STUDIES OF INTERFACIAL ADHESION AND COPPER PLATING CHEMISTRY FOR METALLIZATION OF THROUGH-PACKAGE-VIAS IN GLASS INTERPOSERS

A Dissertation
Presented to
The Academic Faculty

by

Timothy Huang

In Partial Fulfillment
of the Requirements for the Degree
Doctor of Philosophy in the
School of Materials Science and Engineering

Georgia Institute of Technology
December 2017

STUDIES OF INTERFACIAL ADHESION AND COPPER PLATING CHEMISTRY FOR METALLIZATION OF THROUGH-PACKAGE-VIAS IN GLASS INTERPOSERS

Approved by:

Dr. Rao R. Tummala, Advisor
School of Materials Science and Engineering
Georgia Institute of Technology

Dr. Dong Qin
School of Materials Science and Engineering
Georgia Institute of Technology

Dr. Preet Singh
School of Materials Science and Engineering
Georgia Institute of Technology

Dr. Venkatesh Sundaram
School of Electrical and Computer Engineering
Georgia Institute of Technology

Dr. Rahul Manepalli
Intel Corporation

Date Approved: October 31, 2017

ACKNOLWEDGEMENTS

First and foremost, I would like to thank my advisor, Prof. Rao Tummala, for his guidance and mentorship throughout my time as a graduate research assistant at the Georgia Tech Packaging Research Center (GT-PRC). He gave me the opportunity to work in a unique research environment in a field that I was passionate about, in a way that helped immensely in preparing for my future career. I am very grateful for my research mentors at GT-PRC, Dr. Venky Sundaram and Dr. Himani Sharma, who closely guided my research projects. I would also like to thank Prof. Dong Qin, Prof. Preet Singh, and Dr. Rahul Manepalli for serving as members of my committee and providing valuable feedback.

Completing this research would not have been possibile without the help and support from my colleages at GT-PRC and GT-PRC's industry sponsors. Specifically, I am thankful for the technical assistance and discussions I had with Yoichiro Sato (AGC), Tomonori Ogawa (AGC), Akira Mieno (Atotech), Robin Taylor (Atotech), Peter Haack (Atotech), Rahul Manepalli (Intel), and Sashi Kandanur (Intel).

I am also indebted to everyone to assisted or trained me the in lab to complete my experiments. I would like to thank Vijay Sukumaran, Kaushik Ramachandran, and Dr. Fuhan Liu for their training in the cleanroom during my first year at GT-PRC. I received support in fabrication and characterization from Yuya Suzuki, Jialing Tong, Bruce Chou, Nathan Huang, Hao Lu, Zihan Wu, Chandra Nair, Tailong Shi, Grant Spurney, Kaya Demir, Scott McCann, Vanessa Smet, and Fabian Benthaus (TU Dresden). I am also very grateful to Prof. El-Sayed and his research group, especially Jane Wu and Dr. Sajanlal Panikkanvalappil, for their assistance with in-situ Raman measurements. Finally, it would

not have been possible to complete my work without Chris White, Jason Bishop, and everyone else who maintains the lab tools and equipment.

There are also many to thank for their administrative support in GT-PRC and in the Materials Science and Engineering (MSE) department. Many thanks to Patricia Allen, Karen May, and Brian McGlade for helping me take care of conference calls, meetings with industry visitors, sample shipments, and preparing the logistics for my dissertation proposal and defense. I would also like to thank the MSE graduate office, especially Susan Bowman, Teresa Nelson, and Dracy Blackwell who kept track of my degree completion progress.

I would to thank all of my friends and colleagues for making my time in Atlanta memorable. Finally, I would like to thank my family and loved ones for their unconditional support in helping me pursue my goals.

TABLE OF CONTENTS

LIST OF TABLES

LIST OF FIGURES

LIST OF SYMBOLS AND ABBREVIATIONS

BTA	Benzotriazole
CE	Counter electrode
CMP	Chemical mechanical polishing
CTE	Coefficient of thermal expansion
DB	Diazine black
DRIE	Deep reactive ion etching
EMI	Electromagnetic interference
FTIR	Fourier transform infrared spectroscopy
HAST	Highly accelerated stress testing
HBM	High bandwidth memory
IC	Integrated circuit
JGB	Janus Green B
LSV	Linear sweep voltammetry
MPS	3-mercapto-1-propanesulfonate
η	Overpotential
PAG	Polyalkylene glycol
PEG	Polyethylene glycol
PEI	Polyethyleneimine
PPG	Polypropylene glycol
PVD	Physical vapor deposition
PVP	Polyvinyl pyrrolidone

PWB	Printed wiring board
R_a	Roughness (average)
RDE	Rotating disc electrode
RDL	Redistribution layer
RE	Reference electrode
SAP	Semi-additive process
SERS	Surface enhanced Raman spectroscopy
SPE	Screen printed electrode
SPS	Bis(sodium sulfopropyl) disulfide
STM	Scanning tunneling microscopy
TCT	Thermal cycle testing
TPV	Through-package-via
TSV	Through silicon via
VMS	Virgin makeup solution
WE	Working electrode
XPS	X-ray photoelectron spectroscopy

SUMMARY

High quality copper plating in blind-vias and through-vias is crucial to achieve high electrical performance and reliability from the integrated circuit (IC) to the package substrate and printed wiring board (PWB). Cu has been deposited and patterned by several chemical and vapor deposition methods, but the most common approach for high volume manufacturing is electroless and electrolytic Cu plating. In efforts to meet the ever-increasing demand for improved system performance, recent trends in microelectronic packaging require finer Cu lines, micro vias, and fine-pitch Cu-filled through-package-vias (TPVs). Additionally, non-traditional package substrate materials such as glass are being investigated for their electrically insulating properties. These trends pose various material and process-related challenges in achieving high quality Cu metallization. Poor adhesion between copper and glass can result in electrical failures caused by delamination. Low-quality Cu filling in high-aspect ratio TPVs can lead to void formation and mechanical reliability failures. These challenges associated with poor-quality Cu metallization can be addressed through a better understanding of copper to glass adhesion and Cu deposition mechanisms. Therefore, there is a strong need to investigate the fundamental aspects related to Cu adhesion and Cu plating chemistry.

The objective of this research was to develop a fundamental understanding of various aspects related to copper deposition on glass for advanced package and interposer applications. This included investigating the following topics: 1) metallization and adhesion of Cu to ultra-thin glass substrates with small diameter, fine-pitch TPVs, 2) electrochemical characteristics of organic additives in electrolytic Cu plating, and 3) the

mechanism of how organic additives in electrolytic Cu plating enable void-free Cu filling in vias.

Various Cu to glass adhesion mechanisms were investigated. Glass surface roughness was first studied as an approach to enable direct electroless Cu deposition. The feasibility was evaluated by determining the minimum required surface roughness and the interfacial failure mechanism by x-ray photoelectron spectroscopy (XPS). Then, a via-first process using a thin epoxy-based adhesion layer was developed. The process enabled electroless Cu deposition to ultra-thin glass substrates (100 μm) with small diameter (20 μm), fine pitch (40 μm) TPVs. Cu metallized glass substrates with TPVs passed thermomechanical reliability with strong adhesion after thermal cycle testing and highly accelerated stress testing.

The impact of organic additives on electrolytic copper plating behavior was studied by electrochemical characterization. Using cyclic voltammetry and injection chronopotentiometry, the potential dependence and polarization kinetics of individual additives and combinations of additives were characterized. Their impact on Cu filling performance in blind-vias was investigated, and a mechanism was proposed to describe the additive interactions with the Cu via during plating. Finally, surface enhanced Raman spectroscopy (SERS) was used for in-situ observation of the chemical interactions between organic additives and the Cu surface during electroplating.

CHAPTER 1

INTRODUCTION

From the integrated circuit (IC) to the package substrate and printed wiring board (PWB), copper has emerged as the preferred metal for electrically connecting components in most electronic systems. The high electrical conductivity, good corrosion resistance, and high thermal conductivity of copper are some of the desired properties that makes copper the front-up material for electrical interconnections. Cu has been deposited and patterned by several chemical and vapor deposition methods, but the most common approach for high volume manufacturing has been electroless and electrolytic Cu plating. In efforts to meet the ever-increasing demand for improved system performance, recent trends in microelectronic packaging require finer Cu lines, micro vias, and fine-pitch Cu-filled through-package-vias (TPVs). Additionally, non-traditional package substrate materials such as glass are being investigated for their electrically insulating properties. These trends pose various material and process challenges to fabricate high-quality copper wiring as fine-line wiring for redistribution layers (RDLs) and as filled TPVs. These challenges can lead to grave electrical failures caused by delamination from poor adhesion between copper and glass. Low-quality Cu filling in high-aspect ratio TPVs can lead to void formation and mechanical reliability failures. These challenges with poor-quality copper metallization can be addressed through a better understanding of copper to glass adhesion and copper deposition mechanisms. With the lack of literature in Cu metallization of glass TPVs, there is a strong need to investigate the various fundamental aspects related to adhesion and Cu plating chemistry.

The objective of this research is to develop a fundamental understanding of various aspects related to copper deposition on glass for advanced package and interposer applications: 1) metallization and adhesion of Cu to ultra-thin glass substrates with small diameter, fine-pitch TPVs, 2) electrolytic Cu deposition as affected by organic bath additives, and 3) processes for achieving void-free, fully-filled Cu TPVs in glass.

1.1 Motivation for Advanced Device and System Packaging

It is well known that increased performance in computing requires advancements in IC manufacturing technologies. However, commensurate advances in the IC packaging substrate are needed as well to maximize the overall package performance. Traditionally, active ICs are packaged individually to a package substrate which provides the necessary connections for power and signal to the IC from the PWB. As seen in Figure 1.1, the wiring is designed and routed such that it distributes, or "fans out", the smaller IC pitch at the die towards the larger board pitch at the PWB. This electrical routing is typically fabricated by subtractive or semi-additive processes (SAP), a repeated process comprised of metallization and patterning of conductive wires on multiple layers of dielectric films, with adjacent layers connected by vertically metallized holes, or vias.

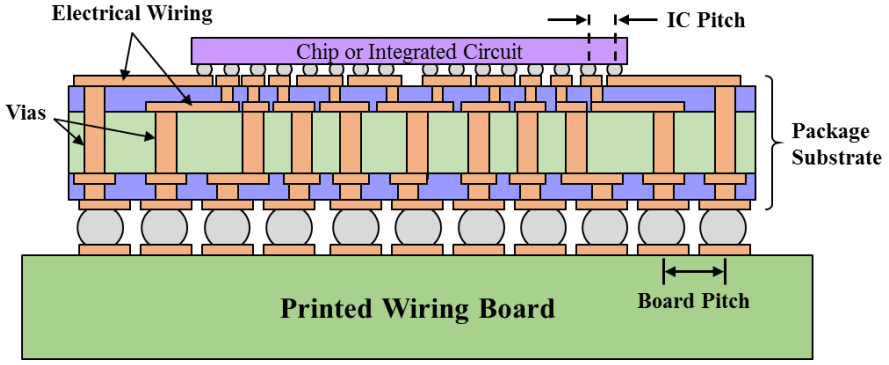

Figure 1.1. Schematic of a traditional IC package substrate connecting the IC to the PWB [1].

Since the 1990s, organic-based composites such as FR-4 have been used as electronic package substrates. Made of an epoxy-based matrix with woven glass fibers and/or silica fillers, this package substrate has the properties to support fabrication for high-performance and consumer products. With a Young's modulus of 10-20 GPa, it is stiff enough to be used for thin packaging in mobile applications such as smartphones. A combination of electroless and electrolytic Cu plating is the widely used for Cu metallization as it is a low-cost and high-throughput process.

Demands for higher performance and multifunctionality in modern systems such as servers requires faster data transmission and miniaturized integration between heterogeneous components in the system. Considering the package substrate material, there are several inherent characteristics of organic-based substrates which limit their ability to support the increased performance demands in the future. Organic-based substrates have relatively high surface roughness, which imposes fabrication-related limitations of the smallest achievable dimensions of Cu wire patterning. And with lower thickness packages, its relatively low stiffness leads to warpage-related challenges for fabrication of high Cu wiring density and through vias.

While advances in die-level manufacturing have decreased the IC node dimensions by three orders of magnitude in the last four decades, packaging dimensions have reduced by less than a factor of ten (Figure 1.2). The next section discusses advanced packaging architectures and substrate materials that are designed to meet the future demands for performance by bridging the IC-package gap.

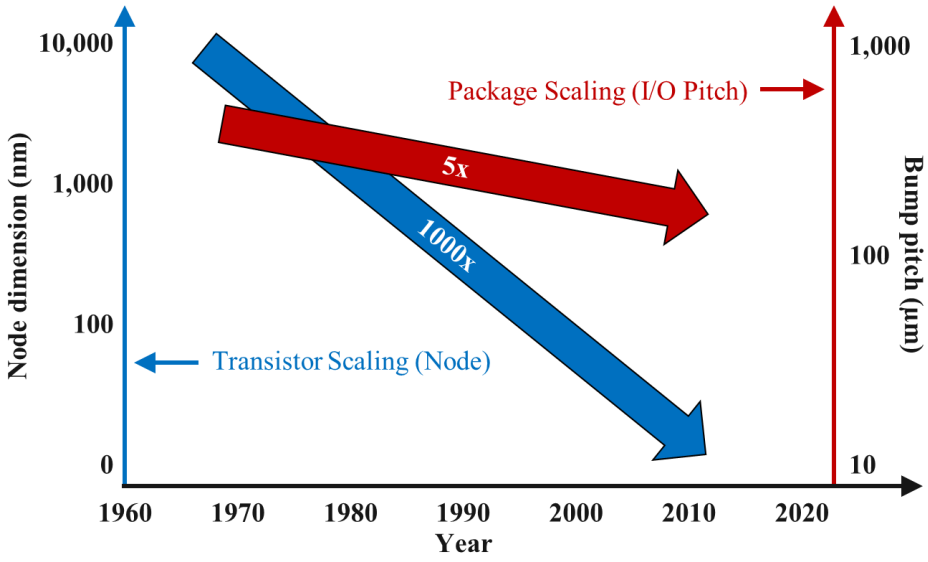

Figure 1.2. Progress in transistor scaling vs. package scaling over time (R. Tummala, 2016).

1.2 Recent Trends in IC Package Substrates

Demands for increased I/O density to achieve high logic-memory bandwidth are leading to the development of inorganic-based interposers with advanced packaging architectures such as 2.5D and 3D system packages (Figure 1.3). The interposers serve as an intermediate substrate between the IC and the traditional organic package. Fabricated with advanced packaging materials and technologies, the interposers are designed with fine-pitch wiring and high I/O density. Multiple chips are assembled on a single interposer to minimize the interconnect length and delay, resulting in improved chip-to-chip speed and performance. Two key technologies in these advanced interposer designs are:

1) High-density Cu wiring between chips
2) Fully-filled fine-pitch Cu through-package-vias (TPVs)

Together, these features support the high I/O density between heterogeneous ICs and from the ICs to the rest of the system.

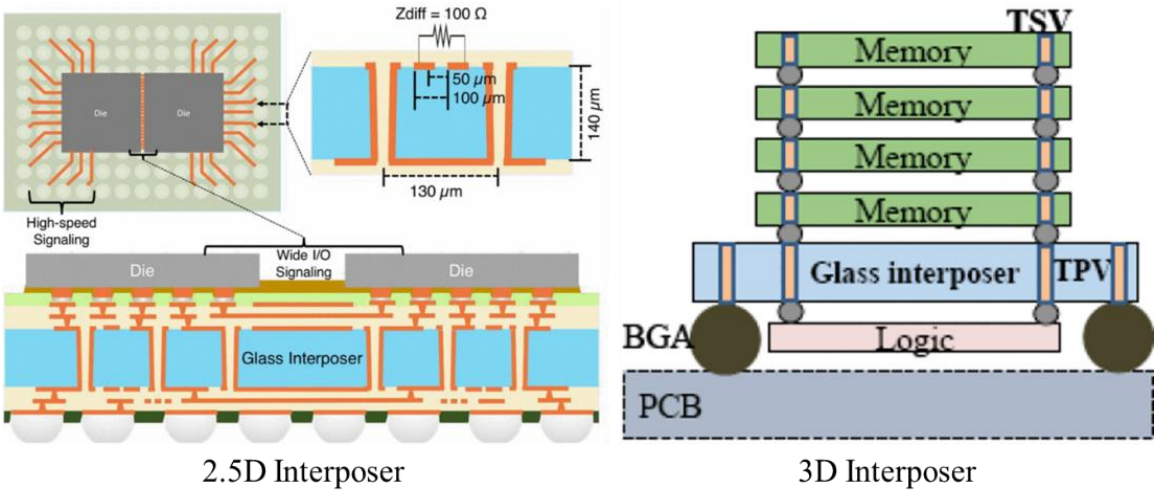

Figure 1.3. Schematic of 2.5D (left) and 3D (right) interposer architectures for multichip packaging (GT-PRC) [2, 3].

Fabrication of fine-pitch wiring and the production of small-diameter vias with high processing accuracy and yield is most feasible on substrates that are smooth and have high resistance to warpage, i.e. high Young's modulus. For optimal electrical performance with high frequency signals, the substrate should be an electrically insulating material with a low dielectric constant and low loss tangent. Other desirable substrate characteristics include strong chemical resistance and a coefficient of thermal expansion (CTE) close to that of the active Si die(s) to minimize warpage and maximize thermo-mechanical reliability. For these reasons, inorganic materials such as silicon and glass have been recently studied as advanced interposer substrates. Table 1 shows how silicon and glass compare to traditional packaging materials in terms of material properties and processing costs.

Table 1. Summary of properties for various package substrate materials [1].

Characteristic	Material property	Ceramic	Organic	Silicon	Glass
Electrical	Dielectric constant @ 1 MHz	9.5-10	4.5-4.8	11.9	4.6
	Resistivity (ohm·m)	$> 10^{10}$	$> 10^{10}$	0.02 - 10	$> 10^{10}$
Mechanical	Young's Modulus (GPa)	300 - 500	10 - 20	130	60 - 80
	CTE (ppm/K)	4 - 8.5	18 - 20	2.6 - 3.0	3.3
Thermal	Thermal conductivity (W/m·K)	20 - 40	0 - 1	100 - 150	1.1 - 1.2
Processing	Minimum via diameter (μm)	50	20	10	20
	Minimum line/space wiring (μm)	50	10	< 1	2
	Through-via formation and metallization feasibility	Low	Medium	Low	Medium
Relative cost	Per area at 25 μm I/O pitch	High	Medium	High	Low

1.2.1. Silicon-based Interposers

Silicon is the most studied material for use as interposer substrates. This is largely due to the well-established infrastructure for silicon processing, such as Bosch processing for through-silicon-via (TSV) formation, small-feature patterning capabilities, chemical-mechanical planarization, and other well-developed processing techniques. Silicon also has many desirable material properties including a high Young's modulus (130 GPa) and a CTE matched to the silicon IC. Its single crystalline nature inherently has a low surface roughness (≤ 1 nm) which allows for Cu line patterning to ≤ 1 μm dimensions. TSVs can be made with a minimum diameter around 10 μm to support high I/O densities [1].

An example of a 2.5D Si interposer with filled Cu TSVs and fine-pitch wiring is shown in Figure 1.4. Advanced Micro Devices used this architecture to support their High Bandwidth Memory (HBM) technology, using a 2.5D interposer combined with 3D IC

stacking for ultra-high logic-memory bandwidth in high-performance graphics processing applications (Figure 1.5).

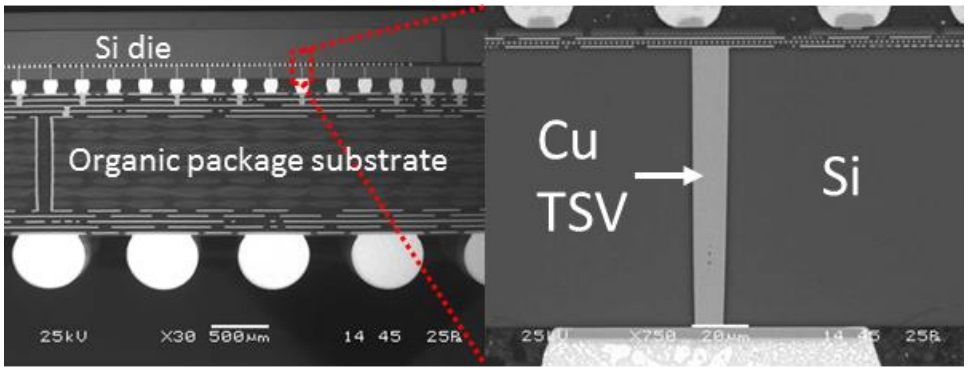

Figure 1.4. Scanning electron micrograph of silicon interposer between die and organic substrate (Xilinx, 2011) [4].

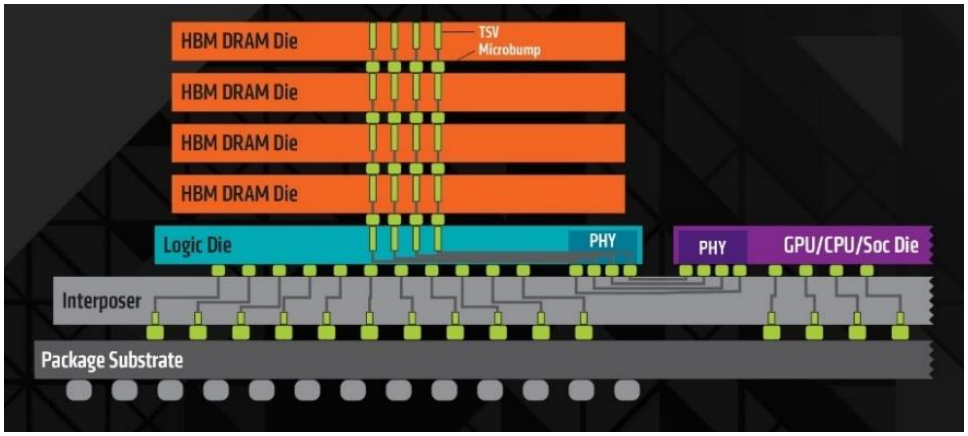

Figure 1.5. AMD's HMB technology using a Si interposer (AMD, 2015).

1.2.2. Glass as a Potential Interposer and Package Substrate

Despite the initial adoption of silicon-based interposers, there is still a need for lower-cost alternatives with similar levels of performance. Glass is widely recognized as a potential alternative to silicon as an interposer substrate material due to its superior

electrically insulating properties, lower raw material costs, and its potential for large scale panel processing [5]. Like silicon, glass has several advantageous mechanical properties over organic-based substrates including a high Young's modulus of 60-80 GPa and nanometer-scale surface roughness. However, the lower dielectric constant and lower loss tangent of glass compared to silicon allows for significantly reduced loss of electrical signals, making glass especially attractive at higher operating frequencies [6]. Glass substrate manufacturing is less demanding than the processing required for high-purity, single crystal silicon. Finally, glass has the potential for large-size, panel-scalable processing (current Generation 8.5 size panels are 220 cm x 250 cm), which will allow for higher throughput and reduced cost per unit. In contrast, the processing area of Si is limited to circular wafers of limited diameter, where the current state of the art is 45 cm in diameter. For these reasons, glass has the potential to be the optimal packaging substrate for advanced computing applications in terms of performance and cost.

Recently, glass interposer manufacturing and processing technologies have seen rapid improvements in several areas such as decreased glass substrate thickness (to <50 μm), reduced through-via diameter (to 20 μm), and improved speed and quality of through-via formation. These advancements are critical for glass to be a competitive substrate material for high-performance interposer substrates that require high-I/O density and superior electrical performance.

1.3 Need for Cu filled Vias in Glass Interposers and Packages

One aspect that remains a challenge for the adoption of glass substrates for interposer applications is the lack of low-cost, high-performance Cu metallization of glass with TPVs. Figure 1.6 illustrates the need for understanding key Cu deposition steps in SAP for glass

interposer fabrication. A thorough understanding of Cu to glass adhesion and viable Cu deposition techniques as well as the electrochemical details of electrolytic Cu plating are necessary to produce reliable, high-performance glass-based interposers that are compatible with SAP.

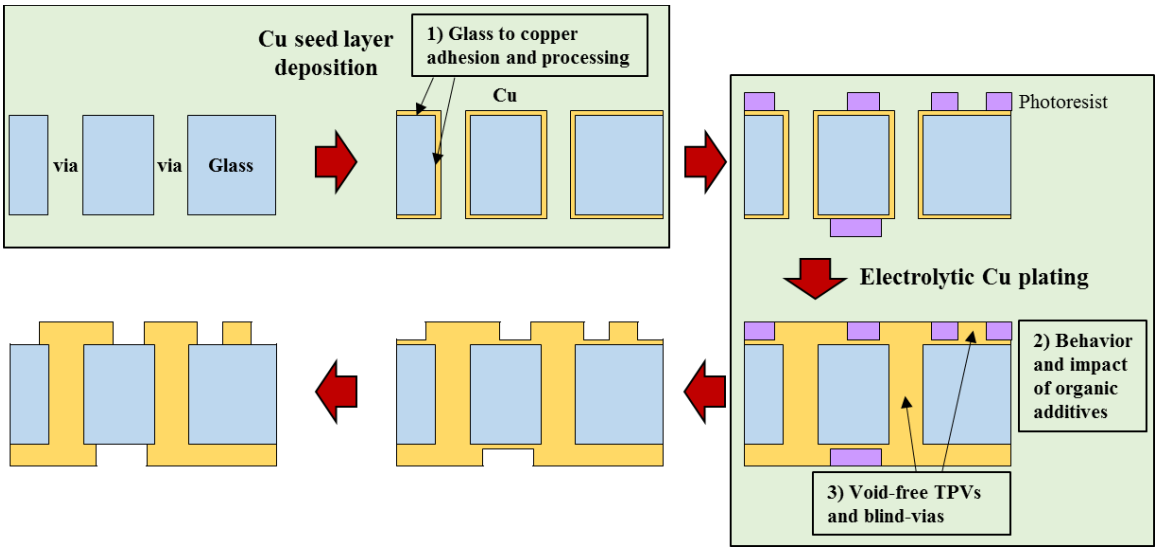

Figure 1.6. Process flow of semi-additive process in a glass interposer with key Cu metallization steps and research objectives highlighted.

1.3.1. Need for Cu to Glass Adhesion

In SAP, a seed layer of Cu is typically deposited by either electroless Cu or by physical vapor deposition (PVD). However, the adhesion between Cu and glass is inherently weak due to their contrasting material structures and lack of strong chemical bonding. Effective Cu deposition methods require an intermediate adhesion layer. Additionally, the high CTE mismatch between Cu and glass will lead to thermal-induced stresses from temperature cycling, which may result in thermo-mechanical failures in the lifespan of the package. These challenges are illustrated in Figure 1.7.

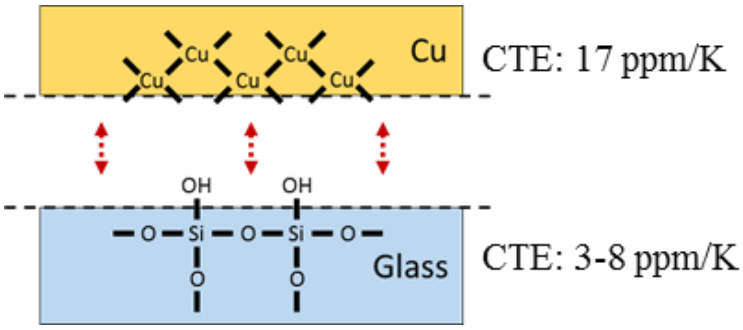

Figure 1.7. Adhesion-related challenges at the Cu/glass interface.

Cu seed layer deposition processes are further constrained by the need to deposit Cu uniformly on the glass surface as well as inside the high-aspect ratio through-vias with strong adhesion (Figure 1.8).

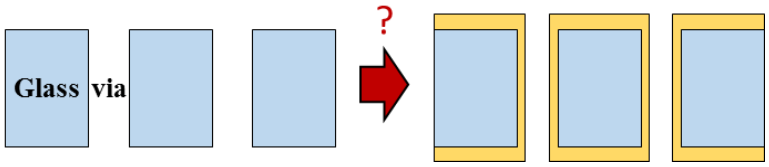

Figure 1.8. Process-related challenges in depositing Cu in high-aspect ratio TPVs.

1.3.2. Need for Understanding Role of Organic Additives in Electrolytic Cu Plating

After the Cu seed layer is deposited, electrolytic plating is used to deposit Cu to the desired thickness. Electrolytic plating inside the through-vias can be conformally or fully-filled. Fully-filled Cu vias are desired over conformally plated Cu vias for several reasons including lower DC resistance, improved power delivery, and superior heat dissipation when used as thermal vias. Fully-filled vias can be formed by electrolytic Cu deposition when the plating conditions allow for "superfilling," a via filling behavior characterized by selectively enhanced plating inside the vias relative to outside of the vias. Superfilling is

achieved through the careful selection of organic molecule additives which either inhibit or promote Cu^{2+} reduction depending on the additive's interaction with the Cu surface with a cathodic potential. While many organic additives have been studied in-depth, there remains a lacking correlation between a given additive's organic structure, electrochemical characteristics, and via filling performance (Figure 1.9).

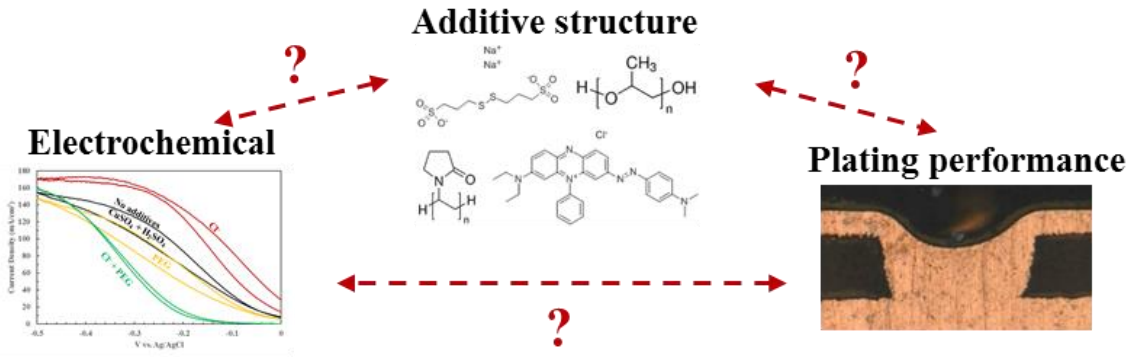

Figure 1.9. Lacking correlation between various aspects of organic additives in electrolytic Cu plating.

1.4 Research Objectives

Based on the above motivations and challenges, this research aims to develop an understanding of the mechanisms for Cu deposition by SAP on ultra-thin (≤ 100 µm) glass substrates with small diameter (≤ 60 µm), fine-pitch (≤ 120 µm) TPVs. This thesis is comprised of three major research objectives:

1. Understand and propose mechanism of copper adhesion to the glass surface and through-glass-via sidewalls.
2. Determine electrochemical characteristics of organic additives in electrolytic Cu plating baths

3. Understand mechanism of organic additives' impact on Cu via filling

The first objective is to determine which Cu seed deposition methods are viable for a given set of glass substrate parameters such as glass thickness, via diameter, and aspect ratio. Metal-to-glass interfaces are prone to mechanical interfacial failures due to lack of strong adhesion. Designing a reliable Cu deposition method requires an understating of copper adhesion mechanisms with adhesion-promoting surfaces or materials. This includes correlating interfacial and surface characterizations with adhesion test results as a function of deposition techniques. Furthermore, the Cu deposition techniques must be able to metallize the glass surface as well as the TPV sidewalls to form continuous, conformal seed layers in preparation for electrolytic plating.

The second objective focuses on the electrolytic Cu deposition process as it relates to filling in vias. Via filling by electrolytic plating is achieved through careful selection of organic molecule additives to the Cu electrolyte to selectively promote Cu^{2+} reduction inside the vias while inhibiting the process outside of the vias. A fundamental understanding of how the organic additive structure influences Cu reduction, and therefore Cu filling performance, will be developed. Organic additives will be characterized by electroanalytical methods such as cyclic voltammetry and injection potentiometry. Additives will be characterized individually to determine their adsorption and polarization kinetics, and then in combination with others to investigate how their behavior changes.

The third objective is to understand the mechanism by which the organic additives affect Cu via filling. This involves using in-situ spectroscopic techniques to better understand the chemical interactions between the additives and the Cu surface. Finally, the blind-via filling performance will be characterized for several combinations of additives.

The results will be combined with their electrochemically determined adsorption properties to propose a mechanism for void-free superfilling in blind-vias.

1.5 Research Challenges and Tasks

The research challenges and tasks associated with the objectives are briefly summarized in

Table 2.

Table 2. Summary of research objectives, challenges, and tasks.

No.	Objectives	Challenges	Tasks
1	Metallization and adhesion of Cu to glass	• Weak Cu to glass adhesion • Thermomechanical reliability	• Develop understanding of Cu to glass adhesion mechanisms • Develop via-first glass metallization process
2	Determine role of organic additives in electrolytic Cu plating baths	• Lacking correlation between additive structure, electrochemical behavior, and plating performance	• Electroanalytical characterization • In-situ chemical characterization • Structural characterization
3	Cu filled glass vias	• Costly processing • Void-free Cu filling in glass TPVs	• Develop process guidelines • Demonstrate high-quality Cu filling in glass TPVs

Chapter 2 will describe in detail the previous research related to each challenge to achieve the objectives of this research. Chapters 3, 4, and 5 describe the results for each research task.

CHAPTER 2

LITERATURE REVIEW

This chapter summarizes key findings from previous work in each of the research objectives. The first research objective relates to adhesion between glass and the Cu seed layer. The Cu thin (500 nm or less) seed deposition must be performed in a way that achieves strong adhesion and by a process that allows for conformational deposition inside the glass TPVs. The next research objective focuses on understanding the fundamental role of organic additives and their impact on electrolytic Cu plating. The last research objective is to investigate processes for filling glass TPVs without voids.

2.1 Metallization and Adhesion of Copper to Glass Interposers

Achieving high-quality metallization of TPVs in ultra-thin glass with strong adhesion and thermo-mechanical reliability is challenging for several reasons. Fundamentally, copper and glass do not adhere well due to their differing chemical structures: the covalent oxide network of silica-based glass and the metallic lattice of copper do not readily form chemical bonds at the interface. In addition to the fundamental challenges associated with Cu to glass adhesion, there are process-related challenges in depositing Cu in a way that is conformal with the glass TPVs. This section provides an overview of previous efforts made in these key areas related to the first metallization step of semi-additive processing, Cu seed deposition.

2.1.1. Copper to Glass Bonding and Adhesion Mechanisms

Chemical bonding can be promoted by chemically treating the glass surface prior to electroless Cu deposition. Some examples of this approach use self-assembled monolayers

of molecules containing alkyl silane end groups which chemically bond to glass and amino based end groups which promote adhesion to Cu (Figure 2.1) [7, 8]. While these wet chemical-based glass surface treatments have enabled adhesion of electroless Cu of sub-micron thickness, maintaining adhesion after electrolytic Cu plating to greater thicknesses remains a challenge, as made evident by the lack of demonstrated applications.

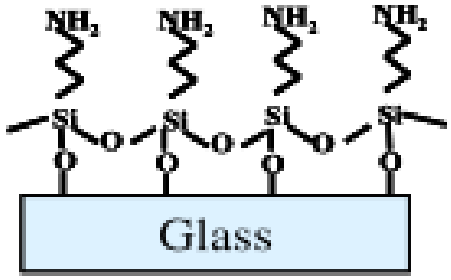

Figure 2.1. Glass functionalized with aminopropyl trimethoxysilane to promote adhesion to electroless Cu [8].

Achieving the strongest adhesion between metals and glass is done through different approaches to attain chemical bonding. Depositing certain metals such as Ti or Cr by physical vapor deposition (PVD) result in the formation of a thin interfacial oxide layer of TiO_2 or Cr_xO_y, respectively, between the metal and glass. The formation of this oxide layer is thermodynamically driven by the respective oxides' high heat of formation and oxygen supplied by the glass [9-14]. Since this process is done in a vacuum, Cu can be subsequently deposited by PVD to form metallic bonds with the Ti or Cr without forming an oxidized layer beneath the Cu.

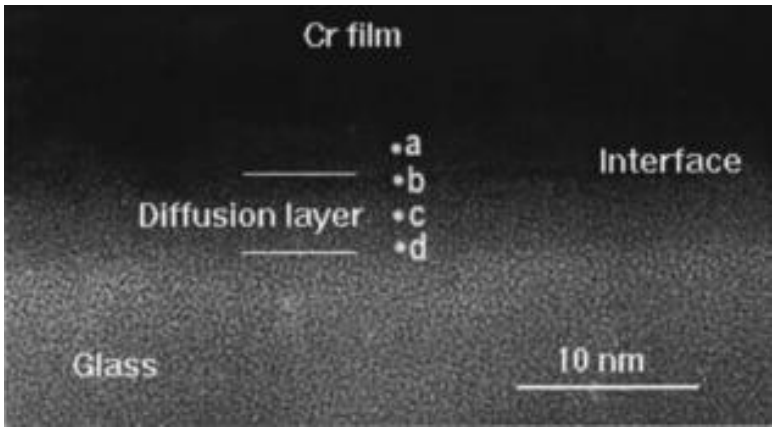

Figure 2.2. Transmission electron micrograph of Cr/glass interface with thin Cr_xO_y layer formed [13].

A mechanical-based adhesion mechanism can be used in place of or in conjunction with chemical-based adhesion. Mechanical adhesion is introduced by roughening the glass surface, leading to mechanical anchoring at the copper-glass interface [15-17]. However, it was shown that roughness in conductor interfaces can degrade high-frequency electrical performance because of the skin-effect [18].

2.1.2. Processes for Cu Seed Layer Deposition in Glass TPVs

Beyond adhesion, other challenges exist which limit certain metallization approaches and technologies based on aspects which may inhibit industrial practicality. The high degree of mismatch in the CTE of glass (3 ppm/K) and copper (17 ppm/K) will further challenge the interfacial adhesion when subjected to stresses in thermal cycle testing (TCT), an industry-standard reliability test. Finally, the requirement of small diameter, high-aspect ratio TPVs in glass is challenging for metallization techniques which are non-conformal in nature (e.g., PVD methods such as sputtering). Several methods have been recently demonstrated to address some of these challenges, all of which utilize an intermediate adhesion layer between glass and copper.

Copper metallization processes of glass interposers found in the literature can be divided into two categories: via-last, where TPVs are formed after other prior processing, and via-first, where TPVs in glass are formed before any subsequent processing. One via-last process, shown in Figure 2.3, demonstrated that laminating a polymer film onto glass followed by TPV formation and electroless metallization yields a stable structure [19-21]. The polymer film serves as an intermediate adhesion layer by forming chemical bonds to glass through silane-based coupling agents on one side and mechanical anchoring to electroless copper on the other side. The polymer also functions as a mechanical stress buffer and aids in the handling of ultra-thin glass.

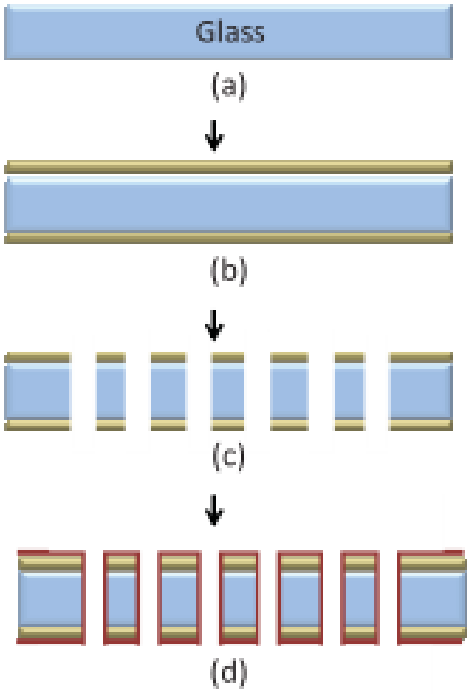

Figure 2.3. Schematic of a via-last process for metallizing glass interposer substrates [5].

Recently, however, glass substrate manufacturers have developed via formation technologies which are incompatible when polymer films are present. The most recent demonstrations have focused on via-first metallization processes in glass. Sputtering titanium or chromium, which are known to form chemical bonds to glass, followed by a metal which does not adhere strongly to glass directly is a well-known method of depositing metals onto glass. Due to the line-of-sight nature of sputtering, depositing metal onto the TPV sidewalls which are parallel to the flux of sputtering is not as straightforward as the planar surface which is perpendicular to the flux of sputtering. It follows that there is an inherent upper limit to the aspect ratio of vias which can be metallized conformally by sputtering before the TPV centers are unable to receive sufficient sputtering flux. This challenge is illustrated in Figure 2.4, where sputtering is unable to conformally deposit on the sidewalls near the center of the vias.

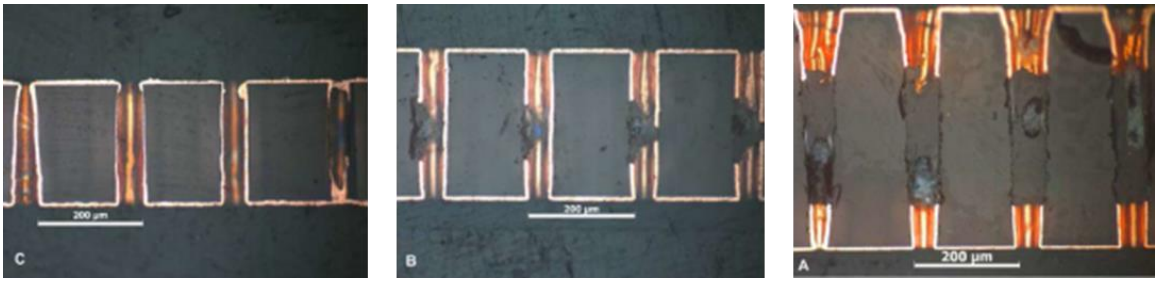

Figure 2.4. Cross section micrographs of glass vias with increasing aspect ratio after Cu sputtering [22].

A method to address this issue was demonstrated by subsequently using electroless metallization to fill any discontinuities in the previous sputtering step [22]. Another recently demonstrated glass metallization technology uses a thin metal-oxide film which

forms chemical bonds to glass and mechanical bonding to electroless copper. The deposition is done by sol-gel processing to enable conformal TPV coverage [23-27].

2.2 Role of Organic Additives in Electrolytic Cu Plating

Once a Cu seed layer is deposited on the substrate, semi-additive processing continues with wiring structures patterned by photolithography, followed by electrolytic Cu plating. Different classes of organic additives are added to the Cu plating electrolyte to affect Cu plating in a way that promotes a plating behavior known "superfilling" in blind-via structures. This section reviews various methods of characterization to observe how the organic molecules affect the Cu electroplating process.

2.2.1. Organic Additive Classifications and Functions

A typical electrolytic copper plating bath is composed of both inorganic and organic components. The essential inorganic elements that make up the aqueous electrolyte solution include a copper salt, acid, and chloride ions. Copper salt (typically $CuSO_4$) ionizes in the aqueous solution to cupric ion (Cu^{2+}), which is reduced and deposited at the negatively charged cathodic substrate by the following reaction:

$$Cu^{2+} + 2e^{-} \rightarrow Cu(s)$$

Acid is added to provide sufficient ionic conductivity in the electrolyte solution; sulfuric acid is normally used for this purpose. An anodic reaction of Cu oxidation occurs at the counter electrode, which has a positive potential with respect to the cathode:

$$Cu(s) \rightarrow Cu^{2+} + 2e^{-}$$

Chloride ions can be added as either NaCl or HCl, and these ions are required to facilitate the interaction between the Cu cathode and the organic additives. The organic additives are included as specific modifiers to the plating behavior and are generally

categorized as suppressors, accelerators, and levelers, based on their function. Table 3 summarizes the acid Cu plating bath components, typically used materials and concentrations, and their function.

Table 3. Summary of typical electrolytic bath components.

Component	Chemical	Concentration	Purpose
Cu^{2+}	$CuSO_4$	0.16 – 0.88 M	Cu^{2+} source
Acid	H_2SO_4	0.1 – 1.8 M	Ionic conductivity
Cl^-	NaCl HCl	30 – 70 ppm	Enables interaction between Cu electrode and organic additives
Accelerator (Thiol-based)	Bis(sodium sulfopropyl) disulfide (SPS)	5-10 ppm	Catalyzes delivery of Cu^{2+} to Cu surface
Suppressor (Alkylene glycol)	Polyethylene glycol (PEG) Polypropylene glycol (PPG) PEG-PPG copolymers	200 – 700 ppm	Creates physical diffusion layer to inhibit Cu^{2+} migration to Cu surface
Leveler (Aromatic nitrogen-based)	Janus Green B (JGB) Diazine Black (DB) Polyvinylpyrrolidone (PVP) Benzotriazole (BTA)	Varies by molecule	Selectively inhibits Cu plating in regions of high current density (peaks of Cu surface) to preferentially plate in troughs

The function of these additives is based on their effect on the Cu plating behavior and plating rate. Accelerator molecules bind to the copper cathode by a sulfur containing end group and effectively catalyze the delivery and reduction of Cu^{2+} in solution to the cathode surface. Suppressors are generally some form of alkylene glycol. These molecules coordinate and bond with CuCl formed on the cathode surface, and the bulky molecule serves as a physical diffusion barrier to inhibit the rate of Cu^{2+} to the Cu surface. Leveler molecules contain nitrogen atoms which coordinate with the Cu cathode to selectively inhibit Cu plating in regions of high current density, which tend to be topographical peaks in the Cu surface, and this results in preferential plating in trough-like features. By employing the appropriate combination of additives, Cu plating can be carried out to create

void-free fully-filled Cu blind via structures through the plating behavior known as "superfilling," as seen in [28].

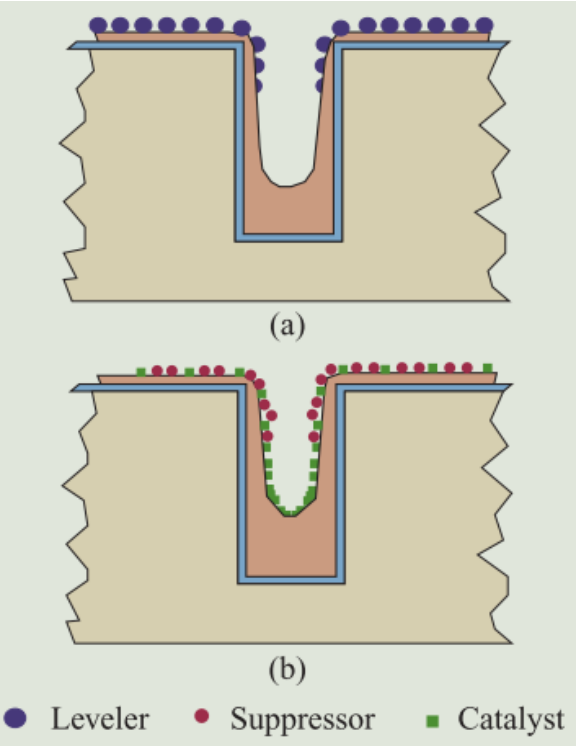

Figure 2.5. Schematic of superfilling mechanisms achieved by (a) strong differential inhibition of plating outside of the vias by leveler and suppressor and (b) selective adsorption and activity of catalyst or accelerator in the bottom of the vias [29].

2.2.2. Electroanalytical Characterization of Organic Additives

Alkokar and Landau utilized electroanalytical techniques such as galvanostatic potentiometry to characterize the transient adsorption of accelerator and suppressor [30]. The plating overpotential was monitored as a function of time after injecting SPS and PEG with varying sequence and combination to the electrolyte. A galvanostatic potential drop indicates accelerated behavior and inferred adsorption of SPS while the opposite infers the adsorption of PEG. The observed competitive adsorption behavior of SPS and PEG on the

Cu electrode was used to propose a mechanism of how the two interact to achieve superfilling. While PEG has fast adsorption kinetics compared to SPS, it is diffusion limited in the confined space deep inside the via. SPS therefore selectively adsorbs closer to the via bottom, enhancing plating at the bottom while PEG suppresses plating towards the top of the via and on the Cu surface outside the via. This behavior is illustrated in Figure 2.6.

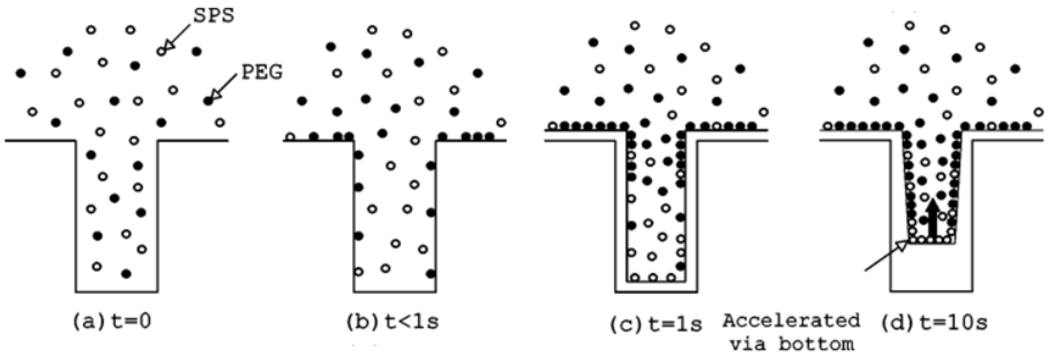

Figure 2.6. Proposed mechanism of competitive adsorption of SPS and PEG in Cu superfilling by Akolkar and Landau *[30]*.

Other electroanalytical techniques used to characterize the plating behavior as affected by organic additives include cyclic voltammetry and rotating ring-disk technique, as shown by Moffat et al. and Vereecken et al., respectively [29, 31]. The results using these techniques and analysis are consistent regarding the behavior of the PEG-SPS-Cl system [32]. More detailed analysis of suppressor behavior has been done to investigate the effect of PEG molecular weight [33] as well as a proposed way to categorize suppressors based on synergistic and antagonistic effects [34]. The adsorption kinetics of PEG have also been studied in detail using microfluidic cells [35]. In addition to PEG,

polypropylene glycol (PPG) and triblock copolymers of PEG and PPG has been characterized and compared with PEG [36].

Likewise, in-depth characteristics of various leveler molecules including polyethyleneimine (PEI), polyvinylpyrrolidone (PVP), Janus Green B (JGB), diazine black (DB), and more have been investigated and characterized [37-42]. In particular, the adsorption and inhibition mechanism of PVP has been studied to great detail [38, 43-45].

2.2.3. In-Situ Observation of Organic Additive Interactions with Cu Surface

The previously mentioned techniques characterize the effects of organic additives indirectly, either by using electroanalytical data to infer and propose the molecular interactions or by ex-situ material characterization of the Cu deposit. One area of ongoing research is in developing a fundamental understanding of the structure-performance relationship of various additives at the molecular level. In-situ techniques are therefore desired to observe the direct interaction of the plating bath components with the Cu electrode under various conditions. These techniques can ultimately enable a predictive understanding of how a given organic additive will behave based on its molecular structure.

Two methods which have been used for in-situ observation of the Cu plating surface are scanning tunneling microscopy (STM) [34] and surface enhanced Raman scattering (SERS) [46-48]. Raman scattering is a spectroscopic characterization technique in which laser-induced interactions with a molecule is observed. The vast majority of photon interactions will result in elastic, Raleigh scattering. However, a small fraction of photons interacts by inelastic scattering where the measured energy difference is related to excited vibrational bonding modes of molecules in the material. The observed inelastic scattering is collected over a spectrum, and characteristic peaks can be associated with the presence

of certain molecular bonds. SERS is a specialized Raman technique which utilizes a phenomenon where the Raman signal is dramatically enhanced through electromagnetic resonance with surface plasmons in specific materials. The effect is limited to noble metals whose surfaces are roughened or nano-structured because the vertical (relative to the substrate) Raman signal must resonate directionally with the surface. Since Cu film growth by electrolytic plating is inherently rough, SERS has been used to gain insight into the chemical interaction of model additives such as PEG and SPS with the copper cathode. For example, Gewirth et al. observed the Cu surface with a range of applied potentials while changing the electrolytic bath components. By systematically adding 3-mercapto-1-propanesulfonate (MPS) or its derivative structures (butanesulfonate and butanethiol) in an aqueous solution of $CuSO_4$ and H_2SO_4 with and without Cl^-, comparative analysis of the SERS spectra led them to the conclusion that the SPS molecule binds to the Cu surface by the -SH thiolate group rather than the $-SO_3$ sulfonate group. They also showed that the presence of Cl^- modifies the Cu surface to enhance $Cu\text{-}S_{thiolate}$ adsorption (Figure 2.7) [48]. Similar experiments verified the molecular interaction between Cu, Cl^-, and PEG [46].

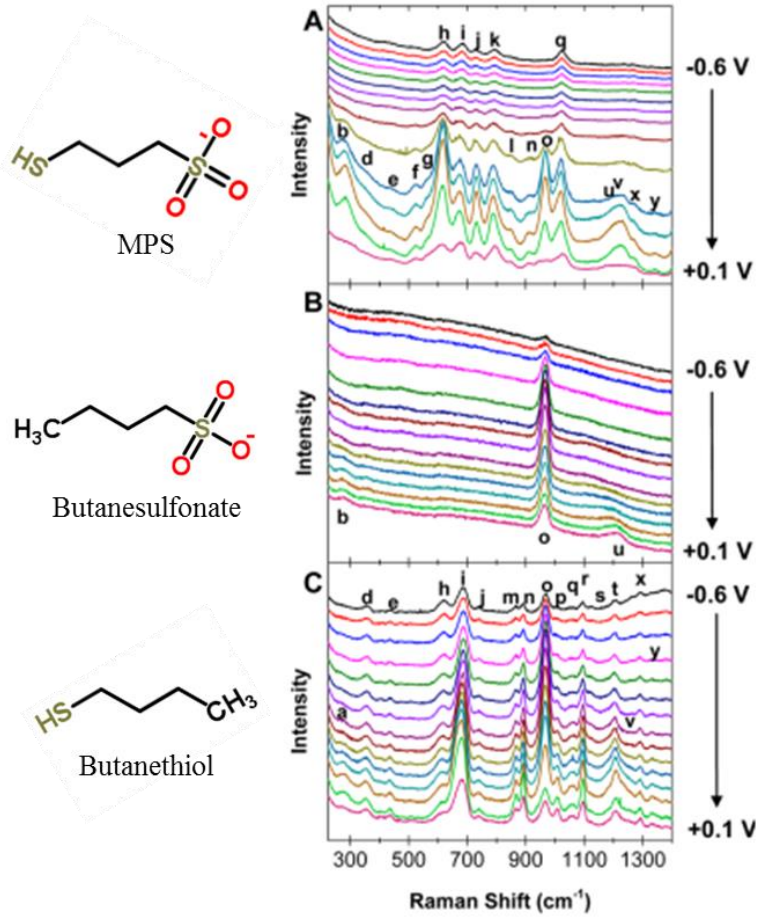

Figure 2.7. SERS spectra of $CuSO_4$, H_2SO_4, Cl^-, and (A) MPS, (B) butanesulfonate, and (C) butanethiol on Cu surface *[48]*.

2.3 Cu Filled Vias in Glass Interposers

Very little previous work was found in demonstrating fully-filled Cu TPVs in glass interposers. A very novel approach was described by Lee et al. which involves bottom-up plating of Cu into TGVs made by a wafer-level packaging approach (Figure 2.8) [49]. In this process, a silicon mold is created by patterning inverse pillar structures in a silicon substrate by deep reactive ion etching (DRIE). A borosilicate glass wafer is bonded to the mold and reflowed at 1025 °C. After reflow, the glass has filled the patterned Si mold and is planarized by chemical mechanical polishing (CMP). Then, the inverse pillar structures

in the Si mold are etched by DRIE to reveal vias in the reflowed glass. The glass vias are then filled with Cu by electrolytic plating directly on the bottom of the Si mold. After bottom-up filling, the surface is planarized by CMP again and the top layer of the substrate is metallized. Finally, the bottom of the vias are revealed by CMP and then metallized. While novel, such a process heavily relies on high-cost, low-throughput processing methods such as DRIE and glass reflow. Furthermore, it has low potential for being panel-scalable.

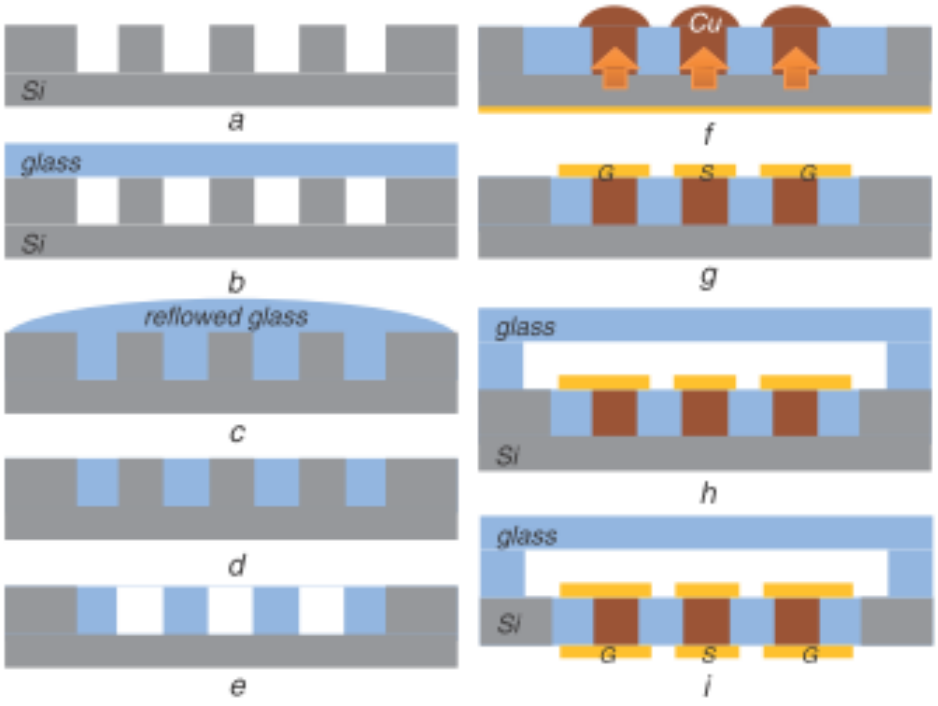

Figure 2.8. Fabrication process flow of a wafer-level RF MEMS package *[49]*.

A more manufacturable approach was demonstrated by Corning Inc. in 2013 [14]. The process is similar to what is typically used for fabricating Si interposers. The process begins with blind vias formed in a thick glass substrate (Figure 2.9a). The blind vias are drilled to a depth greater than the desired final substrate thickness. Ti/Cu is then deposited

by physical vapor deposition (PVD), forming a seed layer for subsequent bottom-up filling of Cu and planarization (Figure 2.9b). Next, the glass substrate undergoes back grinding to reveal the bottom of the blind vias, and then another Cu metallization step is used to complete the metallized glass substrate (Figure 2.9c).

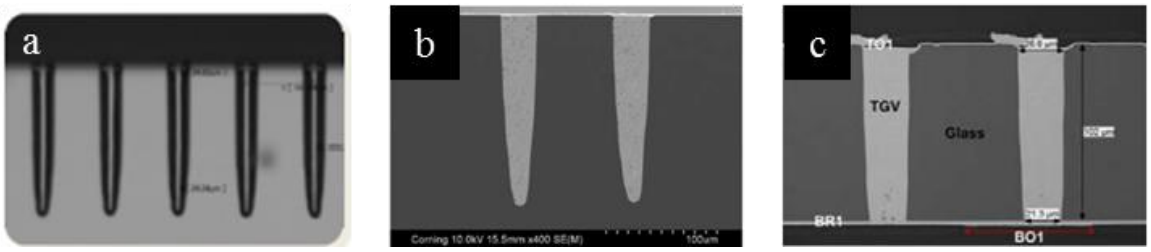

Figure 2.9. SEM cross sections showing various stages of a Si interposer-type fabrication process of filling glass vias with copper *[14]*.

As seen in the previous examples, fully-filled Cu vias in glass interposers have only been demonstrated using bottom-up filling of blind-via structures followed by back grind and CMP to reveal the other side of the vias. No previous literature was found which started with an ultra-thin glass substrate containing vias.

CHAPTER 3

METALLIZATION AND ADHESION OF COPPER TO GLASS

As mentioned previously, the inherently weak adhesion between Cu and glass is one of the major challenges with using glass as an electronic packaging substrate. Due to the differences in their chemical structures, most metallic materials such as Cu do not bond strongly to the oxide networks of silicate glasses. This results in insufficient adhesion and failure to meet reliability criteria in assembled packages. One approach that has been demonstrated to circumvent this is to coat both sides of glass with a polymer film before the glass through package vias (TPVs) are made. After the creation of vias by excimer laser ablation, the polymer surface and the roughened-glass via sidewalls can be metallized by standard electroless processes [19]. The major disadvantage of this approach is its limited compatibility with via-formation methods. Glass manufacturers have recently developed proprietary TPV formation processes, some of which are not fully compatible with polymer-coated glass. Direct metallization of copper on smooth glass surfaces without polymer also provides more opportunities for lower cost, miniaturization as well as reliability and electrical performance improvements.

In general, covalent-bonded oxide networks such as glass bond directly to materials composed of oxides or oxide interfaces that are stable. Since Cu is composed of metallic-bonded atoms, some surface modification that results in an oxide formation can be expected to result in enhanced bonding. Surface modifications can be physical (e.g., mechanical interlocking) or chemical, with the latter being ideal. For good chemical adhesion between bare copper metal and glass, fundamental adhesion theory states that it

is important to have an intermediate metal oxide interface for strong and lasting adhesion. Based on this fundamental principle, a process that enhances chemical bonding through gradual, continuous material-property changes in the transition from glass to metal oxide to metal is preferred over mechanical-based methods to achieve strong adhesion. For example, it is well known that certain, reactive metals with high oxygen affinity (e.g., Cr, Ti, Zr, Mg) exhibit strong bonding "directly" to glass by forming thin oxide layers at the interfaces [9, 13]. These oxides are very stable even at high temperatures and in reducing gas atmospheres. While standard vacuum deposition techniques benefit from this approach by depositing an adhesion layer such as Ti between Cu and glass, new innovations [17, 50] are required to achieve this intermediate "adherence oxide" layer with wet metallization techniques as described next.

3.1 Roughness-based Adhesion of Glass to Cu

Electroless copper deposition is a standard wet metallization process typically used for organic substrates. It is a relatively low-cost, wet processing method involving a series of steps which includes chemical surface treatments, deposition of catalyst (typically Pd/Sn) particles, and electroless copper reduction on the catalyst particles. This creates three separate, ionic-bonded interfaces between the glass (negatively charged OH^- surface), conditioner (positively charged polymer electrolyte), and catalyst (negatively charged surface) (Figure 3.1). Except for the bonding between the Pd catalyst and the electroless-deposited Cu, each of the interfaces between glass and catalyst rely on ionic bonding. To improve adhesion, surface etching and roughening is a typical part of electroless plating for organic substrates. Adhesion is improved through increased surface area and mechanical interlocking with the roughened surface. However, increasing the surface

roughness of the glass-metal interface will result in higher conductor losses, especially at higher frequencies due to the skin-effect [18]. Additionally, glass roughening processes are difficult to control precisely and can introduce flaws or cracks, resulting in increased risk of mechanical failure. Since chemical, covalent bonds are not directly made between the Cu and the glass oxide network, glass surface roughness is mandatory for achieving sufficient adhesion. To maximize electrical performance and mechanical integrity, it is therefore of interest to find the minimum roughness required to achieve sufficient adhesion through roughening for electroless plating.

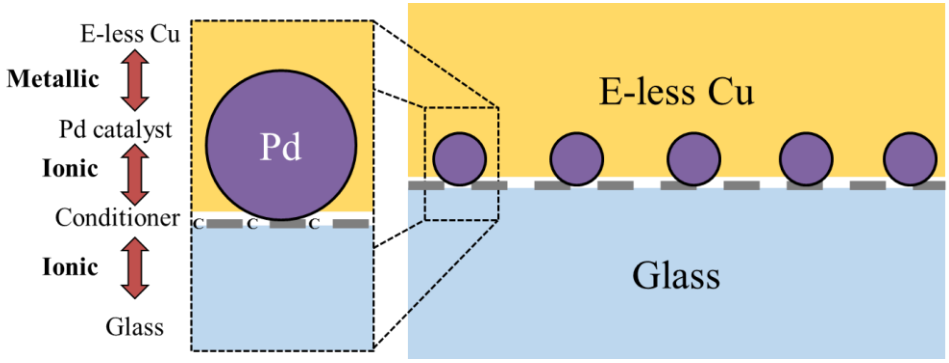

Figure 3.1. Schematic of chemical interfaces between electroless Cu and glass (not to scale).

3.1.1. Electroless Cu Deposition

Smooth and roughened glass-substrates were provided by Corning, Inc. and Life BioScience, Inc. Roughened samples were characterized by atomic force microscopy (Veeco AFM) prior to processing to obtain roughness (R_a), and ranged from < 1 nm to 0.559 μm.

Electroless Cu deposition was used to form a thin layer of copper on the roughened glass substrates. The electroless-plating steps are substrate cleaning, conditioning

(deposition of polymer electrolyte), catalyst deposition, catalyst activation, and finally electroless copper deposition. Triple rinses in water were performed between each step. Electroless deposition was performed until 0.2 μm of Cu was deposited. Finally, samples were annealed at 155°C for 30 minutes in air. Tape-tests were then performed according to IPC-TM-650 test standards.

3.1.2. Tape Test Results and Failure Analysis

Results of the tape-test of electroless Cu on glass are shown in Figure 3.2, in the order of increasing adhesion. It can be seen that there is a regime of surface roughness values (R_a) where the structure of peeled copper changes. In the samples with worst adhesion, Cu outside of the tape dimensions were peeled, as can be seen by the jagged peels in Figure 3.2(a, b). As the adhesion increases, the copper film does not peel beyond the edge of the tape (Figure 3.2(c)), and then smaller amounts of Cu peel from the glass (Figure 3.2(d-f)). Finally, the glass chemically roughened to 0.559 μm passed the tape test, exhibiting no peeled Cu (Figure 3.2(g)).

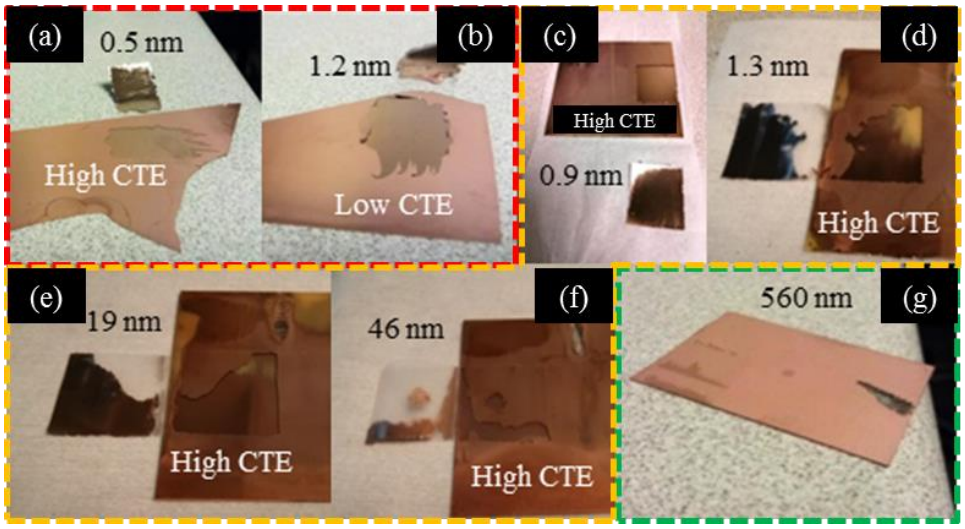

Figure 3.2. Tape tests for electroless copper on various glasses: (a) Corning SGW8.5 (R_a = 0.5 nm) (b) Corning SGW3 (R_a = 1.2 nm) (c) Corning SGW3 (R_a = 0.9 nm) (d) Corning SGW8.5 (R_a = 1.3 nm) (e) Corning SGW8.5 (R_a = 19 nm) (f) Corning SGW8.5 (R_a = 46 nm) (g) Life BioScience APEX (R_a = 0.559 µm).

The large range in tape-test results for similar roughness values (Fig. 2a-d) can be attributed to several factors. Roughness values were measured with AFM and could vary depending on the selected area because the topography was generally not homogenous in the areas inspected (10x10 µm and 30x30 µm). The values in this range are within the instrumental error. In addition to surface roughness, adhesion to glass depends on the glass chemical composition. High CTE glasses (SGW8.5) are composed of more glass network-modifying ions than low CTE glasses (SGW3); as these ions are positively charged, they can assist with adhesion to the Pd catalysts.

For samples which failed the tape-test, the substrate and peeled interfaces were analyzed by X-ray photoelectron spectroscopy (XPS) (Thermo K-Alpha XPS) for the presence of Cu, Si, and C [15]. Representative XPS elemental Pd and survey scans of the peeled Cu and the exposed glass are shown in Figure 3.3. It is apparent that Pd was detected

only on the peeled Cu, while C was detected only on the glass surface. Assuming that the only source of carbon in the system is the polymer electrolyte conditioner, this suggests that the weakest interface in the electroless copper-glass is that between the conditioner and the Pd catalyst.

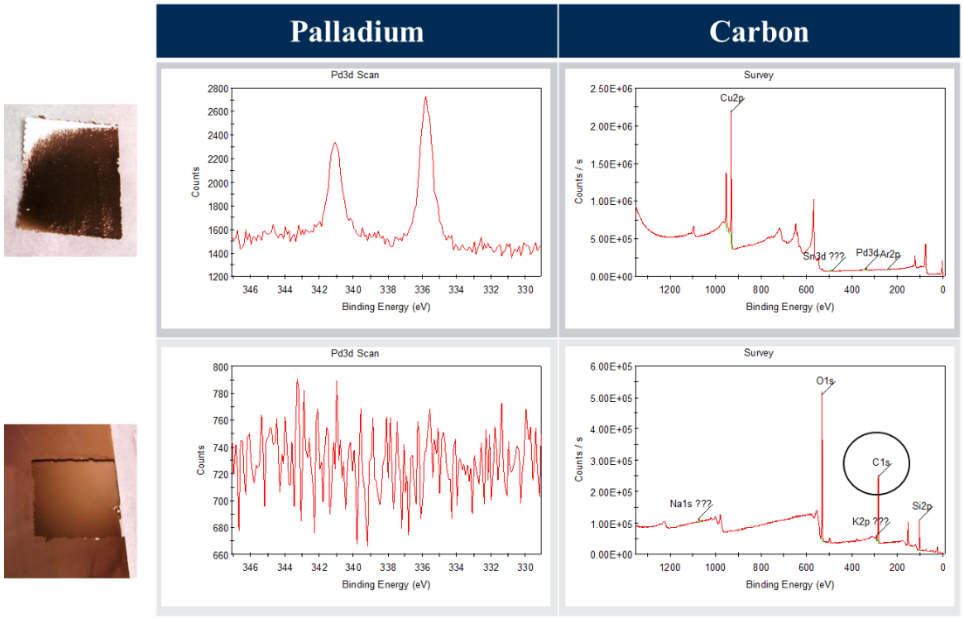

Figure 3.3. XPS elemental Pd and survey scans of the peeled Cu and the exposed glass.

With the current electroless process, a surface roughness on the order of hundreds of nanometers is necessary to achieve sufficient adhesion to pass the tape test. Based on the skin-effect, Brist et al. [18] modeled the effects of surface roughness on electrical loss and introduces an additional electrical loss factor K_{sr}, where a value of 1 represents the factor for smooth surfaces (i.e., no additional loss). At an electrical frequency of 10 GHz, surface roughness values of 0.2 μm and 0.6 μm result in K_{sr} values of ~1.1 and 1.55, respectively [18]; i.e., Cu with 0.6 μm roughness will have 55% more loss (dB/length) than smooth Cu.

3.1.3. Sputtered Cu

To investigate the effects of the sputtered Cu seed-layer thickness and total thickness of the Cu layer, three different seed layer thicknesses (200, 500, and 800 nm) were sputtered on unroughened glass. Each film was electroplated to a total Cu thickness of 5 μm and 10 μm, for a total of six different samples. Peel-tests of these samples showed no significant correlation with the seed-layer thickness for the ranges investigated.

Peel-testing for smooth and roughened (R_a = 10, 50, 100, 200, 300, 400, 500, 1000 nm) glass electroplated to 10 μm Cu was performed before and after thermal shock testing (5 μm thick Cu strips tore during peel testing, and could not be measured). Prior to thermal shock testing, smooth glass exhibited peel strength values over 0.2 kg/cm (Fig. 4). On the other hand, the Cu lines on all roughened glass samples could not be peeled from the glass and therefore exceeded the strength limits that the technique can measure. After 1000 thermal shock cycles, the smooth glass was again the only peelable sample, and did not show any significant change in peel strength when compared to those from pre-thermal shock testing.

In the microelectronics packaging industry, a typical benchmark for the peel strength is 0.7 kg/cm for Cu thickness of 30 μm on organic substrates. The peel strength W_o of a metal strip as a function of film thickness t_s has been modeled by Bikerman to follow the relationship [51]:

$$W_o \propto {t_s}^{3/4}$$

Using this relationship, a comparable peel strength value for Cu plated to 10 μm thickness was calculated to be 0.18 kg/cm. As seen in Figure 3.4, the peel strengths before and after thermal shock testing were

over 0.25 kg/cm, well-above this scaled benchmark value.

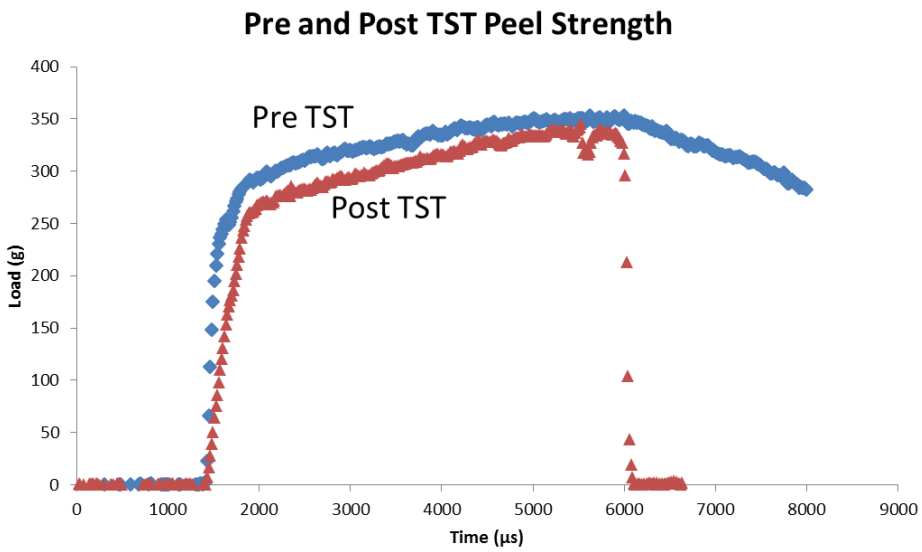

Figure 3.4. Peel strength of 10 µm Cu on smooth glass before and after 1000 thermal shock testing (TCT) cycles.

3.2 Via-First Process for Electroless Cu Metallization

Via metallization processes can be divided into two categories: via-last, where TPVs are formed after other prior processing, and via-first, where TPVs in glass are formed before any subsequent processing. One via-last process, shown in Figure 2.3, demonstrated that laminating a polymer film onto glass followed by TPV formation and electroless metallization yields a stable structure [19-21]. The polymer film serves as an intermediate adhesion layer by forming chemical bonds to glass through silane coupling agents on one side and mechanical anchoring to electroless copper on the other side. The polymer also functions as a mechanical stress buffer and aids in the handling of ultra-thin glass.

Recently, however, glass substrate manufacturers have developed via formation technologies which are incompatible when polymer films are present. The most recent demonstrations have focused on via-first metallization processes in glass. Sputtering

titanium or chromium, which are known to form chemical bonds to glass, followed by the desired metal which does not adhere strongly to glass directly is a well-known method of depositing metals onto glass [9-14]. Due to the line-of-sight nature of sputtering, depositing metal onto the TPV sidewalls which are parallel to the flux of sputtering is not as straightforward as the planar surface which is perpendicular to the flux of sputtering. It follows that there is an inherent upper limit to the aspect ratio of vias which can be metallized conformally by sputtering before the TPV centers are unable to receive sufficient sputtering flux.

This section describes a novel process which utilizes a thin, patternable polymer film as an intermediate layer between glass and electroless copper. The reduced polymer thickness facilitates the patterning process to re-expose the glass vias. Finally, a copper seed layer is deposited by electroless metallization, making the substrate ready for semi-additive processing. The methodology of each processing step is described, and a fully fabricated two metal layer structure is proven to be thermo-mechanically reliable after thermal cycle testing to 1000 cycles and highly-accelerated-stress-testing (HAST) for 96 hours.

The basic process flow for the via-first metallization process is shown in Figure 3.5. TPVs are initially formed in a glass panel. Then, a thin polymer film is laminated on both sides of the substrate, covering the vias. Next, the polymer areas over the vias are patterned to open the vias. Details of each processing step are described in the following sub-sections.

Glass substrates were prepared as follows. Low CTE (~3 ppm/K) glass substrates of 100 μm and 130 μm thickness were used (EN-A1 from Asahi Glass Co. and SGW3 from Corning Inc.). Substrates were panels 76.2 mm x 76.2 mm or larger in size. For daisy chain

resistance structures, glass through-vias with 60 µm entrance diameter and 120 µm pitch were formed into arrays by the glass supplier. Glass substrates were cleaned with acetone and isopropyl alcohol, followed by an O_2 plasma clean. Finally, a silanization step was done to promote chemical adhesion between the polymer and glass [5].

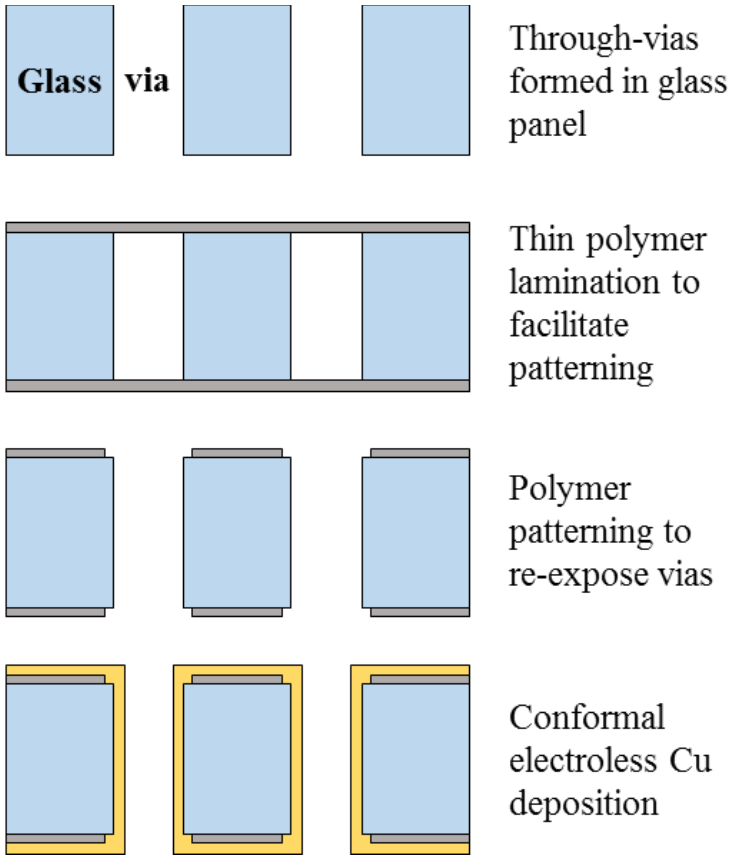

Figure 3.5. Schematic process flow of metallizing glass interposers by a via-first process.

3.2.1. Polymer Preparation and Lamination

In this process, the laminated polymer film will ideally "tent" over the vias; i.e., the film lies over without flowing inside the vias. However, polymers are expected to flow with decreased viscosity at the elevated temperatures during the curing process. Polymer

flow into the vias will increase the thickness of polymer in the TPV region, making it difficult for subsequent etch patterning. Steps were taken to partially pre-cure the polymer film prior to lamination in order to reduce the viscosity of the curing polymer and therefore the degree of flowing into the vias.

An epoxy-based polymer film of 5 μm thickness was chosen as the dry film polymer due to its excellent dielectric properties and known compatibility with electroless copper plating. Normally stored at -40 °C, the polymer films were exposed to elevated temperatures for extended periods of time, and Fourier transform infrared spectroscopy (FTIR) was used to qualitatively observe the degree of pre-curing in the epoxy-based films prior to lamination. The uncured film is composed of an epoxy resin and phenol-based hardener. During the curing process, they are exposed to elevated temperatures and react to form a cross-linked polymer network (Figure 3.6(a)). The degree of curing can therefore be qualitatively observed by the reduction in absorption intensity of the uncured epoxy group at 912 cm^{-1} [52]. The FTIR absorbance spectrum of the polymer film after three different curing conditions is shown in Figure 3.6(b) and the corresponding cross sections after lamination are shown in Figure 3.7. The fully cured film was prepared by heating at 180°C for 30 min and produced the lowest absorption intensity, as expected. In contrast, the uncured film produced the highest absorption intensity, and lamination onto the glass resulted in a significant amount of polymer flow into the TPVs, leaving an air-filled void, as shown in Figure 3.7(a). The film was then kept at room temperature for 12 hours prior to lamination. A slightly diminished absorption intensity was observed compared to the uncured film, indicating that a small degree of pre-curing has occurred. The result was confirmed by observing the cross section of the laminated film, which shows a significantly

reduced volume of polymer flow into the TPV after lamination (Figure 3.7(b)) compared to the case with no pre-curing. Finally, the polymer was kept at room temperature for 12 hours followed by heating at 100 °C for 20 min. The epoxide absorption intensity was further reduced and the cross section after lamination shows that with sufficient pre-curing the polymer can completely tent the TPVs (Figure 3.7(c)). This tented structure is ideal for subsequent polymer patterning to re-expose the TPVs.

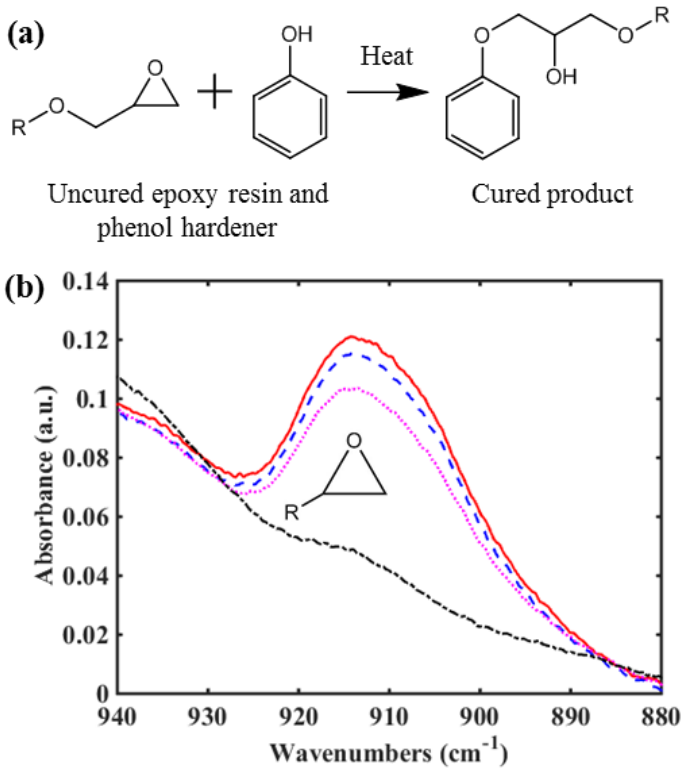

Figure 3.6. (a) Reaction of uncured epoxy resin and phenol-based hardener during polymer curing. (b) FTIR absorption spectra showing epoxy peak after various amounts of polymer curing: (—) uncured; (- -) pre-cured at room temperature for 12 h; (·····) pre-cured at room temperature for 12 h followed by 100 °C for 20 min; (---) fully cured at 180 °C for 30 min.

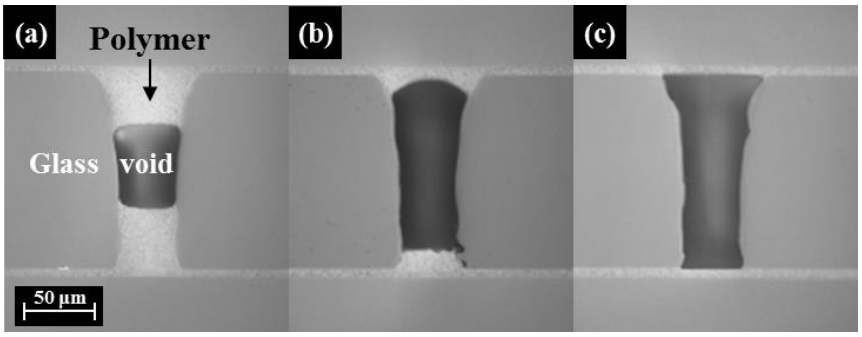

Figure 3.7. Optical micrographs of cross sections after lamination with various degrees of polymer pre-curing. (a) With no pre-curing, significant flow of polymer into vias is observed. (b) After a low amount of pre-curing, polymer flow is reduced but still apparent. (c) With sufficient pre-curing, polymer flow is prevented and tenting is achieved.

3.2.2. Polymer Patterning

There are many methods of etch patterning thin polymer films. This study investigates plasma etching and laser ablation as they are scalable and widely adopted technologies in panel-size microelectronics fabrication.

Plasma etching requires an etch mask to differentiate the polymer regions over the vias from the regions over blank glass. Dry film photoresist with a thickness greater than the underlying polymer film was used as the etch mask. After lamination onto the polymer-tented glass substrate, the photoresist was exposed and developed to expose the tenting polymer regions over the vias. An RF plasma (400 W power) of O_2 and CF_4 gas (1:1 mixture) at 100 °C was used to etch the exposed polymer over a duration of about 15 min. Finally, the photoresist was stripped. Figure 3.8(a) shows a top-down view after patterning by plasma etching, and it is apparent that the glass vias have been fully exposed.

Two different lasers were used to directly pattern the laminated polymer films. One was a CO_2 laser ($\lambda = 10.6$ µm) with a maximum output of 80 W, which used ten pulses at about 20% power. The second was a UV laser ($\lambda = 266$ nm), which only required one pulse

at 90% power. Top-down micrographs of polymer-tented glass substrates patterned by CO_2 and UV lasers can be seen in Figure 3.8(b) and (c), respectively.

The results from each patterning technique are comparable. In all cases, the etched polymer region has a diameter of about 80 μm, and a small (~5 μm) ring of bare glass is left exposed around the glass TPVs. Of these technologies, laser ablation is a relatively simpler process as it does not require additional steps for lithography. However, laser ablation has the potential to induce unwanted modification to the underlying glass and has a lower theoretical throughput compared to plasma etching, which is a planar process. This metallization process is not limited to these examples. Any polymer patterning method can be used provided it results in fully opened vias and that the polymer provides strong interfacial adhesion to subsequent electroless metallization and meets the necessary dielectric requirements.

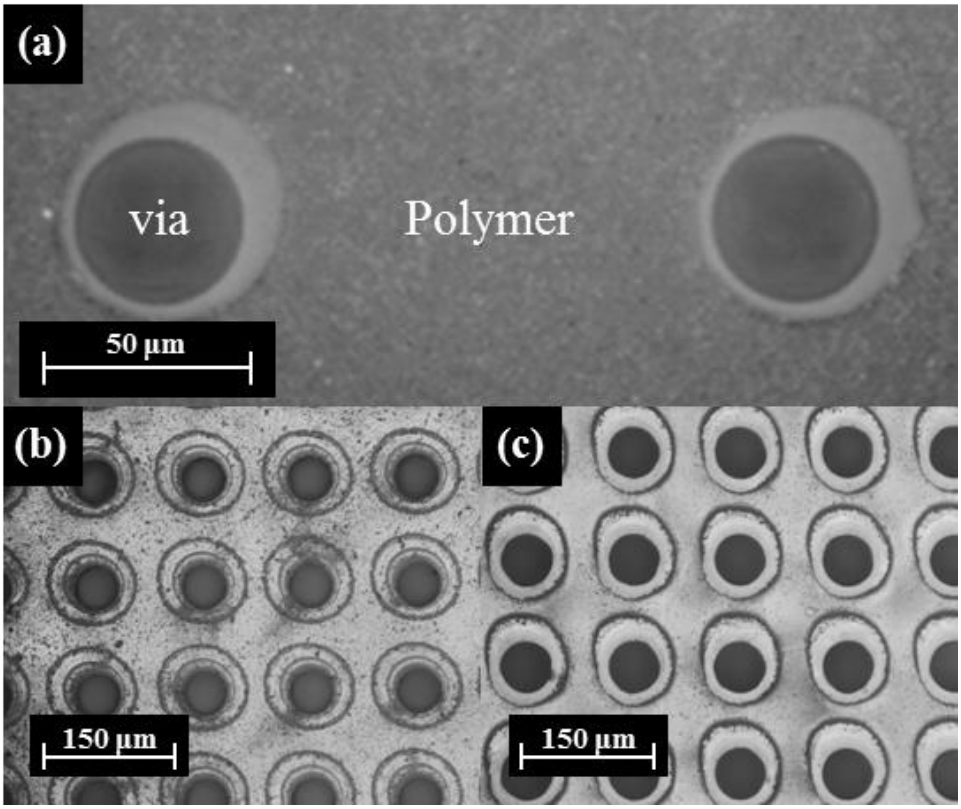

Figure 3.8. Top-down optical micrographs of vias after polymer material was patterned by (a) plasma etching, (b) CO_2, and (c) UV laser ablation.

3.2.3. Cu Metallization

After polymer films were patterned, about 350 nm of copper was conformally deposited using a commercial electroless plating bath (Atotech Inc.). Electroless copper deposition resulted in continuous, conformal coverage on the polymer-laminated surface and on the sidewalls of the glass vias. After electroless plating, copper daisy chains were fabricated by semi-additive processing with a final copper thickness of about 20 µm and annealed at 160 °C for 1 hour. For this study, the vias were conformally plated by electrolytic Cu deposition. Compared to fully-filled vias, conformal plating provides comparable electrical performance in RF and millimeter-wave applications due to the skin effect [53] while reducing processing costs.

The fabricated daisy chains were observed to be free of any apparent blisters, delamination, or other metallization defects on the surface (Figure 3.9). Cross sections of the conformal-plated daisy chains were prepared to assess the metallization coverage at each interface. As seen in Figure 3.10, about 20 μm of copper was deposited after electrolytic plating without any observable defects at the copper/glass or copper/polymer interfaces.

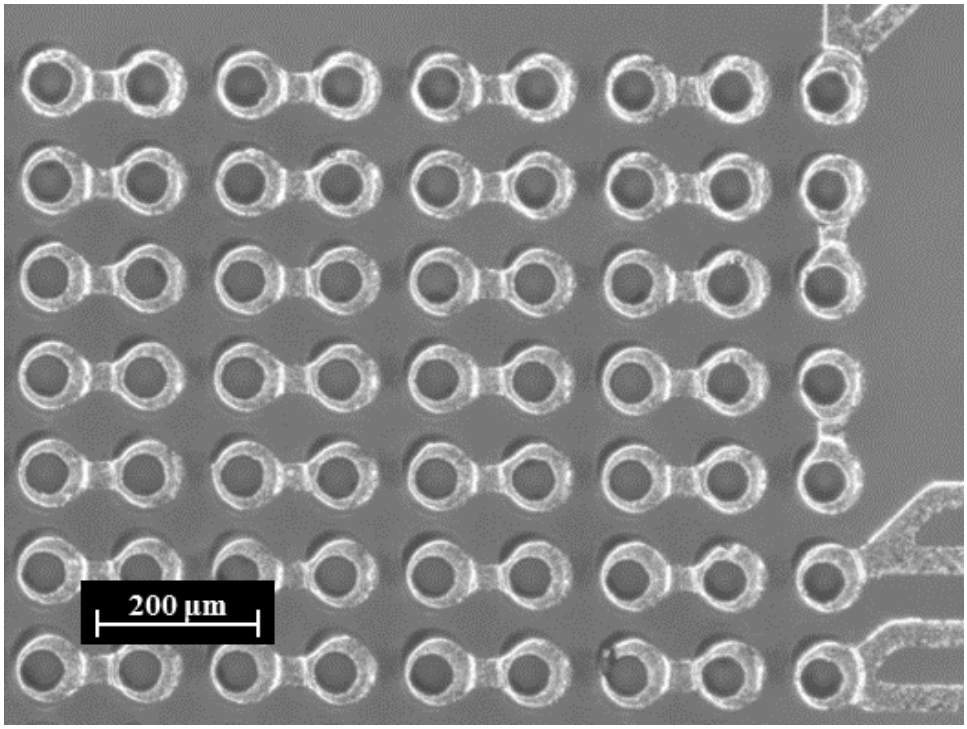

Figure 3.9. Top-down optical micrograph of fabricated daisy chain structures after semi-additive processing.

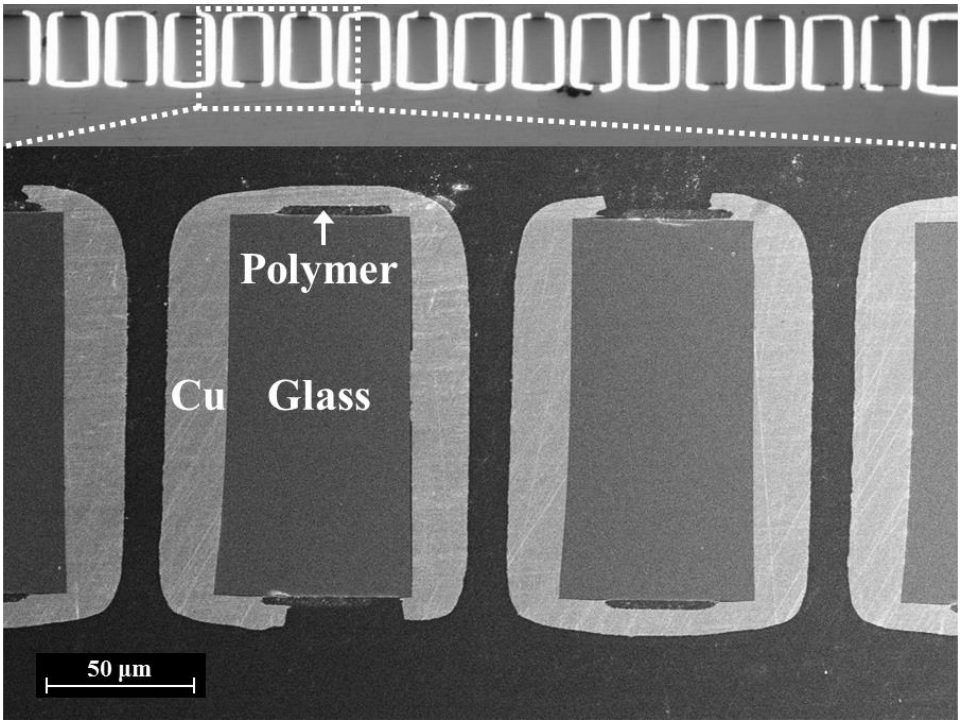

Figure 3.10. Top: optical micrograph of a daisy chain cross section after completed fabrication. Bottom: scanning electron micrograph showing continuous and void-free copper metallization of vias in glass.

3.2.4. Reliability Testing – HAST and Peel Testing

Copper peel testing was performed to determine if the copper adhesion to the polymer film was negatively impacted by introducing the pre-curing step compared to the standard polymer lamination and curing procedure. Substrates were prepared with and without tenting lamination conditions, followed by electroless copper deposition and electrolytic plating to a final thickness of 25 µm. In HAST, the polymer absorbs moisture which migrates to the Cu-polymer interface where Cu oxidation is induced. The formation of CuO and Cu_2O creates a weak interface with the bulk metallic Cu and leads to reduced adhesion strength [54]. To investigate the effect of modifying the dielectric processing conditions on Cu adhesion, peel tests were conducted at an angle of 90° before and after 24, 48, and

96 hours of unbiased HAST performed according to JEDEC Standard JESD22-A118 Condition A, having a temperature of 130 °C and a relative humidity of 85%.

The peel strength results are shown in Figure 3.11. As expected, the peel strength decreased in both cases with increased exposure to HAST conditions. After 48 hours of exposure, the peel strength ceased to decrease and remained constant. At all times, however, the difference in peel strength between samples with and without tenting conditions was within the measured deviation. Since the failure for all samples was at the interface between copper and polymer, this suggests that changes in the lamination conditions had a negligible effect on the mechanism of mechanical failure at the Cu-polymer interface. Adhesion between the copper and polymer is strongly determined by the roughness induced as part of the preparation for electroless plating. The modified pre-curing procedure of this polymer film therefore does not have a significant effect on the resulting Cu-polymer interfacial strength characteristics.

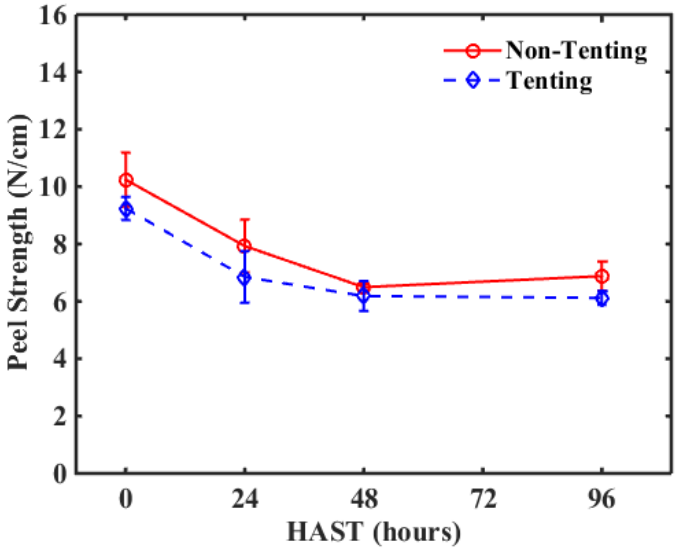

Figure 3.11. Comparison of 90° peel strength of copper on polymer laminated with tenting and non-tenting conditions. Error bars represent one standard deviation.

3.2.5. Reliability Testing – Thermal Cycle Testing

For daisy chain resistance and thermal cycle testing, structures consisting of Kelvin resistance structures were designed with eight different lengths ranging from 2 to 66 vias in the 16 x 16 array of vias as depicted in Figure 3.12. Daisy chain resistances were measured before and throughout 1000 thermal cycles using the standard four-point method of driving a 50 mA current source from one end of the chain to the other and sensing the voltage drop using a multi-meter (Keithley Instruments). Thermal cycle testing was performed according to JEDEC Standard JESD22-A104D Condition B, having a maximum and minimum temperature of 125 °C and -55 °C, respectively. A soak time of 15 min was used at the maximum and minimum temperatures.

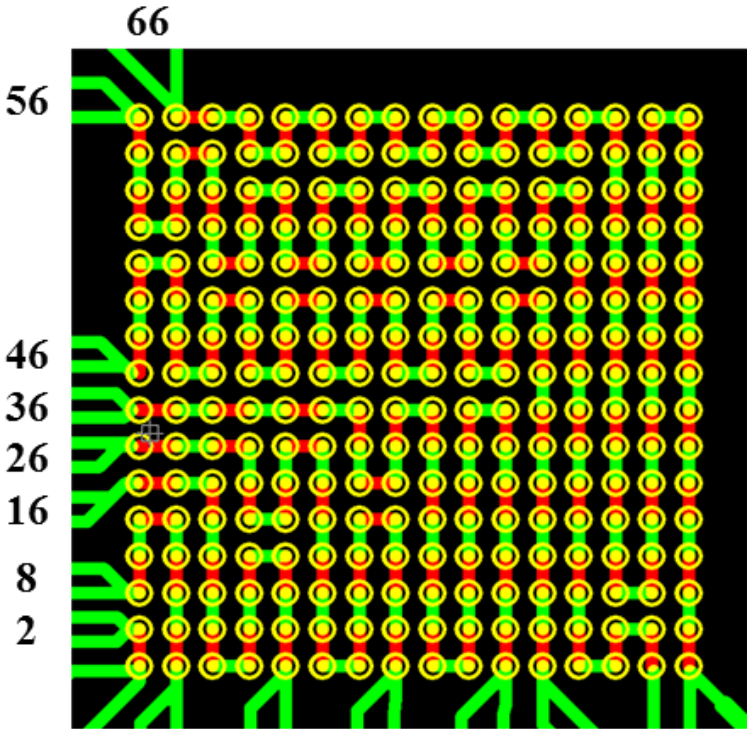

Figure 3.12. Design of daisy chain structures. The number of vias in each daisy chain is labeled near the traces for the respective daisy chain. Green and red lines represent copper traces on the top and bottom sides of the glass, respectively, and the yellow rings represent the glass vias.

The initial resistances for one set of daisy chains are shown in Figure 3.13. A least-squares linear fit set with a y-intercept of zero yielded a slope corresponding to a resistance of 10.0 mOhms per via and a correlation coefficient of 0.9922. As expected, the data correlates well with the linear fit since the total resistance is determined by the length of the copper daisy chain and is directly proportional to the number of vias in the chain. The daisy chain resistance was then monitored after 250, 500, and 1000 thermal cycles (Figure 3.14). The standard deviation in the resistance amongst daisy chains of the same length was less than 10%. However, the largest change in resistance for any daisy chain with a length of 66 vias was only 1.18% after 1000 thermal cycles. The deviation in resistance amongst daisy chains of the same length is attributed to variations in electrolytic plated copper thickness from sample to sample. Therefore, the change in resistance was negligible for any individual daisy chain.

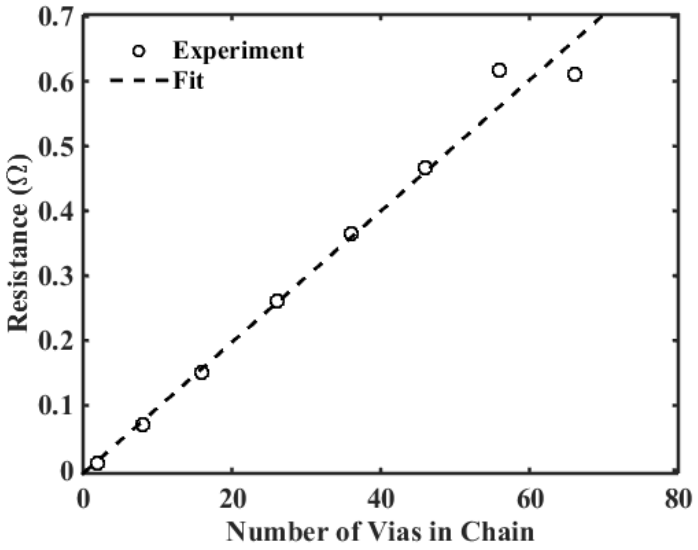

Figure 3.13. Initial resistance of eight daisy chains from one 16 x 16 array of vias.

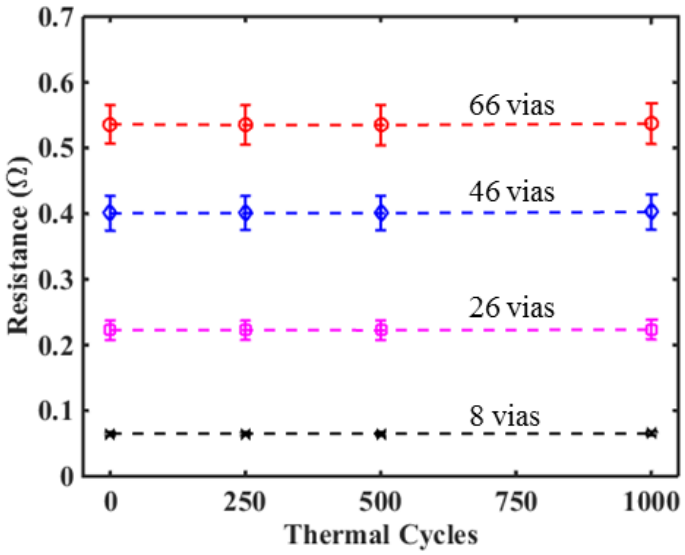

Figure 3.14. Daisy chain resistance measured throughout thermal cycle testing. Four of eight measured daisy chain lengths are shown for simplicity. Error bars represent one standard deviation.

No copper delamination was observed by optical inspection of the surface and in the vias after cross sectioning. This process involves the plating of copper directly on the glass via sidewall without a polymer adhesion layer. On the smooth glass surface (R_a < 1 nm), copper is mechanically anchored to the rough polymer film. At the via sidewall interface, the necessary adhesion between copper and bare glass is attributed to mechanical anchoring of copper to the micro and nano-roughened via sidewall which results from glass via formation processing [19, 55, 56]. A previous study showed that a sub-micro roughened glass surface was sufficient to pass a tape test after electroless copper deposition [57]. As expected, the robustness of the Cu/polymer/glass structure was validated and is consistent with previous studies using a similar structure, despite not having a polymer coating on the via sidewalls.

3.2.6. Process Applications and Dimensional Scalability

The via-first process demonstrated is not limited to any specific polymer materials and processing techniques. In general, any polymer film that is compatible with electroless metal deposition can be used in conjunction with an appropriate patterning process. For example, a photo-sensitive polymer film may be used for direct patterning instead of laser ablation. Depending on the needs of specific applications, the most suitable materials and processes can be chosen accordingly.

Finer via pitch is desirable in digital high-performance applications such as 2.5D and 3D IC. A preliminary test was done to assess the capability of the via-first process to metallize glass with small diameter and fine-pitch vias. Glass substrates were obtained having 100 μm thickness and vias with an entrance and exit diameter of 20 and 10 μm, respectively, and 40 μm pitch. The previously described processes were successfully completed, and a cross section of the metallized glass with daisy chain structures is shown in Figure 3.15. The copper coverage is uniform along the polymer-lined surface and the sidewalls of the glass vias. In this case, the via aspect ratio was as high as 10. The aspect ratio, higher than what is readily achievable by sputtering, is limited only by the practical limits of electroless and electrolytic copper deposition. The smallest diameter and finest achievable pitch depends on the polymer patterning capability because the amount of excess polymer etched around the glass vias will limit the amount of polymer coverage between adjacent vias. Fine pitch metallization requires the diameter of the etched polymer region to be as close as possible to that of the underlying glass via.

The ability to scale to fine pitch is not only desirable in digital high-performance applications. Closely packed vias can be used to design impedance-matched high speed

signals from chip to board [58], with via guard wall acting as electromagnetic interference (EMI) shield to protect the adjacent signals from cross-talk [59]. The high speed and EMI shielded signals are crucial for radio frequency, millimeter wave, and optoelectronic applications [2]. Closely packed power and ground vias can also mitigate the power handling concerns of conformal filled vias to ensure power that integrity is met.

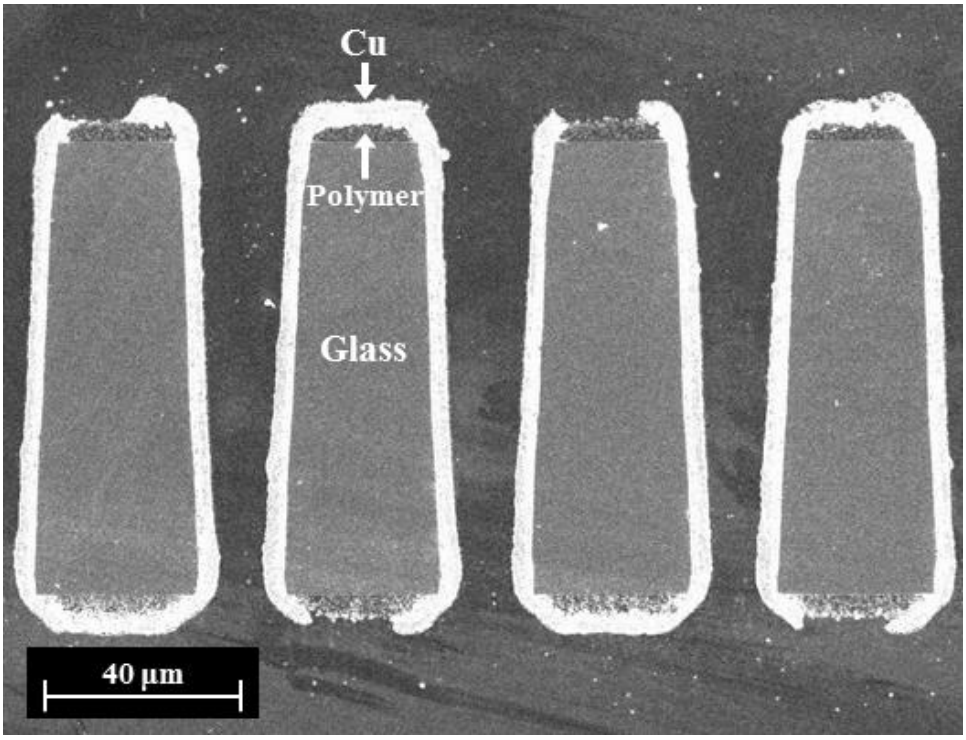

Figure 3.15. Scanning electron micrograph of cross section showing glass of 100 µm thickness with vias of diameter 20 µm and 40 µm pitch after polymer lamination, polymer patterning, electroless copper deposition, and semi-additive processing.

3.3 Summary

Several methods of Cu to glass metallization were investigated. The feasibility of roughness-based adhesion of glass substrates to electroless deposited Cu and sputtered Cu was determined by tape testing, peel testing, and interfacial failure analysis. Tape test

results after electroless Cu showed that a surface average roughness on the order of several hundred nanometers is necessary to pass the tape test. Interfacial failure analysis performed by XPS on failed tape test samples suggested that the weak interface between Cu and glass is determined by the weak adhesion of glass to the Pd catalyst nanoparticles used in electroless Cu deposition. In contrast, sputtered Cu with a sputtered Ti adhesion layer passed the tape test for all roughness values, including smooth, unroughened glass. Additionally, the sputtered Cu seed layer with electrolytic plating exhibited satisfactory peel strength to smooth glass, and exemplary peel strength to all roughened glass. However, roughening glass substrates is undesirable due to reduced electrical performance and the requirement for additional glass processing. While PVD methods such as sputtering create strong interfacial bonds between glass and Cu, the line-of-sight nature prevents ideal metallization of high aspect ratio vias in glass.

A novel, via-first method for electroless Cu deposition to glass using an intermediate polymer adhesion layer was developed to address the challenges mentioned above. Glass substrates containing through-vias are laminated by a thin polymer film which serves as an intermediate adhesion layer between the glass and electroless Cu. The lamination process was optimized to tent over the vias. Then, the through-vias are re-exposed by one of several methods before being conformally coated with electroless Cu seed layer. Reliability test structures were patterned by semi-additive processing and showed the structure to be stable after 1000 thermal cycles. Finally, the dimensional scalability of the process was demonstrated by metallizing ultra-fine pitch (40 μm), small diameter (20 μm) vias in 100 μm thick glass substrates.

CHAPTER 4

ELECTROCHEMICAL CHARACTERIZATION OF ORGANIC ADDITIVES IN ELECTROLYTIC COPPER PLATING BATHS

Fully-filled Cu blind-vias are typically fabricated by depositing a thin, conformal Cu seed layer followed by electrolytic Cu plating in an aqueous electrolyte comprised of an acid, Cu salt, and organic additives. The organic additives are crucial for modifying the Cu^{2+} reduction rate in a way that achieves "bottom-up filling" or "superfilling" in vias, where Cu plating is promoted inside the vias while inhibiting plating on the surface regions outside the vias [28]. The effect of a given additive on the Cu^{2+} reduction kinetics, and therefore the via filling profile, depends on where the additive molecules adsorb relative to the via geometry, its interaction with the Cu cathode surface, and other additives in the electrolyte. Akolkar and Moffat studied the interactions between common accelerator and suppressor additives and proposed a widely-accepted model of superfilling, where differences in additive transport kinetics determine the additive distribution inside the vias [30, 60]. Various aspects of the widely used polyethylene glycol (PEG) suppressor additive have been studied, such as the effect of molecular weight and its interaction with chloride ion at the Cu cathode [32, 33, 35, 46]. Similarly, several leveler additives have been investigated on an individual basis with the goal of determining the effects of molecular weight and concentration on Cu plating behavior [38, 44, 45]. Common suppressor and leveler additives have been categorized as "synergistic" and "antagonistic", depending on their effect on the Cu^{2+} reduction potential when combined with accelerator additives [34].

While many additives have been investigated and some combinations are known to promote superfilling behavior in certain blind-via geometries, there remains a limited understanding of the mechanisms by which various combinations of additives interact with the Cu cathode surface, and how these interactions ultimately affect Cu via filling performance. This chapter aims to develop an understanding of how additives interact with the Cu electrode and with each other through systematic combinations of additives observed by cyclic voltammetry and injection chronopotentiometry.

4.1 Electrochemical Characterization Details

This section contains details regarding the organic additives used for this study and the experimental conditions for electrochemical characterization.

4.1.1. Organic Additives Chosen for Study

A virgin makeup solution (VMS) was prepared as an additive-free base electrolyte. The VMS bath was comprised of $CuSO_4$ (50 g/l), H_2SO_4 (100 g/l), and Cl^- ion (70 ppm). $CuSO_4$ was added in the form of $CuSO_4{\cdot}5(H_2O)$ (78 g/l), and Cl^- was supplied by NaCl (115 ppm). Bis(sodium sulfopropyl) disulfide (SPS) was used as the accelerator additive. Suppressor additives chosen for investigation were polyethylene glycol (PEG) (M_n = 3,350 g/mol) and polypropylene glycol (PPG) (M_n = 1,000 g/mol). Polyvinylpyrrolidone (PVP) (M_w = 55,000 g/mol) was used as the leveler. Additive concentrations were 10 ppm SPS, 300 ppm PEG or PPG, and 10 ppm PVP unless otherwise stated. A summary of materials used is listed in Table 4, and the molecular structures of additives are illustrated in Figure 4.1.

Table 4. Virgin makeup solution (VMS) and organic additives used for study.

Component	Chemical	Concentration and Mw
VMS	$CuSO_4 \cdot 5(H_2O)$	50 g/l ($CuSO_4$)
	H_2SO_4	100 g/l (H_2SO_4)
	NaCl	70 ppm (Cl^-)
Accelerator	Bis(sodium sulfopropyl) disulfide (SPS)	10-100 ppm
Suppressor	Polyethylene glycol (PEG)	100-500 ppm Mn ~3350 g/mol
	Polypropylene glycol (PPG)	100-500 ppm Mn ~1000 g/mol
Leveler	Polyvinyl pyrrolidone (PVP)	5-25 ppm Mw ~55000 g/mol

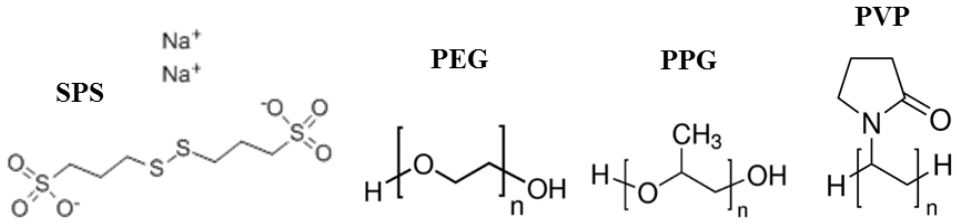

Figure 4.1. Molecular structures of additives used for study.

4.1.2. Electrochemical Cell and Experimental Details

Electroanalytical characterization was performed using a Pt rotating disc electrode (RDE) with a 0.4 cm diameter. The rotation speed of the RDE was kept at 200 rpm. A high-purity Cu sheet was used as the counter electrode. About 200 nm of Cu was deposited by electrolytic plating in VMS prior to each measurement. All reported potentials are with

reference to a $Hg/Hg_2SO_4/K_2SO_4$ (sat.) electrode. The electrodes were mounted with fixed positions in a 100 ml PTFE beaker.

Cyclic voltammetry was performed using a CH Instruments 600C Electrochemical Analyzer. The potential was swept from the open circuit potential to -1.0 V and back at a rate of 10 mV/sec while monitoring the current between the counter and working electrode (Figure 4.2(a)).

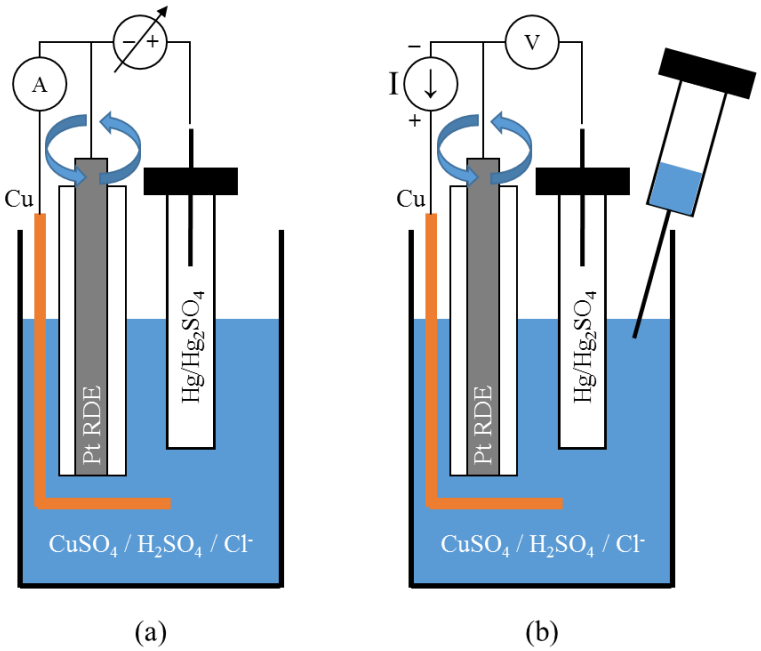

Figure 4.2. Diagram of electrochemical cells used for (a) cyclic voltammetry and (b) injection chronopotentiometry.

For injection chronopotentiometry, the potential between the reference and working electrodes was measured as additives were injected with a syringe containing the desired additives in VMS during plating on the Pt RDE (Figure 4.2(b)). The rotation rate was fixed

at 200 rpm and the current density was fixed at 20.9 mA/cm^2. The response time of injection was less than one second.

4.2 Cyclic Voltammetry

This section contains results which investigate the impact of organic additives on current-potential response during electrolytic Cu plating. The results are organized by different combinations of organic additive classes.

4.2.1. Suppressor and Accelerator

The electrochemical characterization of VMS with suppressor only was first studied before investigating the behavior of additive combinations. The effect of PEG concentration on the current-potential response was investigated, and the results are shown in Figure 4.3. The open circuit potential was roughly -0.37 V, and for all concentrations of PEG, the plating current was suppressed to around -0.65 V (Figure 4.3(a)). Beyond this potential, the rate of current rise during the forward (negative) potential scan decreased as the PEG concentration was increased from 100-200 ppm. The linear sweep voltammograms (LSV) are indistinguishable from 200-500 ppm of PEG, showing that the effect of PEG concentration was saturated after a particular concentration. Figure 4.3(b) shows the entirety of the forward and reserve scans of cyclic voltammetry, illustrated over time for clarity. PEG showed similar behavior during the forward and reverse scans.

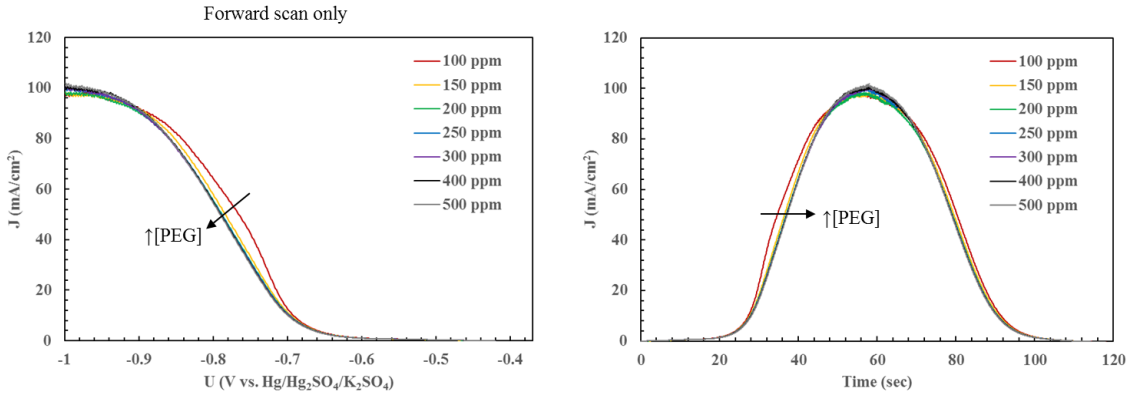

Figure 4.3. (a) Linear sweep voltammogram showing effect of PEG concentration on current-potential response during forward (negative) potential scan. (b) Current response during the forward and reverse potential scans.

Figure 4.4 shows the electrochemical response of PPG with the same range of concentrations. In the forward scan, all concentrations of PPG effectively suppressed plating current to around -0.65 V, which was similar to that of PEG. However, the behavior beyond this potential was strongly dependent on the concentration of PPG. In the 100-250 ppm range, the current was reduced for potentials between -0.65 V and -0.85 V before reaching a maximum current density around 100 mA/cm^2 (Figure 4.4(a)). Beyond -0.85 V shows that PPG concentrations greater than 300 ppm showed an increase in the maximum current density with PPG concentration. The current response during the forward and reserve potential scans is shown in Figure 4.4(b). Given the known mechanisms of polyalkylene glycol (PAG) suppression, it is unexpected for the current density to rise with PAG concentration. The significant increase in current beyond -0.85 V may be an indicator of a non-faradaic process which occurs with an "excess" amount of PPG beyond 300 ppm. Further studies are required to elucidate the mechanism of this behavior.

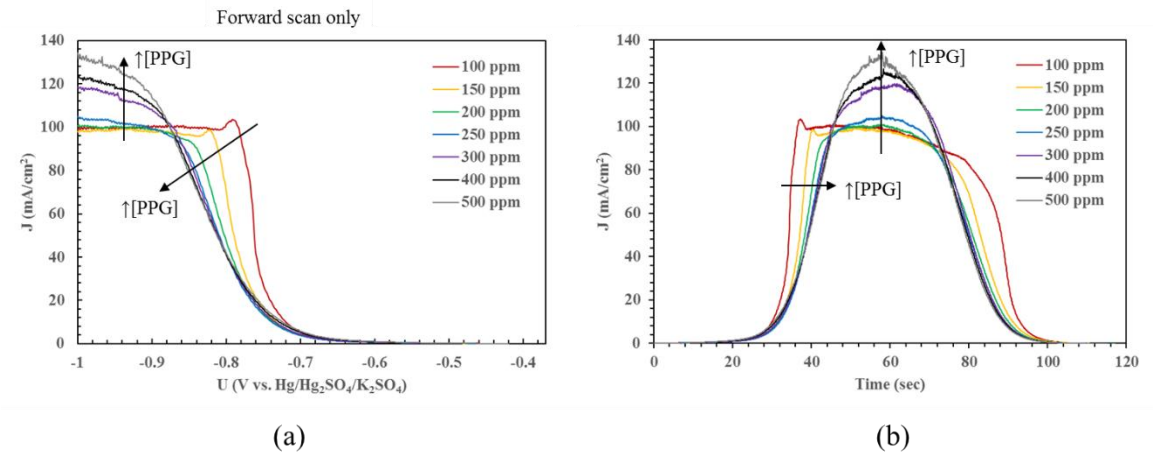

Figure 4.4. (a) Linear sweep voltammogram showing effect of PPG concentration on current-potential response during forward (negative) potential scan. (b) Current response during the forward and reverse potential scans.

Based on the above results, 300 ppm was chosen as the concentration of PAG-type suppressors. Cyclic voltammograms of VMS with PAG-based suppressors only are shown in Figure 4.5. In the forward potential scan, the PEG solution shows strong suppression to roughly -0.60 V before beginning a steady increase in current density. PPG shows suppression to a more negative potential, around -0.70 V, before the current density rises at a higher rate than PEG. While the voltammogram of PEG has minimal hysteresis between the forward and reverse potential scans, there is a larger hysteresis produced by PPG. A maximum current density of about 95 mA/cm^2 was observed for both PAG-type suppressors at -1.0 V.

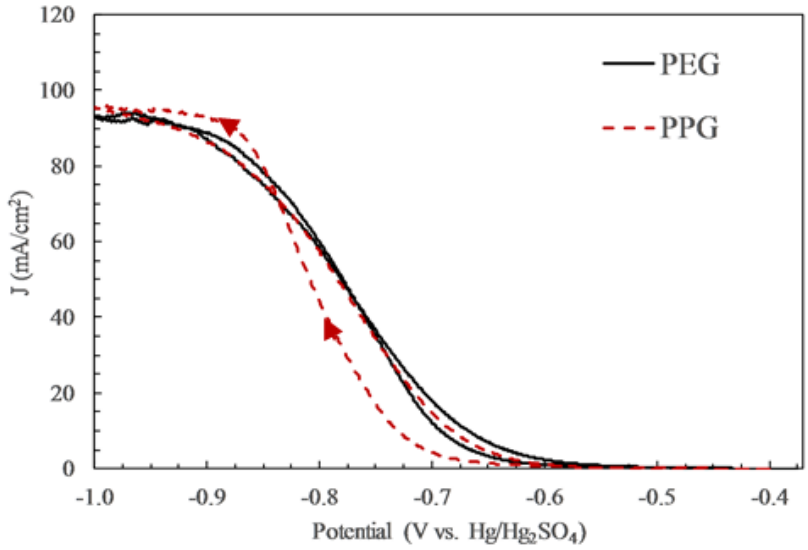

Figure 4.5. Cyclic voltammograms of VMS with PEG (300 ppm) and PPG (300 ppm).

Combinations of SPS accelerator and each of the PAG-type suppressors were prepared, and their cyclic voltammograms are shown in Figure 4.6. The addition of SPS to all PAG-type suppressors resulted in a large hysteresis between the forward and reverse potential scans. This is expected due to the time-dependent interactions between SPS and PAG-type molecules with the Cu electrode [31]. PEG+SPS showed a positive shift in the threshold of suppressed current compared to only PEG, from -0.60 V to -0.55 V, respectively. In contrast, PPG shows little change in its potential range of suppressed current density. At potentials lower than -0.68 V in the forward scan, PPG shows a faster rise in current density compared to PEG, and both PAG-type suppressors with SPS showed a maximum current density of around 105 mA/cm^2. The size of hysteresis between the forward and reserve scans of PPG+SPS was larger than for PEG+SPS.

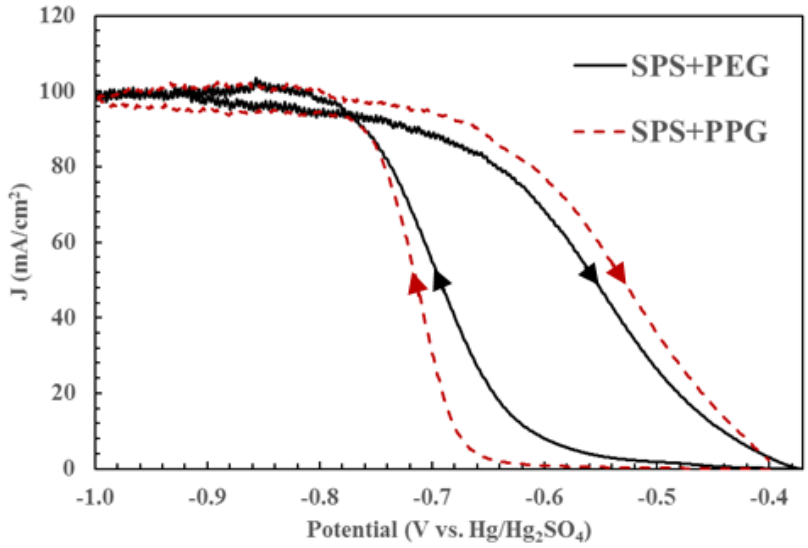

Figure 4.6. Cyclic voltammograms of VMS with SPS+PEG and SPS+PPG.

4.2.2. Leveler and Accelerator

Figure 4.7 shows the effect of PVP concentration (5-25 ppm) on the current-potential response. Similar to PEG, PVP showed a saturated behavior beyond a certain concentration. With a PVP concentration of 5 ppm, the current suppression threshold was very low (~ -0.55 V). A PVP concentration of 10 ppm or more showed suppression to roughly -0.70 V. Beyond -0.70 V, higher concentrations of PVP showed slightly reduced current from -0.70 V to -0.85 V. All concentrations of PVP resulted in a maximum current density of ~100 mA/cm^2.

For all concentrations of PVP, the current density was higher for a given potential during the reverse potential scan than in the forward potential scan (Figure 4.7(b)). Effectively, the suppressive effect of PVP was deactivated before and throughout the reverse potential scan.

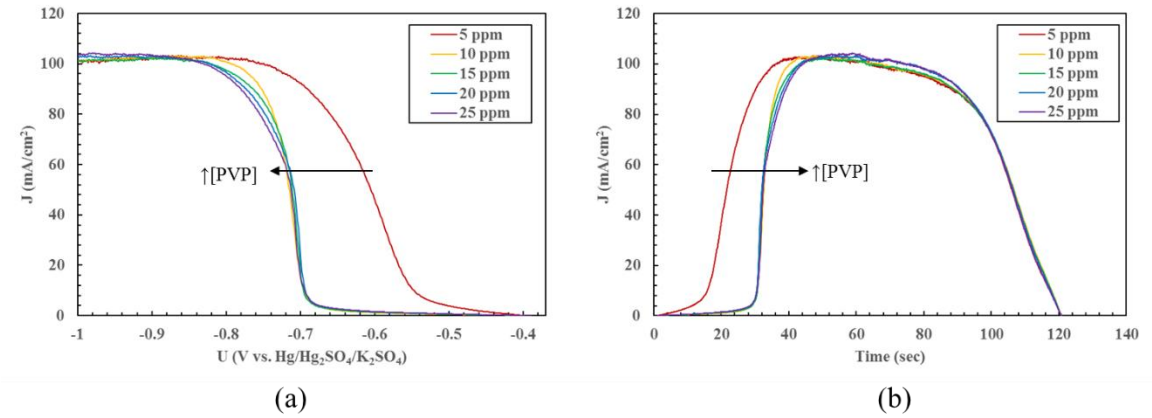

Figure 4.7. (a) Linear sweep voltammogram showing effect of PVP concentration on current-potential response during forward (negative) potential scan. (b) Current response during the forward and reverse potential scans.

Keeping the PVP concentration at 10 ppm, the suppressive reversibility was investigated by performing cyclic voltammetry with two cycles. Each cycle began at the open circuit potential (-0.37 V) and swept to low potential (ranged from -0.65 V to -0.90 V), and finally back to the open circuit potential. The results are shown in Figure 4.8. With the low potential of -0.65, -0.70, or -0.75 V, the cyclic voltammograms of the first and second cycles followed similar behavior. This indicates that the suppressive effects of PVP are reversible in this range. Beyond -0.80 V, the second cyclic voltammograms showed a significant loss in suppressive effectiveness during the forward scan. This result suggests that PVP undergoes an irreversible change in suppressive ability when subjected to potentials more negative than -.80 V vs. Hg/Hg_2SO_4. The mechanism for the reduced activity of PVP is elaborated in Section 4.4.

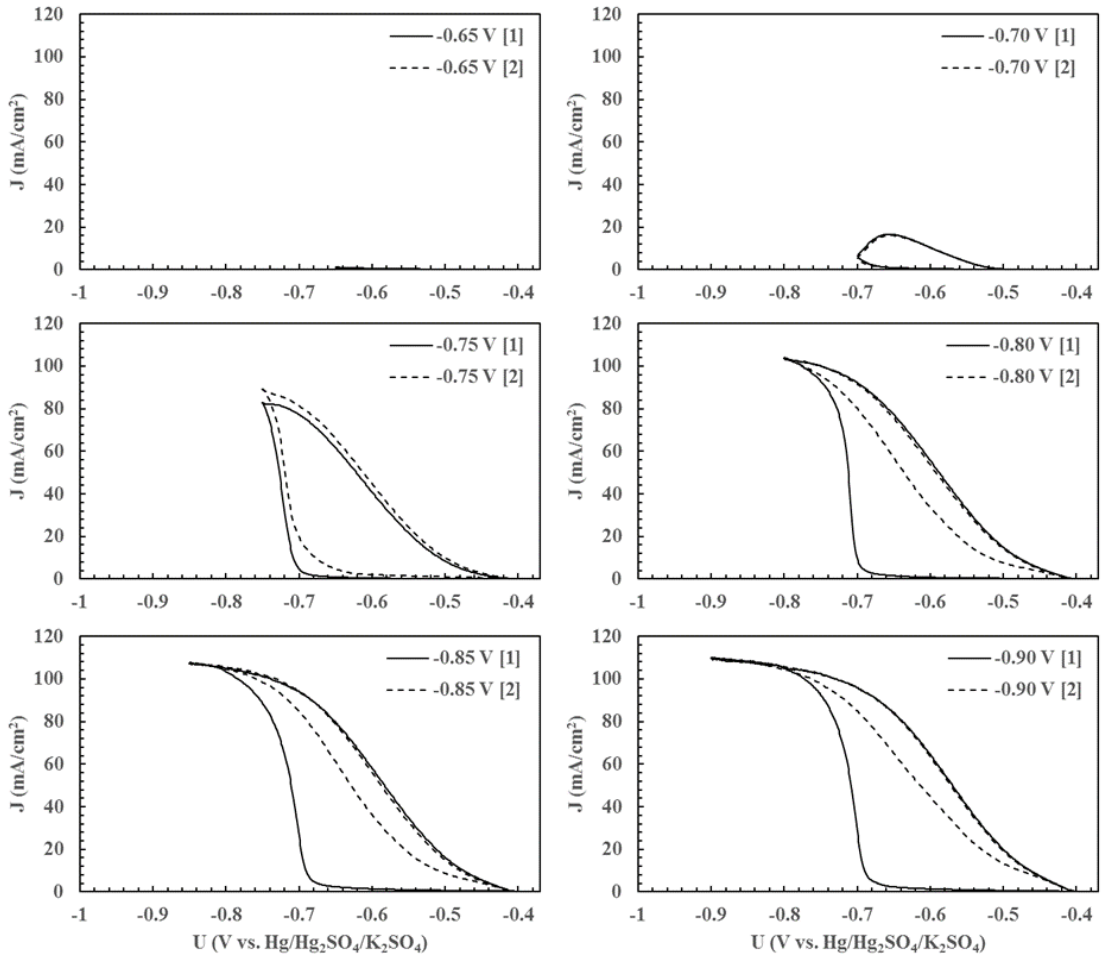

Figure 4.8. Potential dependence of negative potential on two cycle voltammetry of VMS with PVP (10 ppm). Continuous and dashed lines correspond to the first and second cycle, respectively.

The cyclic voltammogram of VMS with combinations of SPS (10 ppm) and PVP (10 ppm) are shown in Figure 4.9. As expected, the current response of only SPS shows an immediate increase in current at the beginning of the forward scan before reaching a maximum current density of 115 mA/cm^2. The solution with only PVP showed strong suppression to about -0.69 V followed by a sharp rise in current density, rising from 5 mA/cm^2 to 85 mA/cm^2 from -0.68 V to -0.72 V in the forward scan. The current density tapered around -0.80 V, reaching a maximum of 96 mA/cm^2. In contrast to the forward

scan, the current density decreased gradually in the reverse scan, resulting in a large hysteresis. The PVP+SPS solution shows similar behavior as the solution with only PVP. The addition of SPS resulted in a more positive potential of suppression threshold (around -0.65 V) and a slightly increased current density in the reverse scan from -0.65 V to -0.37 V.

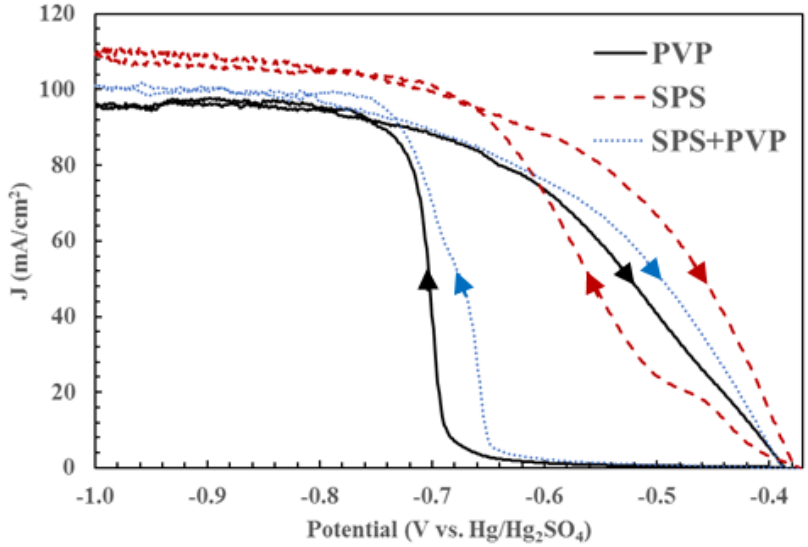

Figure 4.9. Cyclic voltammograms of VMS with PVP only (10 ppm), SPS only (10 ppm), and SPS+PVP (10 ppm each).

4.2.3. Suppressor, Leveler, and Accelerator

Figure 4.10 shows the cyclic voltammograms of solutions containing SPS, PVP, and each of the PAG-type suppressors. The behavior of is similar to the case of SPS+PAG, and the addition of PVP slightly reduced the size of hysteresis for both PAG-based suppressors. Again, the largest hysteresis was observed for the solution containing PPG. Despite the previously shown deactivation of PVP at potentials lower than -0.80 V, the addition of PVP managed to reduce the plating current in the reverse potential scan compared to SPS+PAG. This mechanism for this behavior is hypothesized in Section 4.4.

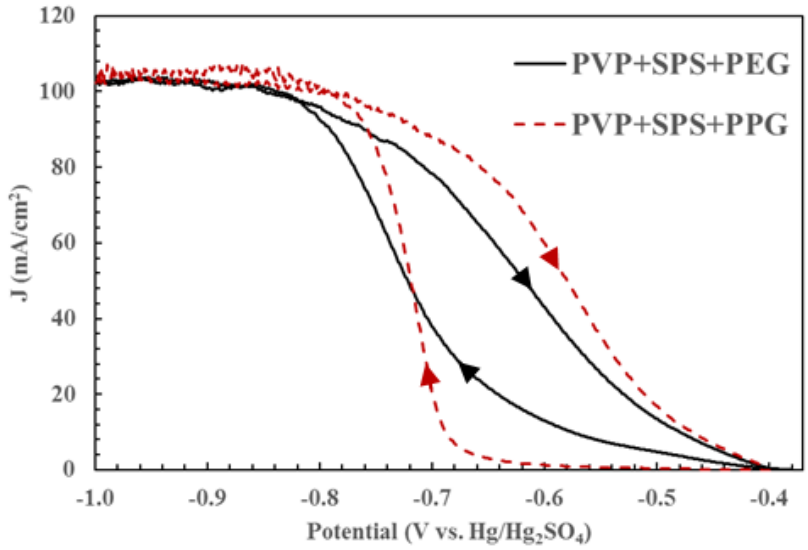

Figure 4.10. Cyclic voltammograms of VMS with PVP+SPS+PEG and PVP+SPS+PPG.

4.3 Injection Chronopotentiometry

This section contains results which investigate the impact of organic additives on potential-time response during galvanostatic Cu plating (20.9 mA/cm^2). The results are organized by different combinations of organic additive classes.

4.3.1. Accelerator

Figure 4.11 shows the potential-time response after injecting SPS with various concentrations into VMS. Higher concentrations of SPS showed both a higher degree of depolarization and a higher rate of depolarization. The depolarization for 10, 50, and 100 ppm increased from 3, 5.5, and 8 mV, respectively. Similarly, the time to depolarize was reduced, requiring roughly 80, 40, or 30 seconds for increased SPS concentration to reach maximum depolarization. This result suggests that the kinetics of SPS adsorption to the Cu electrode are primarily driven by bulk concentration effects.

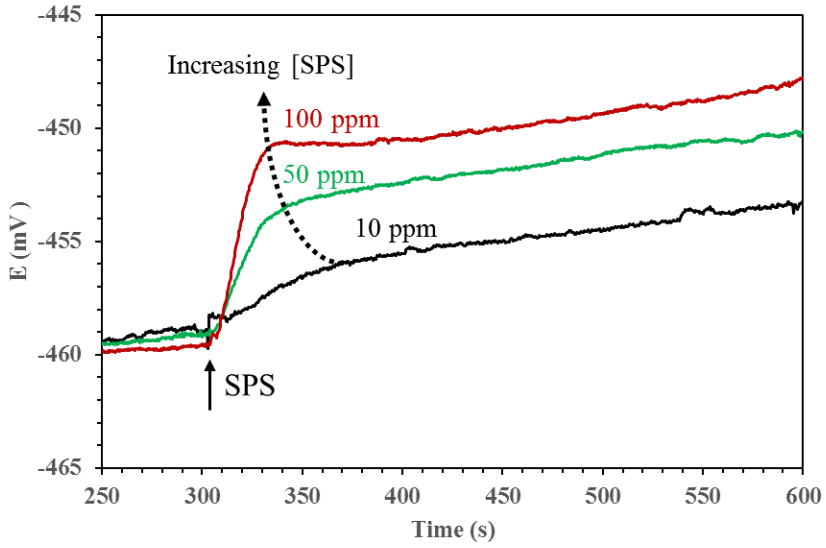

Figure 4.11. Potential-time response after injection of SPS with various concentrations.

4.3.2. Suppressor and Accelerator

Figure 4.12 shows the potential response of the Cu working electrode after injection of each of the PAG-type suppressors into VMS. Both PAG-type suppressors exhibited a fast (<1 second) polarization which was maintained for the duration of plating. The polarization due to PPG was about 40 mV weaker than that of PEG.

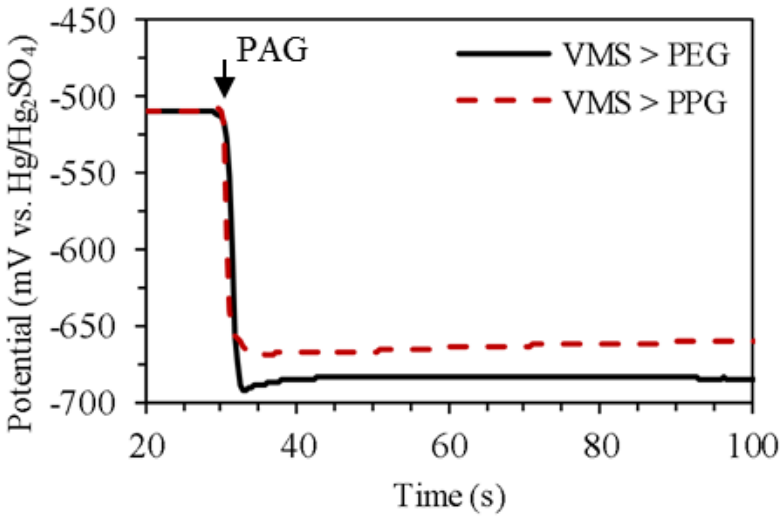

Figure 4.12. Potential-time response after injection of PEG and PPG into VMS.

The potential response of SPS combined with PAG-type suppressors was investigated by sequential and combined injection. By sequentially injecting each additive in a different order, the effect of Cu surface functionalization by one additive on the adsorption characteristics of the other additive can be investigated, while the case of competitive adsorption can be observed when injecting them simultaneously. Figure 4.13 shows the potential response of the following cases: 1) plating in VMS and PAG for 5 minutes followed by injection of SPS, 2) plating in VMS and SPS for 5 minutes followed by injection of PAG, and 3) plating in VMS for 5 minutes followed by injection of PAG+SPS.

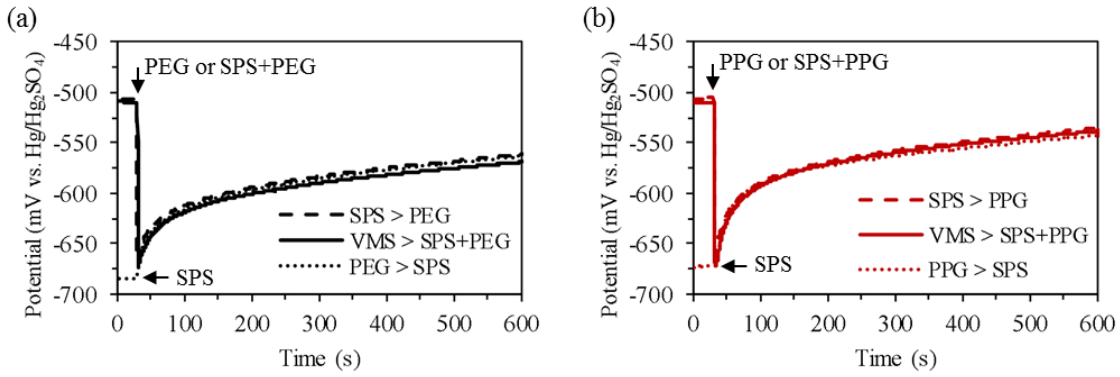

Figure 4.13. Potential-time response injecting different sequences of SPS and (a) PEG and (b) PPG.

In Case 1, addition of SPS of the PAG-modified electrode resulted in depolarization at an initially fast rate, which decreased after about 1 minute and continued at a slower, steady rate. Case 2 and 3 start with a fast (<1 second) polarization which was followed by a depolarization with nearly identical time-dependence as seen after the initial depolarization in Case 1. The solution of PPG+SPS showed greater depolarization compared to that of PEG+SPS (Figure 4.14).

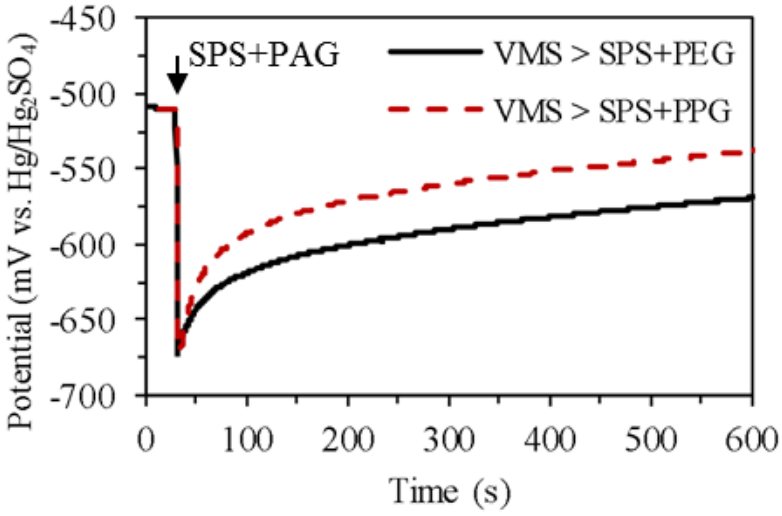

Figure 4.14. Comparison of potential-time response of combined injection of SPS+PEG and SPS+PPG.

The SPS/PAG interactions were further investigated by changing the SPS concentration. PEG (300 ppm) and PPG (300 ppm) were injected into solutions of VMS and SPS (10, 50, or 100 ppm), and the results are shown in Figure 4.15. For all concentrations of SPS, PPG showed significantly faster depolarization kinetics than PEG. Additionally, PPG showed weaker polarization in the initial stage of injection than PEG. The time for PPG to reach maximum polarization was also slightly slower than PEG. These observations strongly suggest that in the presence of SPS, the interaction between PPG and the Cu electrode is weaker than that between PEG and Cu. Both PEG and PPG showed faster depolarization with increasing concentration of SPS. This confirms that PAG adsorption is inhibited by Cu surfaces previously functionalized by SPS.

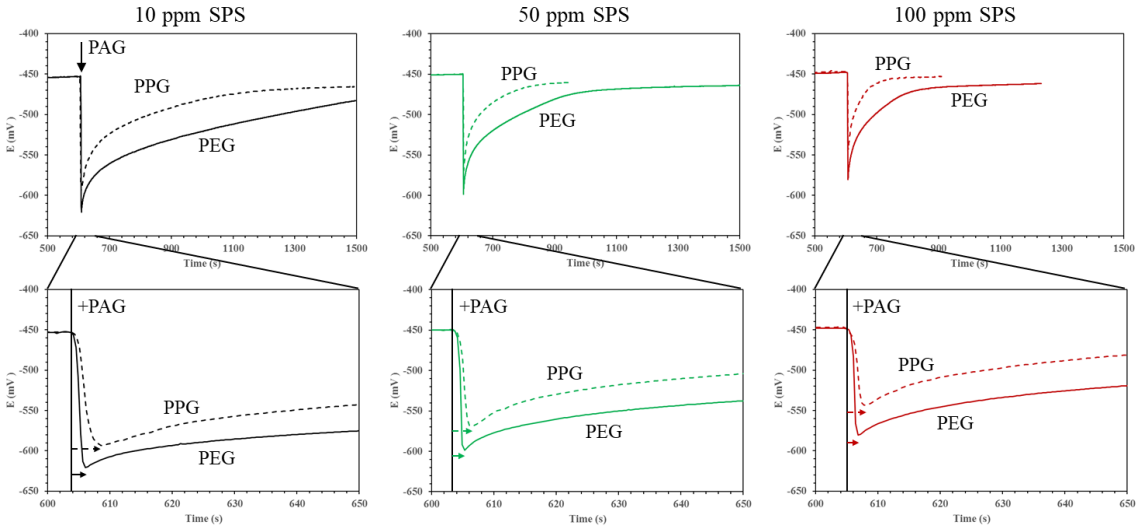

Figure 4.15. Potential-time response of injecting PEG (300 ppm) and PPG (300 ppm) into solution of VMS and SPS with various concentrations.

4.3.3. Leveler, Suppressor, and Accelerator

The potential-time response of PVP and SPS combinations are shown in Figure 4.16. The addition of PVP to VMS resulted in a brief depolarization followed by a gradual polarization which continued for about 10 minutes (not shown). The simultaneous addition of PVP+SPS and the sequentially addition of PVP after SPS resulted in a similar response, characterized by a more rapid polarization compared to that of only PVP. In the case of sequential addition of SPS after PVP, the solution of PVP was allowed to plate for 10 minutes to reach a steady-state potential. Compared to adding SPS after PAG-type suppressors, the addition of SPS after PVP had a minimal effect on the Cu potential as seen by the 5 mV depolarization which did not increase with time.

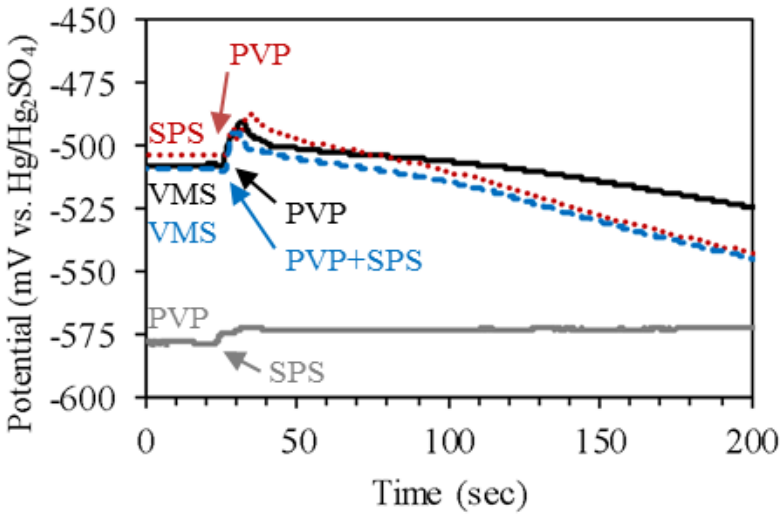

Figure 4.16. Potential-time response after injections of PVP and SPS with different sequences and combinations.

Figure 4.17 shows the sequential and combined additions of PVP and PEG. Adding PVP after PEG resulted in a brief ripple in polarization followed by a slightly increased polarization of about 5 mV after 10-15 seconds. When PEG was added after PVP, the polarization rapidly increased and remained stable after 10-15 seconds. The simultaneous addition of PEG+PVP to VMS shares characteristics of the aforementioned cases: fast polarization with a brief ripple before reaching a steady-state potential after 10-15 seconds. All cases resulted in roughly the same steady-state potential of -700 mV.

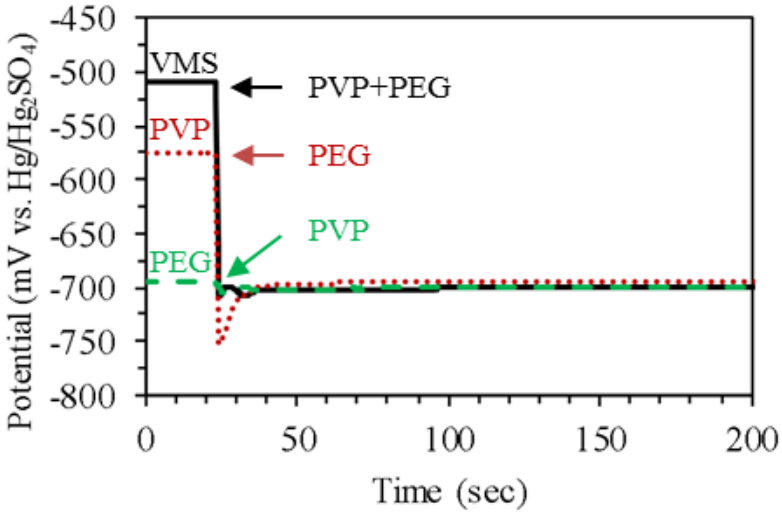

Figure 4.17. Potential-time response after injections of PVP and PEG with different sequences and combinations.

A summary of interactions with SPS, PEG, and PVP are shown in Figure 4.18. On its own, PVP has weak and slow polarization kinetics. The combination of PVP+SPS shows slightly faster polarization. PVP+PEG shows a fast, strong polarization that is maintained over time. In the combination of PEG+SPS, PEG quickly polarizes the Cu electrode but is followed by a continuous depolarization with time due to the presence of SPS. The PVP+PEG+SPS combination shows a hybrid of characteristics: rapid polarization due to PEG, a 30-40 mV depolarization from the addition of SPS compared to PVP+PEG, and a polarization that is maintained due to PVP.

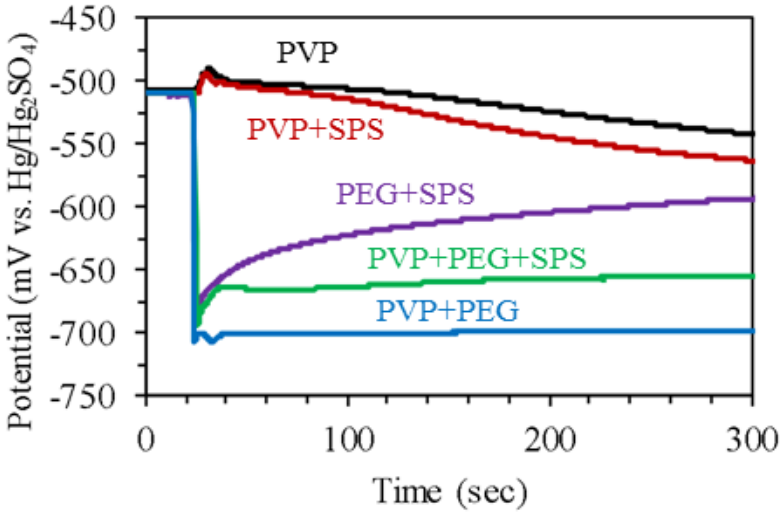

Figure 4.18. Potential-time response after combined injections of PVP, SPS, and PEG.

4.4 Analysis of Electrochemical Behavior of Organic Additive Interactions

This section summarizes the observed behavior of organic additives and how they impact the electrochemical behavior during copper plating.

4.4.1. PEG vs. PPG

In the forward potential scan of cyclic voltammetry with just PAG, PEG suppressed the plating current density to a certain potential before rising steadily at lower potentials and followed a similar path on the reverse scan with minimal hysteresis (Figure 4.5). In contrast, PPG showed a notable difference in the current-potential response of the forward and reverse scans. The forward scan resulted in a stronger suppression followed by a more rapid rise in current density at more negative potentials, while the reverse scan was characterized by a more gradual return to the suppressed state over a wider range of applied potential. In the chronopotentiometry experiments of only PAG, the cathode potential with PPG was about 20 mV more positive than that of PEG (Figure 4.12).

Differences between PEG and PPG remained apparent in the experiments performed with combinations of PAG+SPS. While both PAG+SPS combinations showed the similar hysteresis of current response between forward and reverse potential scans, the PPG+SPS combination resulted in a larger hysteresis with a potential difference of 200 mV between forward and reverse scans when the current density was 50 mA/cm^2 (Figure 4.6). As the hysteresis is attributed to PAG-Cl-Cu interactions being displaced by SPS in favor of S_{thiol}-Cu interactions, this result suggests that PPG has a weaker chemical interaction with the Cl^- modified Cu surface than PEG [29, 31, 48]. This is further exemplified by comparing the potential response after injections of PAG/SPS combinations, where the PPG+SPS combination shows a significantly higher rate of depolarization compared to PEG+SPS (Figure 4.14). According to studies by Feng et al., Cu coordinates with ether oxygen atoms of the alkyl backbone [46]. Compared to PEG, the steric hindrance associated with an additional methyl side chain in PPG may be attributed to inhibit coordination between O-C-C-O and the Cl^- modified Cu surface.

The potential response of each individual PAG/SPS combination show indistinguishable rates of suppression and depolarization when the order of PAG or SPS injection was changed (Figure 4.13). This suggests that, considering SPS and PAG interactions only, additive adsorption and displacement kinetics are independent of how the Cu cathode surface was previously functionalized. The potential response of PEG/PVP interactions show a similar independence of the order of injection; the strong polarization from PEG is unchanged from the addition of the relatively less polarizing PVP (Figure 4.17).

4.4.2. Role of PVP

The relatively long polarization characteristics observed in PVP injection suggests that its surface functionalization kinetics are slow compared to the PAG-based molecules. This difference is attributed to their large difference in molecular weight, where the transport kinetics of PVP are expected to be slower. The slow rate of PVP-copper functionalization also explains the hysteresis behavior observed in cyclic voltammetry (Figure 4.9). In the forward potential scan, the current density is low, and copper growth is occurring at a rate slow enough for PVP to adsorb and suppress plating. After a potential threshold (-0.69 V) beyond which PVP was unable to suppress the surface, the reverse scan began with a high current density. As the copper growth was faster than PVP could functionalize, the reverse potential scan resulted in a current response representative of a non-suppressed cathode.

Injections of SPS followed by PVP or PVP and SPS simultaneously result in a slightly faster polarization than by PVP alone (Figure 4.16). This result is consistent with previous studies which described the relationship between SPS and PVP as synergistic, where the suppression effect of PVP is enhanced by SPS [34]. When SPS was injected after the potential stabilized with PVP, the result was minimal depolarization which did not increase with time. As described by Schweinsberg et al., PVP is believed to coordinate with the Cu surface through the oxygen in its N=C-O moiety [43]. These observations suggest that the nitrogen containing moiety in PVP's interaction with copper is strong enough to prevent dissociation in favor of S_{thiol}-Cu from SPS.

4.4.3. Combination of Suppressor, Leveler, and Accelerator

When PEG, SPS, and PVP are combined, the behavior can be explained from the individual interactions noted above. As seen in Figure 4.18, the depolarization by SPS dictates the behavior when combined with PEG. However, when SPS is combined with PVP, the polarization is dictated by the suppressive ability of PVP. PEG and PVP combined show a strong, constant polarization with time. When SPS is added, the result is a slight depolarization due to displacement of weak PEG interactions, but is further prevented by the presence of PVP.

4.5 Summary

The interactions between SPS, PAG-type suppressors, and PVP were investigated by comparison of their electroanalytical behavior. Electroanalytical characterization by cyclic voltammetry and chronopotentiometry revealed the polarization and adsorption kinetics of each additive and which additive-copper interactions dominate amongst a given combination of additives. PAG-type suppressors were fast to polarize the Cu electrode with strong suppression, but were susceptible to depolarization and displacement when in the presence of accelerator molecule SPS. In general, PPG has a weaker coordination to Cu than PEG, as indicated by its weaker cathode polarization and faster depolarization with SPS. The PVP leveler adsorbs slowly with weak polarization, but resists depolarization when combined with SPS. The combination of PAG and PVP follows the polarization and adsorption characteristics of PAG. When PAG, PVP, and SPS are combined, the result is the sum of their sub-interactions: a strong, rapid polarization from PAG that is slightly depolarized by SPS, but retains a constant potential with no depolarization over time due to the dominant surface interactions of PVP over SPS.

CHAPTER 5

IMPACT OF ORGANIC ADDITIVES ON COPPER VIA FILL

Increased demands for high-performance and multifunctional electronics in smaller form factors are driving the development of advanced packaging technologies. Achieving high logic-memory bandwidth and I/O density requires the IC package to support high wiring density and fine-pitch through-package-vias (TPVs) as seen in recent 2.5D and 3D system packages [61]. TPVs and blind-vias that are fully-filled with Cu are desired over conformally-plated copper due to lower DC resistance, improved power integrity, and superior thermal dissipation [21]. This chapter investigates the impact of organic additives on blind-via filling. The mechanism of additive interactions during various stages of plating are proposed.

Additionally, surface enhanced Raman spectroscopy (SERS) will be used as a means for in-situ observation of chemical interactions between the organic additives and the surface of the Cu electrode. With an incident laser, Raman active organic ligands are excited to higher energy vibrational states. The energy associated with these excited states (measured as the Raman shift) is collected to generate a spectrum, with characteristic peaks corresponding to the Raman active ligand it originated from. When the laser is focused on a noble metal, such as gold, silver, or copper surface, plasmons at the surface resonate to amplify Raman scattering near the metal interface. When using SERS to probe the Cu electrode surface with a Cu plating electrolyte, specific chemical moieties from each organic additive can be detected. The signal will be theoretically representative of the organic additive moieties that interact at the electrolyte/electrode interface.

5.1 Blind-via Filling

This section contains results showing the impact of organic additives on blind-via filling behavior. The experimental details are explained, followed by cross section analysis. Results from Chapter 4 are used to propose a mechanism for additive interactions during blind-via filling.

5.1.1. Substrate Preparation and Experimental Details

Substrates for blind-via filling were prepared as illustrated in Figure 5.1. A Cu clad FR-4 board was laminated with a dry film epoxy-based dielectric of 20 µm thickness. Arrays of blind-vias having 45 µm diameter were formed by laser ablation. Finally, about 400 nm of seed layer Cu was deposited using a commercial electroless Cu plating bath.

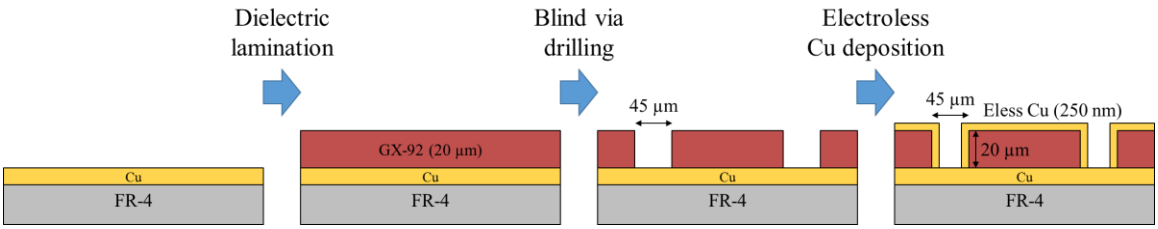

Figure 5.1. Process flow diagram of blind-via substrate fabrication.

Blind-via filling was performed with a current density of 20.9 mA/cm^2 for 15 minutes with mechanical stirring. The reference electrode was $Hg/Hg_2SO_4/K_2SO_4$ (sat.) and a high-purity copper sheet was used as the counter electrode. The electrodes were mounted with fixed positions in a 100 ml PTFE beaker (Figure 5.2). VMS composition and additive concentration is the same as listed in Table 4. The potential between the working and reference electrodes was measured as a function of plating time. Finally, the plated substrates were cut and polished to the center of the vias.

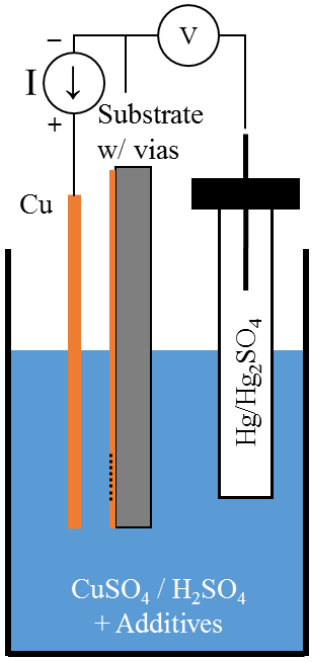

Figure 5.2. Diagram of electrochemical cell setup used for blind-via filling.

5.1.2. Effect of Organic Additives on Blind via Performance

Electrolytic plating with PEG+SPS resulted in a conformal filling profile (Figure 5.3 (a)). The plated copper thickness outside of the via was 8.0 µm while the thickness at the bottom of the via was 5.7 µm, corresponding to a filling ratio of 0.72. The potential response shown in Figure 5.3(b) shows similar behavior as that seen in injection chronopotentiometry of PEG/SPS (Figure 4.13), as characterized by an initially high polarization (-665 mV) followed with a gradual depolarization. Depolarization was observed for about 6-7 minutes before reaching a steady state potential of -550 mV.

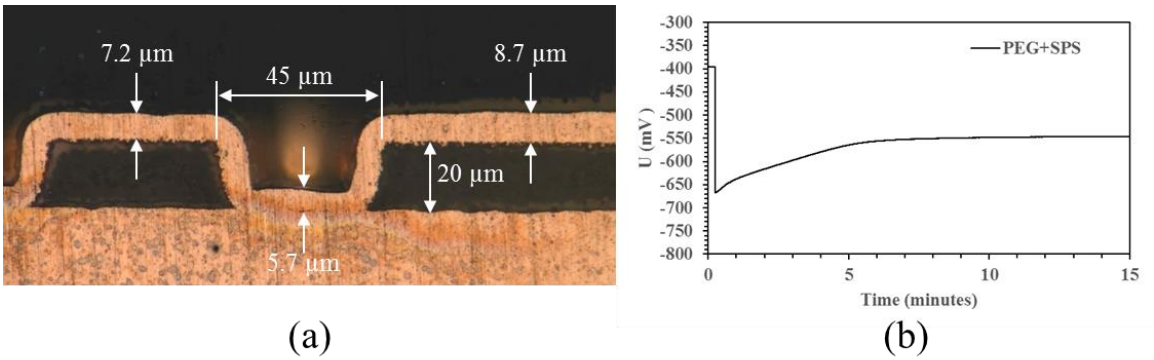

Figure 5.3. (a) Optical micrograph of blind-via cross section after plating with PEG and SPS. (b) Cathode potential measured during plating.

Plating in PVP+SPS resulted in a subconformal filling profile (Figure 5.4 (a)). The plated Cu thickness outside and inside the via was 26.9 µm and 10.9 µm, respectively, corresponding to a filling ratio of 0.41. The angle between the Cu along the sidewalls and the bottom of the via is acute. If plating continued, the plated Cu along the upper corners of the via would close and leave behind a void in the center. While the potential-time characteristics from injection chronopotentiometry imply slow kinetics of PVP adsorption to the Cu surface (Figure 4.16), the potential response collected during the plating of blind-vias showed an immediate, mild polarization to -585 mV which was relatively constant during the 15 minutes of plating (Figure 5.4 (b)).

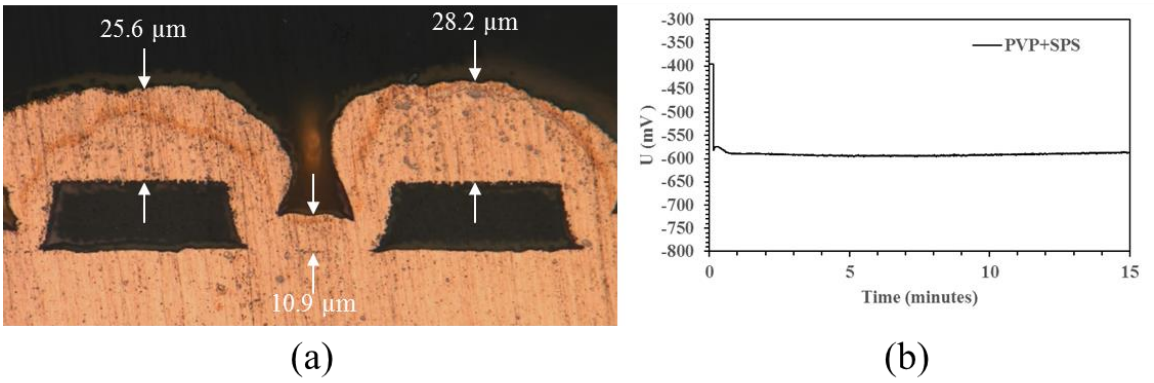

Figure 5.4. (a) Optical micrograph of blind-via cross section after plating with PVP and SPS. (b) Cathode potential measured during plating.

Inspection of plating thickness across the sample revealed a significant difference with respect to location. As shown in Figure 5.5, tens of microns of plating was apparent in regions near the vias while less than 1 µm was plated in regions away from the vias. One difference between these regions is the effective current density. Since the surface area/volume is larger in regions near the vias, specially near the corners, the current density is expected to be higher than the planar regions away from the vias. This observation suggests that the suppressive effectiveness of PVP may depend on current density.

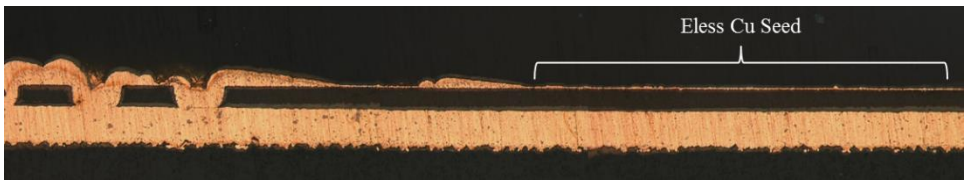

Figure 5.5. Low magnification optical micrograph showing distribution of copper plating thickness near and away from vias.

Figure 5.6 (a) shows the blind-via filling profile after plating with PEG+PVP+SPS. With a filling ratio of 2.11, the fill profile is superconformal, as also indicated by the

concave-up profile in the center of the almost-filled via. Compared to the case of PEG+SPS, significantly more Cu was plated inside the via (15.2 µm), and the plated Cu thickness outside of the via was slightly reduced (7.2 µm). No voids were observed. The potential response was similar to that from injection chronopotentiometry, as characterized by an immediate, strong polarization to -680 mV that was maintained for the entire duration of plating (Figure 5.6 (b)).

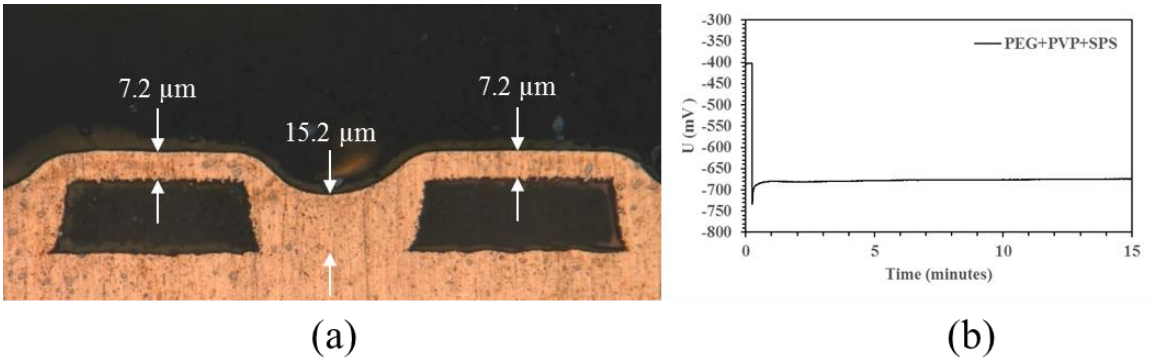

Figure 5.6. (a) Optical micrograph of blind-via cross section after plating with PEG, PVP, and SPS. (b) Cathode potential measured during plating.

5.1.3. Proposed Mechanism of Additive Impact on Filling Behavior

The impact of additives in the filling performance can be correlated with their potential response during plating. With PEG+SPS, a strong overpotential was immediately in effect, which slowly depolarized over the first 6-7 min of plating. Suppression by PEG and depolarization by SPS displacement occurred uniformly over surfaces inside and outside the via structure, resulting in a conformal via fill (Figure 5.7 (a)). Superfilling behavior was previously observed for PEG+SPS combinations, but only for vias small enough where filling was complete within the time scale of SPS displacement, and where

the via geometry allowed for a concentration differential of additives inside and outside the vias [30].

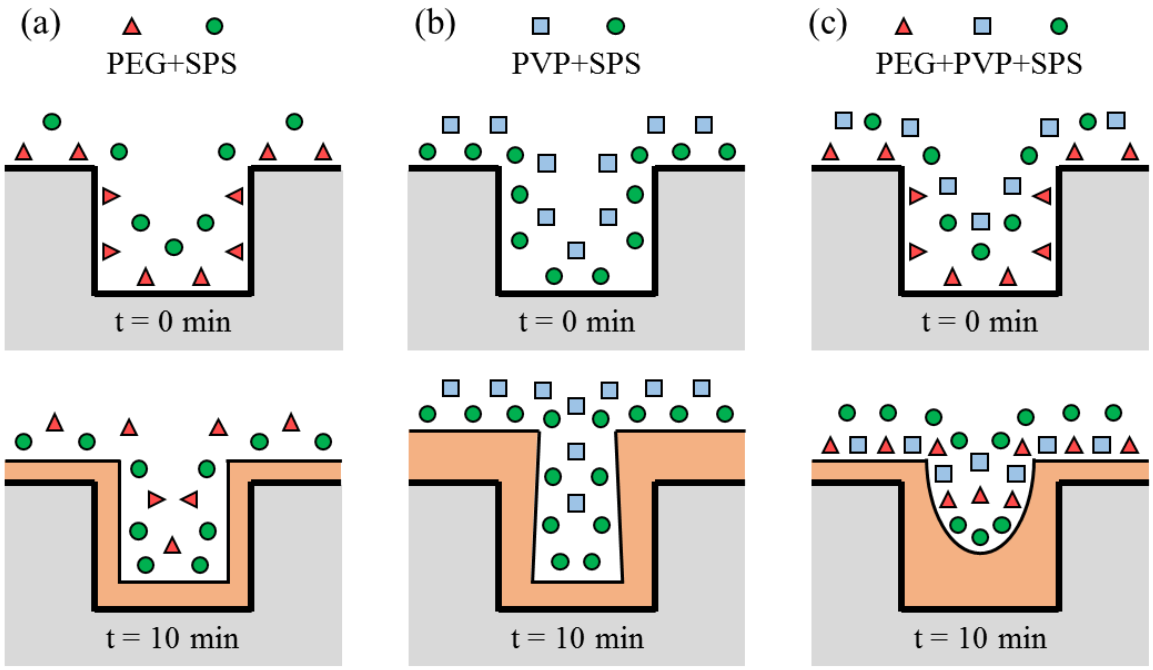

Figure 5.7. Pictorial representation of additive interactions during initial (t = 0 min) and late stages (t = 10 min) of blind-via filling with (a) PEG+SPS, (b) PVP+SPS, and (c) PEG+PVP+SPS.

In the case of PVP+SPS, the cathode overpotential was slightly larger than the depolarized state measured after 7 minutes of plating with PEG+SPS (Figure 5.4(b)). Cu plating was effectively unsuppressed, especially around the upper corners of the via, where current crowding is likely to occur. This case is similar to the condition observed in the reverse potential scan of the cyclic voltammogram of PVP+SPS, where the Cu growth rate exceeded PVP's ability to functionalize and suppress (Figure 4.9). The copper growth in these regions was too fast for PVP to adsorb and affect plating, resulting in subconformal via filling (Figure 5.7 (b)).

The combination of PEG+PVP+SPS resulted in the best blind-via filling performance, with over twice as much Cu plating in the via compared to outside. Whereas PVP alone was shown to be insufficient for suppression outside the vias, PEG provided the fast adsorption and polarization to suppress plating long enough for PVP to be effective. Plating behavior inside the via was likely dictated by the faster adsorption of PEG and SPS than PVP (Figure 5.7 (c)). These conditions created a strong differential in effective copper reduction polarization in the regions inside and outside the vias to achieve superfilling behavior with a filling ratio of 2.11.

5.2 In-Situ SERS Characterization of Organic Additive Interactions

This section contains results from in-situ SERS characterization to investigate the organic additive interactions with the Cu electrode during plating. Pure organic additives are characterized first to determine Raman active ligands. Then, SERS is used in-situ at the Cu electrode during plating with organic additives in solution.

5.2.1. Raman Scattering of Pure Organic Additives

Raman spectra of pure organic additives were collected to determine and identify Raman active ligands. The spectra were collected using a 785 nm laser with a 50x objective lens. Figure 5.8 shows the Raman spectrum of SPS powder with characteristic ligands identified. Notable Raman peaks include those due to S-S stretch (511 cm^{-1}), C-S(sulfonate) stretch (528 cm^{-1}), C-S(thiol) stretch (644 cm^{-1}), CH_2 rock (747 cm^{-1}), S=O stretch (1075 cm^{-1}), and CH_2 scissor (1430 cm^{-1}) [47]. However, the S-S ligand will not be relevant as SPS changes to 3-mercapto-1-propanesulfonate (MPS) during plating. Additionally, the S=O moiety is redundant with the sulfate-based electrolyte used in plating.

Therefore, the C-S(sulfonate), C-S(thiol), and CH_2 peaks will be relevant for in-situ SERS when SPS is used alone, and the CH_2 peaks become redundant if combined with PEG.

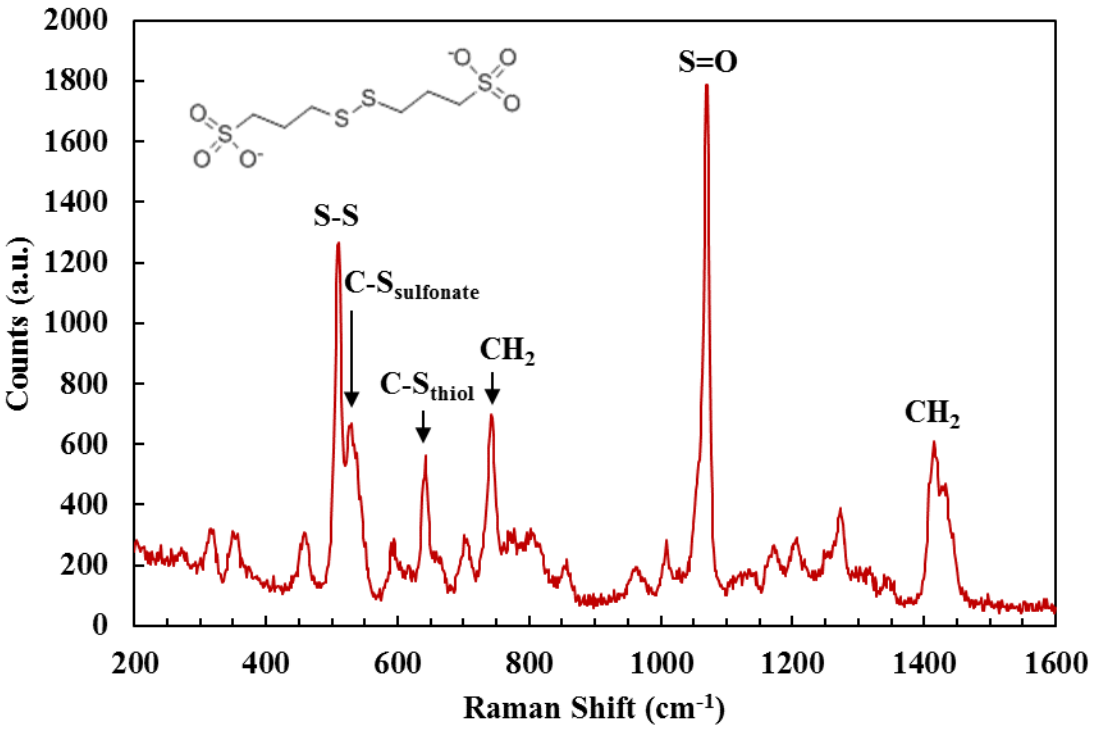

Figure 5.8. Raman spectrum of SPS powder.

Figure 5.9 shows the Raman spectrum of PEG powder. The characteristic peaks correspond to O-C-C (277 cm^{-1} and 534 cm^{-1}), C-O-C (361 cm^{-1}), CH_2 (845 cm^{-1}), and C-O (857 cm^{-1}) [46].

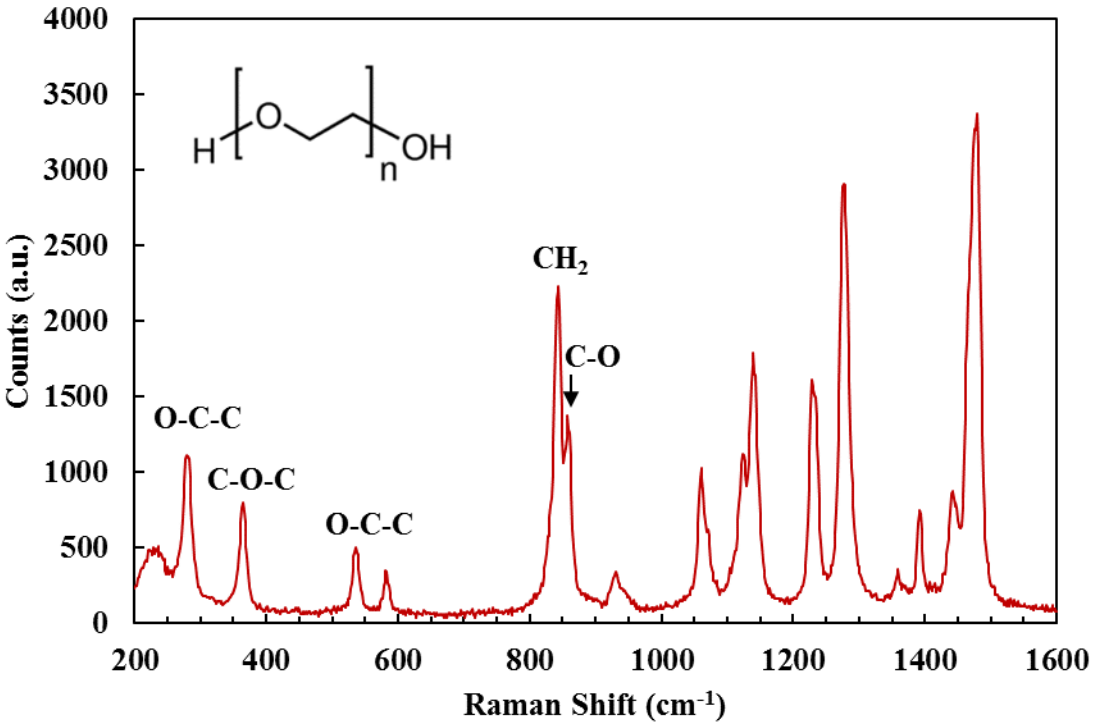

Figure 5.9. Raman spectrum of PEG powder.

The Raman spectrum of PVP powder is shown in Figure 5.10. Characteristic Raman peaks related to PVP include: C-N-C deformation (370 cm^{-1}), O-C=N in-plane deformation (551 cm^{-1}), C-N-C symmetric stretch (750 cm^{-1}), ring breathing (934 cm^{-1}), and C-N-C asymmetric stretch (1230 cm^{-1}) [43].

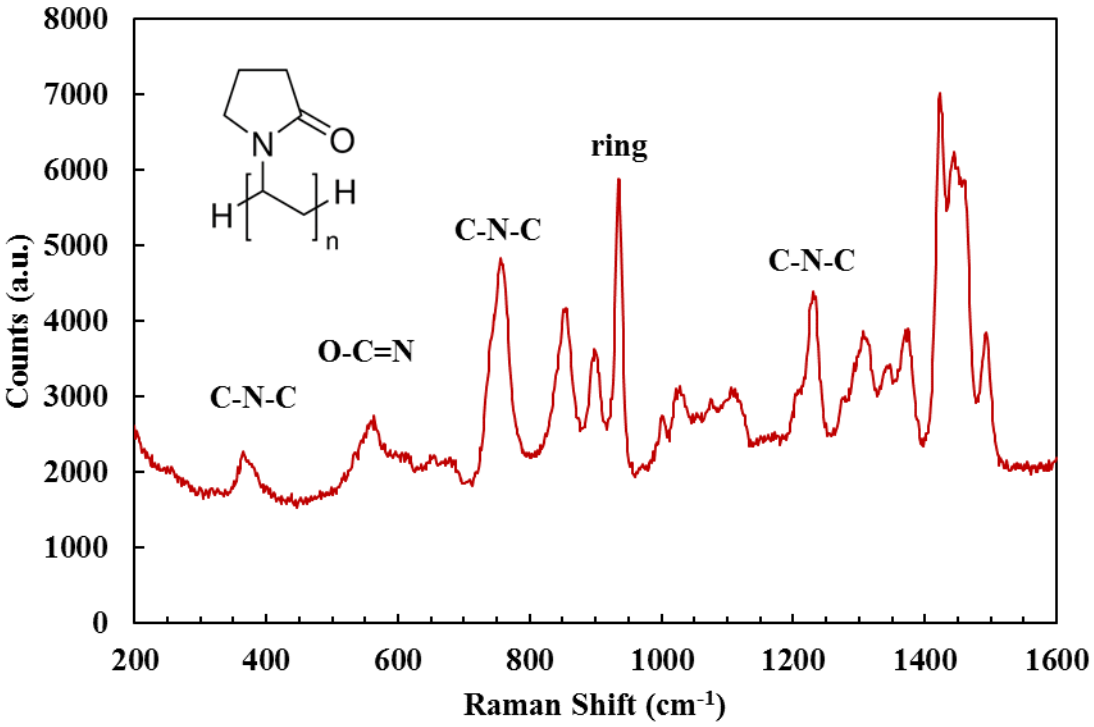

Figure 5.10. Raman spectrum of PVP powder.

5.2.2. Experimental Details for In-Situ SERS Measurements

Due to the physical constraints of the Raman tool, a screen printed electrode (SPE) was chosen as a suitable platform to carry out SERS measurements. The SPE is comprised of a Pt working electrode, Ag/AgCl reference electrode, and Pt counter electrode (Figure 5.11). Again, the composition and VMS and organic additive details are the same as used in previous experiments (Table 4).

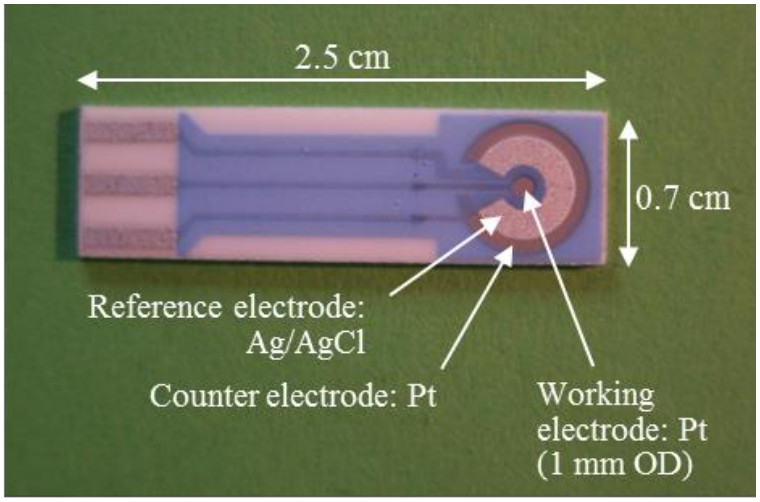

Figure 5.11. Components of screen printed electrode used for SERS.

Figure 5.12(a) shows a schematic of the SPE with electrolyte and incident Raman laser. A photograph of the actual experimental setup is shown in Figure 5.12(b). A red laser (785 nm) was used and focused onto the copper surface with a 20x objective lens. Due to the small working distance, a glass cover slip was required to protect the objective lens from coming in contact with the electrolyte.

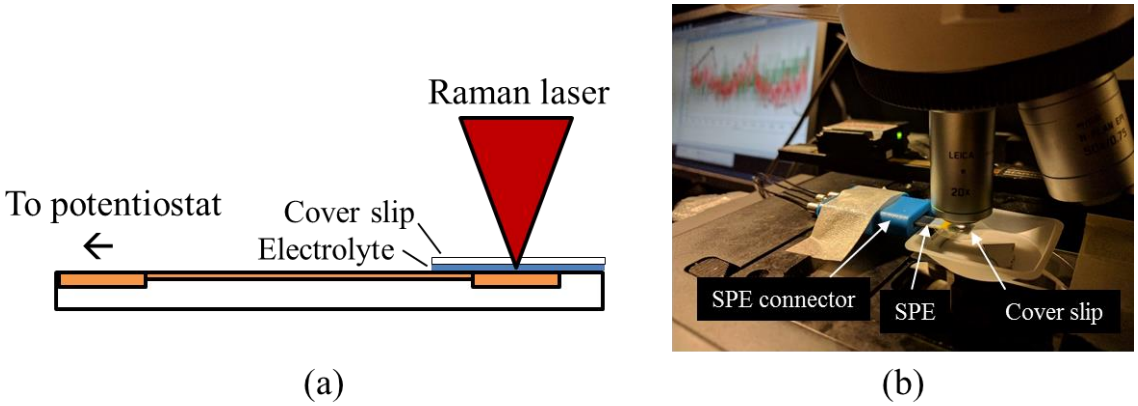

Figure 5.12. (a) Diagram of screen printed electrode and (b) photograph of setup used for SERS.

Based on results from electrochemical characterization, the Cu plating overpotential using the combination of PAG+PVP+SPS was roughly -0.25 V (-0.65 V vs Hg/Hg_2SO_4) to maintain a current density of 20.9 mA/cm^2. Based on this result, an overpotential (η) of -0.25 V was used as the plating condition for SERS measurements. Plating solutions containing the standard virgin makeup solution (VMS) and SPS as accelerator (10 ppm), PEG as suppressor (300 ppm), and PVP as leveler (10 ppm) were prepared and used individually. SERS spectra were collected during plating (η = -0.25 V) and after plating (η = 0 V).

5.2.3. Organic Additive Interactions with Copper as Observed by SERS

The SERS spectra collected with VMS+SPS are shown in Figure 5.13. During plating (η = -0.25 V), peaks corresponding to C-C (1035 cm^{-1}), CH_2 (740 cm^{-1}), and C-S(thiol) (625 cm^{-1} and 691 cm^{-1}) moieties in SPS were apparent. The SERS spectrum collected after plating (η = 0 V) contained the same peaks mentioned previously, but with two additional peaks corresponding to C-S(sulfonate) (520 cm^{-1} and 795 cm^{-1}).

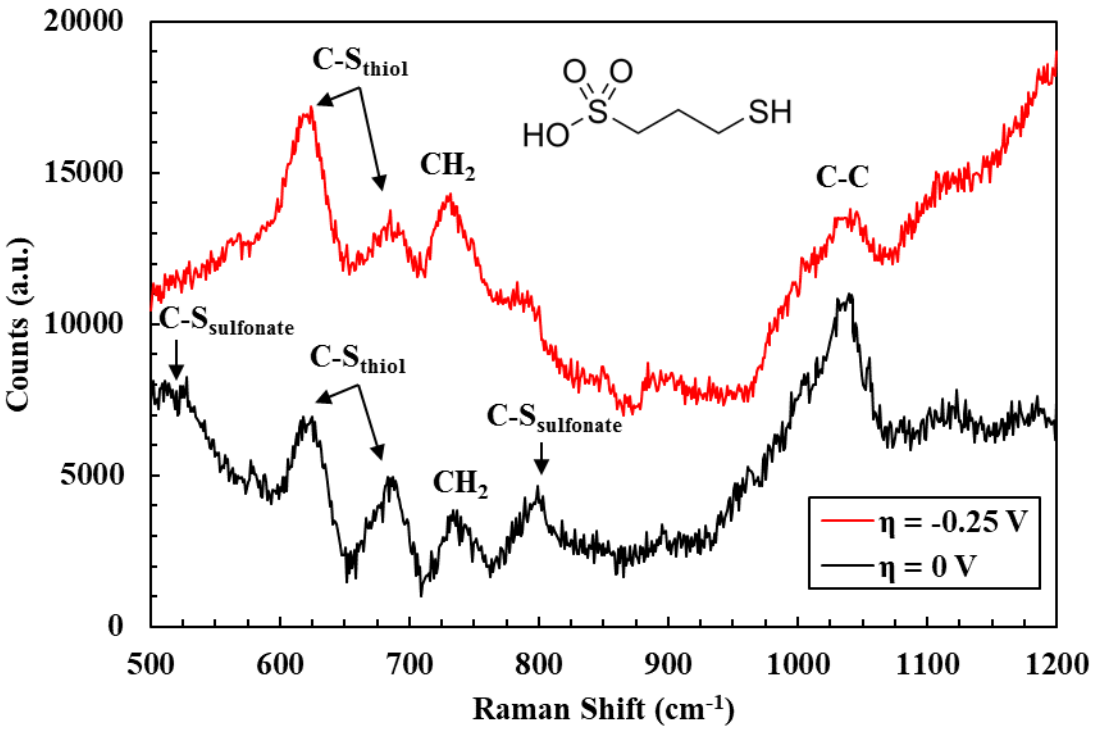

Figure 5.13. SERS spectra of VMS with SPS collected with and without applied potential.

SPS is a short, linear molecule with thiol and sulfonate groups at opposite ends. These spectra suggest that the thiol and sulfonate moieties of SPS interact with the Cu surface before plating (η = 0 V). During plating, the negatively charged sulfonate group is no longer in proximity to the Cu electrode and the only the S(thiol)-Cu ligand remains (Figure 5.14). This is consistent with literature that proposed a similar SPS/Cu interaction, with the electronegative sulfonate group attracting Cu^{2+} ions in solutions as the accelerating mechanism [48].

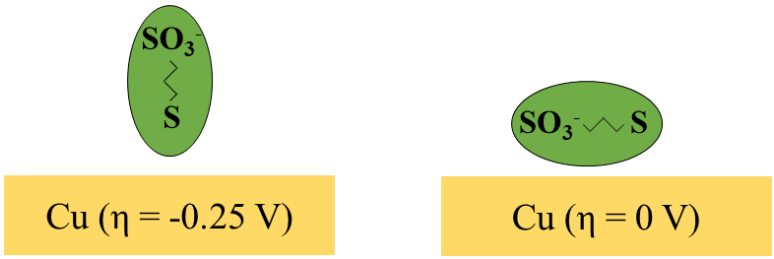

Figure 5.14. Pictorial representation of SPS interactions with the copper electrode with and without applied potential.

Figure 5.15 shows the SERS spectra collected with VMS+PEG. The difference between the spectra with and without applied potential is clear. Without applied potential, no significant SERS peaks are present, and only weak peaks corresponding to SO_4^{2-} (990 cm^{-1}) and O-C-C-O (690 cm^{-1}) are apparent. With applied potential, strong peaks appear which correspond to ligands formed specifically when PEG has formed a complex with Cu/Cl^-: Cu-O (525 cm^{-1}) and O-C-C-O (690 cm^{-1}).

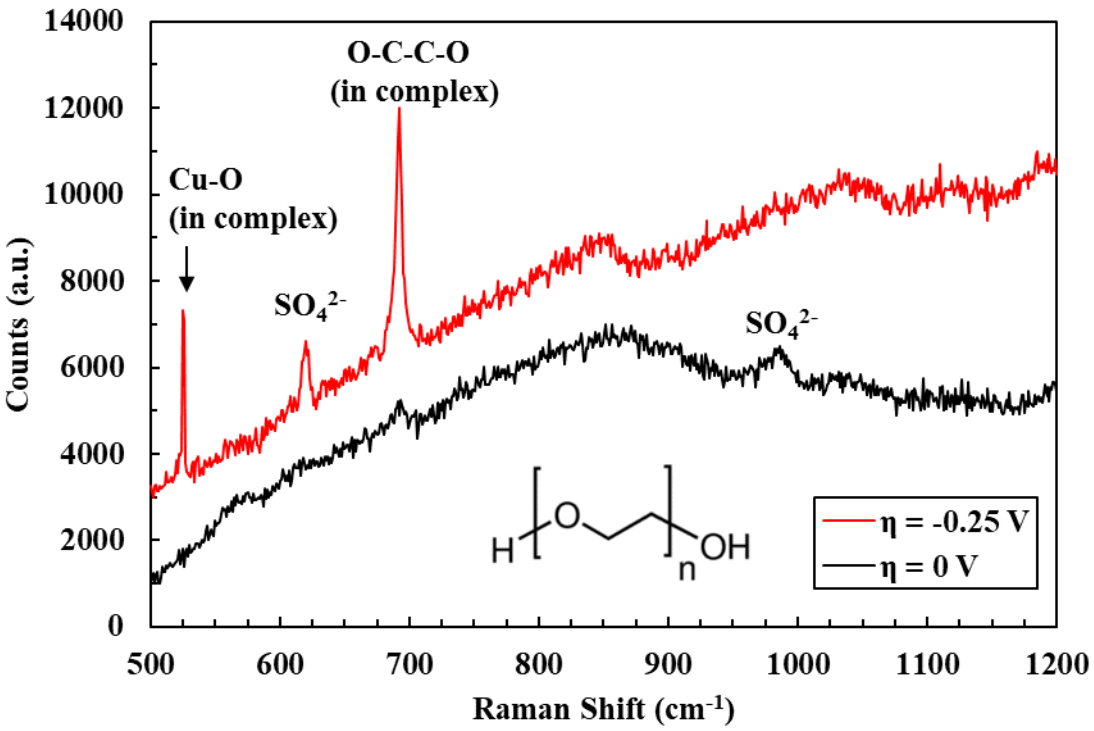

Figure 5.15. SERS spectra of VMS with PEG collected with and without applied potential.

According to prior studies, polyalkylene glycols such as PEG are believed to coordinate to the Cl^- modified Cu surface through the oxygen atoms in the alkyne chain [46]. It was previously believed that PEG's hydrophobicity was the primary driving force guiding the suppressor molecule to the Cu surface. However, this result suggests that electrode potential has a role in Cu/Cl^-/PEG complex formation. Based on these observations, the only mechanism of PEG adsorption is its low surface tension and hydrophobicity, which leads to a relatively weak coordination with the Cu surface. With applied potential, PEG adsorbs more strongly, forming the Cu/Cl/PEG complex (Figure 5.16).

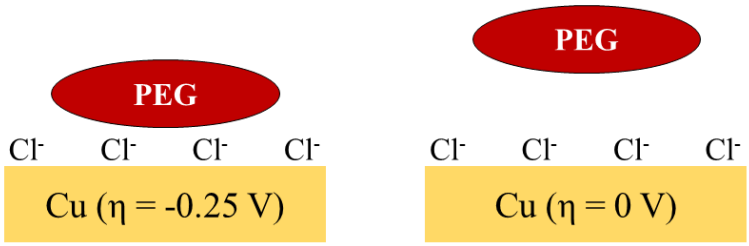

Figure 5.16. Pictorial representation of PEG interactions with the copper electrode with and without applied potential.

A similar trend was found for PVP, where PVP-specific ligands were observed by SERS only with applied potential (Figure 5.17). Specifically, the N=C-O moiety (535 cm^{-1}) appeared weak without potential, but became strongly apparent with potential. According to studies by Schweinsberg et al., PVP coordinates to Cu by coordinating with the originally hydrogenated oxygen in the N=C-OH moiety [43]. The SERS spectra suggest that Cu with negative potential increases the amount of O-C=N coordination (Figure 5.18).

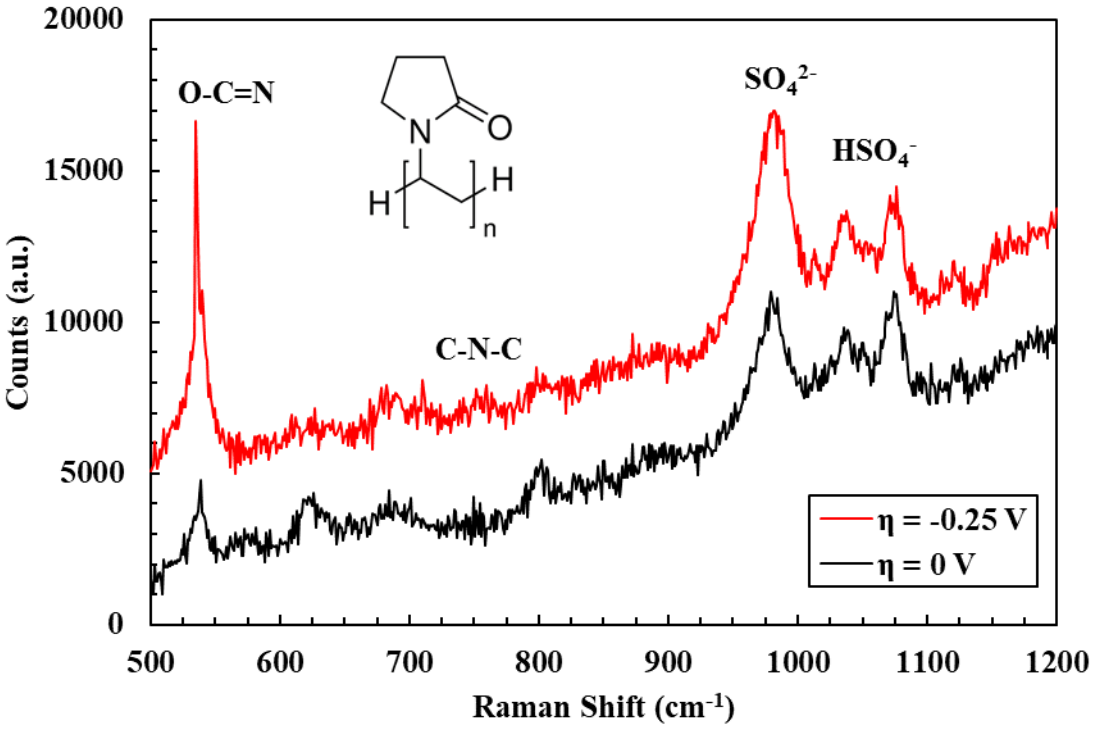

Figure 5.17. SERS spectra of VMS with PVP collected with and without applied potential.

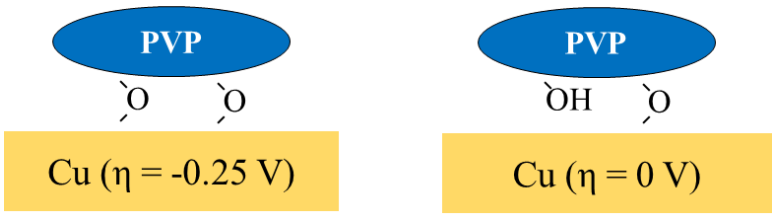

Figure 5.18. Pictorial representation of PVP interactions with the copper electrode with and without applied potential.

5.3 Summary

These electroanalytical observations from Chapter 4 were used to infer the additives' impact on filling behavior in blind-vias. The combination of PEG and SPS resulted in a conformal fill, likely due to uniform polarization by initial PEG adsorption and

depolarization by SPS over all surfaces. PVP alone was unable to suppress plating, especially in the top corner regions of the vias where current density is expected to be high. This resulted in subconformal filling likely to form a void. The PAG, PVP, and SPS combination yielded superfilling behavior as a result of their combined additive interactions. Outside the vias, PAG rapidly polarizes the surface to suppress the plating current, allowing the slower PVP to adsorb. The combination of PVP and PEG allowed for effective suppression outside the vias throughout the entire duration of plating. Inside the vias, PVP was unable to affect plating due to its slow adsorption kinetics, so the plating behavior was dominated by PEG and SPS interactions. By observing the electrochemical behavior of individual and combined additives, an adsorption kinetics and interaction-based mechanism was proposed to which achieves void-free superfilling in relatively large blind-vias.

Initial trials of SERS confirmed the presence of known organic ligands related to each additive and their chemical adsorption to copper. In SPS, the C-S(thiol) ligand was found to coordinate with copper regardless of applied potential, while the C-S(sulfonate) moiety was only strongly apparent without applied potential. PEG showed strong SERS peaks from Cu-O and O-C-C-O ligands specifically related to Cu/Cl^-/PEG complex formation with applied potential. SERS characterization of PVP had similar results, with its N=C-O moiety being more apparent only during plating.

CHAPTER 6

RESEARCH SUMMARY AND FUTURE WORK

This dissertation presented the first comprehensive study of copper metallization of glass with through-package-vias (TPVs) for interposer applications. Copper adhesion to glass and electrochemical interaction of additives in electrolytic plating baths are the two key focus topics of this research. This work is guided from the motivation that a limited knowledge is available in the literature to understand the methods and fundamental mechanisms to achieve copper adhesion and high-quality copper plating in glass with TPVs. Although strong adhesion of copper to glass surfaces can be achieved using adhesion-promoting metal/metal-oxide layers deposited by physical vapor deposition (PVD), adhesion of copper on bare glass using electroless copper deposition to evenly metallize high-aspect ratio TPVs in panel-scalable glass remains a challenge. In addition, a better understanding of fundamental aspects related to electrolytic copper plating is desired. Specifically, the electrochemical properties and mechanism by which organic additives affect copper filling performance in via structures remains largely unknown. Based on these motivations, the objective of this research was to develop fundamental understandings of copper metallization for ultra-thin ($\leq$ 100 μm) glass with small-diameter ($\leq$ 60 μm), fine-pitch ($\leq$ 120 μm) TPVs. The research tasks included investigating interfacial adhesion mechanisms of copper to glass, developing a via-first process for metallizing glass with high-aspect ratio TPVs, and electrochemical characterization of organic additives in electrolytic copper plating to determine their role in via filling.

6.1 Research Summary

6.1.1. Metallization and Adhesion of Copper to Glass Interposers

The feasibility of direct electroless copper deposition to glass was investigated using surface roughness as an adhesive enhancement mechanism. A direct correlation between average surface roughness and adhesive test results was found, and an average surface roughness of several hundreds to 500 nm was required for passing the tape test. Interfacial failure analysis was carried out using a surface-sensitive compositional technique, x-ray photoelectron spectroscopy (XPS). Several high-resolution core-level scans at the peeled copper and glass surfaces showed that weak bonding between glass and palladium inhibited the adhesion of electroless copper to glass.

An alternative means to achieve improved adhesion while minimizing physical and chemical modification of the glass substrate was also developed using a patterned polymer adhesion film. The process was optimized using a 5 μm thick epoxy-based dry film dielectric and polymer patterning techniques. A polymer pre-cure step was developed and the degree of polymerization was characterized by fast Fourier infrared spectroscopy (FTIR). High-quality conformal copper metallization of TPVs with 60 μm diameter and 120 μm pitch in 100 μm thick glass was demonstrated. Adhesion and thermo-mechanical reliability was validated by peel strength and electrical resistance measurements after 1000 thermal cycles. The process was shown to be capable of meeting high I/O density demands as demonstrated by conformal copper metallization of 20 μm diameter TPVs with 40 μm pitch in 100 μm thick glass.

6.1.2. Role of Organic Additives in Electrolytic Copper Plating

Organic molecules were first chosen for each class of additives: bis(sodium sulfopropyl) disulfide (SPS) as accelerator, polyalkylene glycol-based (PAG) suppressors, and polyvinyl pyrrolidone (PVP) as leveler. Electroanalytical techniques such as cyclic voltammetry and chronopotentiometry were used to benchmark the additives individually and in combination with each other. Cyclic voltammetry was used to determine the additives' impact on the current-potential response, while additive injection chronopotentiometry was used to investigate additive adsorption and cathode polarization kinetics. In general, the PAG-based suppressor molecules showed relatively fast (< 10 sec) adsorption kinetics with strong polarization of the copper cathode. Of the PAG-based suppressors, polypropylene glycol (PPG) showed weaker electrochemical suppression than polyethylene glycol (PEG). This was made evident by PPG's weaker polarization of the copper cathode and faster characteristic time to depolarize in the presence of SPS. It is hypothesized that the additional methyl group in the alkyl side-chain of PPG results in steric hindrance between the O-C-C-O coordination to the Cl^- modified Cu surface. While the PVP leveler molecule showed slower adsorption kinetics and weaker polarization than the PAG-based suppressor molecules, it exhibited resilience to depolarization when combined with SPS. The potential response of the SPS-PAG-PVP combination was found to be the sum of their sub-interactions: PAG adsorbs rapidly and strongly polarizes the cathode, but PVP prevents depolarization with time from the SPS.

Surface enhanced Raman spectroscopy (SERS) was used for in-situ chemical observation of additive interactions with the copper surface during plating. Using SERS, characteristic Raman peaks corresponding to organic ligands near or on the copper

electrode are enhanced from surface plasmon resonance. The copper surface was probed by SERS during and after plating in electrolyte containing each type of additive individually. In the case of SPS, it was found that Raman signals corresponding to the sulfonate moiety were only present during plating (negative Cu potential), while the thiol group was present with and without applied potential. Ligands associated with Cu/Cl/PEG complex formation were also present only during plating. While PEG adsorption characteristics are attributed to its hydrophobic nature, this observation suggests that the chemical interactions are potential-dependent. A similar trend was found in PVP interactions, where the O-C=N moiety responsible for coordination with copper was more strongly present during plating.

The final research task of this work was to understand the impact of the additives' electrochemical properties on via filling performance. Blind-vias of 45 μm diameter and 20 μm depth were plated with various additive combinations to observe their impact on filling performance. Two-additive combinations of SPS-PVP and SPS-PEG yielded unsatisfactory via filling, characterized as subconformal and conformal, respectively. In contrast, the three-additive combination with its strong, constant polarization yielded a superconformal via filling behavior. The explanation of these results can be hypothesized based on the results from electrochemical characterization. Consistent with results from cyclic voltammetry, the plating behavior of SPS-PVP appeared to depend on current density. Away from the vias, the low current density surface was strongly suppressed while current crowding near the via corners inhibited the effectiveness of PVP, resulting in a subconformal via fill. As shown from chronopotentiometry measurements, the SPS-

resistant combination of PEG and PVP resulted in sustained suppression in all regions outside of the vias.

6.2 Scientific and Technological Contributions

Key scientific and technological contributions of this research are listed below:

- Determined the limits and interfacial failure mechanism of glass surface roughness as an adhesion enhancement method to electroless copper
- Developed a novel, via-first process to enable electroless copper metallization of glass interposers with high aspect ratio, fine-pitch TPVs using a thin, patternable polymer film. Thermo-mechanical reliability was proven and high-quality metallization of small diameter (20 μm), fine-pitch (40 μm) TPVs in ultra-thin (100 μm) glass was demonstrated.
- Characterized the electrochemical behavior of organic additives individually and in combination to develop fundamental understanding of additives' impact on current-potential and potential-time response
- Investigated the fundamental mechanism of additive-copper interactions by in-situ surface enhanced Raman spectroscopy (SERS)
- Correlated electrochemical characteristics of additive combinations with via filling behavior

6.3 Future Work

While this research investigated several aspects of copper metallization to glass interposers, there remain unanswered questions related to interfacial adhesion and the role of organic additives in electrolytic plating. If direct electroless copper deposition to roughened glass is to be further investigated, the relationships between palladium particle

catalyst size, glass roughness, and peel strength are necessary. Despite the demonstration of thermo-mechanical reliability with the polymer-based adhesion layer in this study, the seemingly resilient copper-glass interface in the TPV sidewall without the assistance of the polymer layer cannot yet be sufficiently explained. Detailed interfacial characterization is required to determine the adhesion mechanism and its limits. The two current hypotheses of copper adhesion to the TPV sidewall need further validation: 1) accurate measurement of TPV sidewall roughness and 2) chemical composition of the glass TPV sidewall as compared to the unmodified glass surface. While electrolytic copper plating is a complex process with many variables worthy of investigation, certain aspects of this research require additional examination. To fully understand the additives' effect on via filling, direct observation, preferably in-situ, of additive-copper interactions inside the via need to be compared with copper surfaces outside the via. Finally, the structure-property-performance relationships should be used to validate plating performance on advanced design rule test vehicles and to develop future guidelines for organic additive design.

6.4 Publications

Publications derived from this research are listed below by publication type.

Peer-reviewed journals

- T. B. Huang, H. Sharma, R. Manepalli, S. Kandanur, V. Sundaram, and R. Tummala, "Electroanalytical Study of Organic Additive Interactions in Copper Plating and their Correlation with Via Fill Behavior," *Journal of Electronic Materials*, (under review).
- T. B. Huang, B. DeProspo, H. Sharma, R. Manepalli, S. Kandanur, V. Sundaram, and R. Tummala, "Mechanism of Organic Additive Interactions

in Electrolytic Copper Plating as Determined by SERS," *Journal of Electronic Materials*, (in preparation).

- T. B. Huang, B. Chou, J. Tong, T. Ogawa, V. Sundaram, and R. Tummala, "Via-First Process to Enable Copper Metallization of Glass Interposers with High-Aspect-Ratio, Fine-Pitch Through-Package-Vias," *IEEE Transactions on Components, Packaging and Manufacturing Technology*, vol. 7, pp. 544-551, 2017.
- T. C. Huang, T. B. Huang, M. R. Pulugurtha, G. Ramos, A. Kilian, R. Taylor, V. Smet, and R. R. Tummala, "Electroless Palladium Autocatalytic Gold Surface Finish with Sub-10μm Solder Microbumps for High Reliability," *Journal of Materials Science: Materials in Electronics*, 2017 (under review).
- K. Ramachandran, T. L. Pruyn, T. Huang, Y. Wang, P. M. Singh, and W. Jud Ready, "Investigation of copper plated-through-holes in glass fiber reinforced epoxy substrates using AC impedance spectroscopy," *Journal of Materials Science: Materials in Electronics*, vol. 26, pp. 2563-2570, 2015.
- S. McCann, G. T. Ostrowicki, A. Tran, T. Huang, T. Bernhard, R. R. Tummala, and S. K. Sitaraman, "Determination of Energy Release Rate through Sequential Crack Extension," *Journal of Electronic Packaging*, vol. 139, 2017.

Conference proceedings

- T. B. Huang, B. Chou, V. Sundaram, H. Sharma, and R. Tummala, "Novel copper metallization schemes on ultra-thin, bare glass interposers with through-vias," *Proc. 2015 IEEE 65th ECTC*, pp. 1208-1212, 2015.

- T. B. Huang, V. Sundaram, P. M. Raj, H. Sharma, and R. Tummala, "Adhesion and reliability of direct Cu metallization of through-package vias in glass interposers," *Proc. 2014 IEEE 64th ECTC*, pp. 2266-2270, 2014.
- S. Viswanathan, T. Ogawa, K. Demir, T. Huang, P. M. Raj, F. Liu, V. Sundaram, and R. Tummala, "High Frequency Electrical Performance and Thermo-Mechanical Reliability of Fine-Pitch, Copper-Metallized Through-Package-Vias (TPVs) in Ultra-Thin Glass Interposers," *Proc. 2017 IEEE 67th ECTC*, pp. 1510-1516, 2017.
- V. Sundaram, J. Tong, K. Demir, T. Huang, A. Shorey, and S. Pollard, "High Reliability and High Performance 30μm Through-Package-Vias in Ultra-Thin Bare Glass Interposer," *International Symposium on Microelectronics*, vol. 2014, pp. 000402-000408, 2014.

REFERENCES

[1] R. Tummala, *Fundamentals of Microsystems Packaging, Second Edition*: McGraw-Hill Education, 2018.

[2] B. Sawyer, B. Chou, J. Tong, W. Vis, S. Deng, H. Tournier, *et al.*, "Design and Demonstration of 2.5D Glass Interposers as a Superior Alternative to Silicon Interposers for 28 Gbps Signal Transmission," in *Proc. 2016 IEEE 66th ECTC*, 2016, pp. 972-977.

[3] G. Kumar, P. M. Raj, J. Cho, S. Gandhi, P. Chakraborti, V. Sundaram, *et al.*, "Coaxial through-package-vias (TPVs) for enhancing power integrity in 3D double-side glass interposers," in *2014 IEEE 64th Electronic Components and Technology Conference (ECTC)*, 2014, pp. 541-547.

[4] B. Banijamali, S. Ramalingam, K. Nagarajan, and R. Chaware, "Advanced reliability study of TSV interposers and interconnects for the 28nm technology FPGA," in *Proc. 2011 IEEE 61st ECTC*, 2011, pp. 285-290.

[5] V. Sukumaran, T. Bandyopadhyay, V. Sundaram, and R. Tummala, "Low-Cost Thin Glass Interposers as a Superior Alternative to Silicon and Organic Interposers for Packaging of 3-D ICs," *IEEE Trans. Compon. Packag. Manuf. Technol.*, vol. 2, pp. 1426-1433, 2012.

[6] J. Tong, K. Panayappan, V. Sundaram, and R. Tummala, "Electrical Comparison between TSV in Silicon and TPV in Glass for Interposer and Package Applications," in *2016 IEEE 66th Electronic Components and Technology Conference (ECTC)*, 2016, pp. 2581-2587.

[7] Z.-C. Liu, Q.-G. He, P. Hou, P.-F. Xiao, N.-Y. He, and Z.-H. Lu, "Electroless plating of copper through successive pretreatment with silane and colloidal silver," *Colloids and Surfaces A: Physicochemical and Engineering Aspects*, vol. 257–258, pp. 283-286, 2005.

[8] W. Su, L. Yao, F. Yang, P. Li, J. Chen, and L. Liang, "Electroless plating of copper on surface-modified glass substrate," *Appl. Surface Sci.*, vol. 257, pp. 8067-8071, 2011.

[9] P. Benjamin and C. Weaver, "The Adhesion of Evaporated Metal Films on Glass," *Proc. Roy. Soc. London A: Mathematical and Physical Sciences*, vol. 261, pp. 516-531, May 23, 1961 1961.

[10] M. P. Borom and J. A. Pask, "Role of “Adherence Oxides” in the Development of Chemical Bonding at Glass-Metal Interfaces," *J. Amer. Ceram. Soc.,* vol. 49, pp. 1-6, 1966.

[11] Y. H. Kim, Y. S. Chaug, N. J. Chou, and J. Kim, "Adhesion of titanium thin film to oxide substrates," *J. Vacuum Sci. & Tech. A,* vol. 5, pp. 2890-2893, 1987.

[12] S. W. Russell, S. A. Rafalski, R. L. Spreitzer, J. Li, M. Moinpour, F. Moghadam, *et al.,* "Enhanced adhesion of copper to dielectrics via titanium and chromium additions and sacrificial reactions," *Thin Solid Films,* vol. 262, pp. 154-167, 1995.

[13] N. Jiang and J. Silcox, "Observations of reaction zones at chromium/oxide glass interfaces," *J. Appl. Phys.,* vol. 87, pp. 3768-3776, 2000.

[14] J. Keech, S. Chaparala, A. Shorey, G. Piech, and S. Pollard, "Fabrication of 3D-IC interposers," in *Proc. 2013 IEEE 63rd ECTC*, 2013, pp. 1829-1833.

[15] C. Xiaoyun, D. Bhatt, D. A. Hutt, K. Williams, and P. P. Conway, "Copper Deposition and Patterning for Glass Substrate Manufacture," in *Proc. 2007 9th EPTC*, 2007, pp. 37-42.

[16] S. Bamberg, B. Beck, H. Brüggmann, F. Brüning, E. Langhammer, C. Lowinski, *et al.*, "P-66: Wet Chemical Metallization for High-End Flat Panel Display Manufacturing," *SID Symp. Dig. of Tech. Papers,* vol. 42, pp. 1351-1354, 2011.

[17] S. Bamberg, M. Merschy, T. Bernhard, F. Bruening, R. Taylor, L. Brandt, *et al.*, "Challenges of Adhesion Promotion for the Metallization of Glass Interposers," in *46th Int. Symp. on Microelectronics*, 2013.

[18] G. Brist, S. Hall, S. Clouser, and T. Liang, "Non-classical conductor losses due to copper foil roughness and treatment," in *Electron. Circuit World Conv.*, 2005, pp. 22-24.

[19] V. Sukumaran, Q. Chen, L. Fuhan, N. Kumbhat, T. Bandyopadhyay, H. Chan, *et al.*, "Through-package-via formation and metallization of glass interposers," in *Proc. 2010 60th ECTC*, 2010, pp. 557-563.

[20] V. Sukumaran, G. Kumar, K. Ramachandran, Y. Suzuki, K. Demir, Y. Sato, *et al.*, "Design, Fabrication, and Characterization of Ultrathin 3-D Glass Interposers With Through-Package-Vias at Same Pitch as TSVs in Silicon," *IEEE Trans. Compon. Packag. Manuf. Technol.,* vol. 4, pp. 786-795, 2014.

[21] S. Cho, V. Sundaram, R. R. Tummala, and Y. K. Joshi, "Impact of Copper Through-Package Vias on Thermal Performance of Glass Interposers," *IEEE Trans. Compon. Packag. Manuf. Technol.,* vol. 5, pp. 1075-1084, 2015.

[22] P. Ogutu, E. Fey, P. Borgesen, and N. Dimitrov, "Hybrid Method for Metallization of Glass Interposers," *J. Electrochem. Soc.*, vol. 160, pp. D3228-D3236, 2013.

[23] H. Fu, S. Hunegnaw, Z. Liu, L. Brandt, and T. Magaya, "Adhesive enabling technology for directly plating copper onto glass/ceramic substrates," in *Proc. 2014 IEEE 64th ECTC*, 2014, pp. 1652-1655.

[24] S. Hunegnaw, L. Brandt, H. Fu, Z. Liu, and T. Magaya, "Adhesion Enabling Technology for Reliable Metallization and Patterning of Glass Interposers," in *Int. Symp. on Microelectronics*, 2014, pp. 000393-000396.

[25] K. Mukai, T. Magaya, L. Brandt, L. Zhiming, H. Fu, and S. Hunegnaw, "Adhesive enabling technology for directly plating copper onto glass," in *Proc. 2014 9th IMPACT*, 2014, pp. 170-173.

[26] S. Hunegnaw, Z. Liu, H. Fu, J. Wang, M. Merschky, K. Mukai, *et al.*, "VitroCoat GI - Ultra-thin adhesive layer for metallization of glass interposer," in *Proc. 2015 10th IMPACT*, 2015, pp. 149-152.

[27] Z. Liu, S. Hunegnaw, H. Fu, J. Wang, T. Magaya, M. Merschky, *et al.*, "A metal oxide adhesion layer prepared with water based coating solution for wet Cu metallization of glass interposer," in *Int. Symp. on Microelectronics*, 2015, pp. 000365-000369.

[28] P. C. Andricacos, C. Uzoh, J. O. Dukovic, J. Horkans, and H. Deligianni, "Damascene copper electroplating for chip interconnections," *IBM Journal of Research and Development*, vol. 42, pp. 567-574, 1998.

[29] P. M. Vereecken, R. A. Binstead, H. Deligianni, and P. C. Andricacos, "The chemistry of additives in damascene copper plating," *IBM Journal of Research and Development*, vol. 49, pp. 3-18, 2005.

[30] R. Akolkar and U. Landau, "A Time-Dependent Transport-Kinetics Model for Additive Interactions in Copper Interconnect Metallization," *Journal of The Electrochemical Society*, vol. 151, pp. C702-C711, November 1, 2004 2004.

[31] T. P. Moffat, D. Wheeler, and D. Josell "Electrodeposition of Copper in the SPS-PEG-Cl Additive System: I. Kinetic Measurements: Influence of SPS," *Journal of The Electrochemical Society*, vol. 151, pp. C262-C271, April 1, 2004 2004.

[32] J. G. Long, P. C. Searson, and P. M. Vereecken, "Electrochemical Characterization of Adsorption-Desorption of the Cuprous-Suppressor-Chloride Complex during Electrodeposition of Copper," *Journal of The Electrochemical Society*, vol. 153, pp. C258-C264, April 1, 2006 2006.

[33] W.-P. Dow, M.-Y. Yen, W.-B. Lin, and S.-W. Ho, "Influence of Molecular Weight of Polyethylene Glycol on Microvia Filling by Copper Electroplating," *Journal of The Electrochemical Society,* vol. 152, pp. C769-C775, November 1, 2005 2005.

[34] P. Broekmann, A. Fluegel, C. Emnet, M. Arnold, C. Roeger-Goepfert, A. Wagner, *et al.*, "Classification of suppressor additives based on synergistic and antagonistic ensemble effects," *Electrochimica Acta,* vol. 56, pp. 4724-4734, 5/1/ 2011.

[35] M. J. Willey and A. C. West, "Microfluidic Studies of Adsorption and Desorption of Polyethylene Glycol during Copper Electrodeposition," *Journal of The Electrochemical Society,* vol. 153, pp. C728-C734, October 1, 2006 2006.

[36] J. W. Gallaway and A. C. West, "PEG, PPG, and Their Triblock Copolymers as Suppressors in Copper Electroplating," *Journal of The Electrochemical Society,* vol. 155, pp. D632-D639, October 1, 2008 2008.

[37] S.-K. Kim, D. Josell, and T. P. Moffat, "Electrodeposition of Cu in the PEI-PEG-Cl-SPS Additive System: Reduction of Overfill Bump Formation During Superfilling," *Journal of The Electrochemical Society,* vol. 153, pp. C616-C622, September 1, 2006 2006.

[38] M. J. Willey, J. Reid, and A. C. West, "Adsorption Kinetics of Polyvinylpyrrolidone during Copper Electrodeposition," *Electrochemical and Solid-State Letters,* vol. 10, pp. D38-D41, April 1, 2007 2007.

[39] W.-P. Dow, C.-C. Li, M.-W. Lin, G.-W. Su, and C.-C. Huang, "Copper Fill of Microvia Using a Thiol-Modified Cu Seed Layer and Various Levelers," *Journal of The Electrochemical Society,* vol. 156, pp. D314-D320, August 1, 2009 2009.

[40] W.-P. Dow, C.-C. Li, Y.-C. Su, S.-P. Shen, C.-C. Huang, C. Lee, *et al.*, "Microvia filling by copper electroplating using diazine black as a leveler," *Electrochimica Acta,* vol. 54, pp. 5894-5901, 10/1/ 2009.

[41] Y.-B. Li, W. Wang, and Y.-L. Li, "Adsorption Behavior and Related Mechanism of Janus Green B during Copper Via-Filling Process," *Journal of The Electrochemical Society,* vol. 156, pp. D119-D124, April 1, 2009 2009.

[42] Z. V. Feng and A. A. Gewirth, "Atomic force microscopic study of polymeric film growth in copper electroplating bath with benzotriazole," *Journal of Electroanalytical Chemistry,* vol. 601, pp. 242-250, 3/15/ 2007.

[43] D. P. Schweinsberg, G. A. Hope, A. Trueman, and V. Otieno-Alego, "An electrochemical and SERS study of the action of polyvinylpyrrolidone and polyethylenimine as inhibitors for copper in aerated H2SO4," *Corrosion Science,* vol. 38, pp. 587-599, 4// 1996.

[44] J. Zhou and J. D. Reid, "Impact of Leveler Molecular Weight and Concentration on Damascene Copper Electroplating," *ECS Transactions*, vol. 2, pp. 77-92, February 7, 2007 2007.

[45] N. T. M. Hai, J. Furrer, F. Stricker, T. M. T. Huynh, I. Gjuroski, N. Luedi, *et al.*, "Polyvinylpyrrolidones (PVPs): Switchable Leveler Additives for Damascene Applications," *Journal of The Electrochemical Society*, vol. 160, pp. D3116-D3125, January 1, 2013 2013.

[46] Z. V. Feng, X. Li, and A. A. Gewirth, "Inhibition Due to the Interaction of Polyethylene Glycol, Chloride, and Copper in Plating Baths: A Surface-Enhanced Raman Study," *The Journal of Physical Chemistry B*, vol. 107, pp. 9415-9423, 2003/09/01 2003.

[47] Z. D. Schultz, Z. V. Feng, M. E. Biggin, and A. A. Gewirth, "Vibrational Spectroscopic and Mass Spectrometric Studies of the Interaction of Bis(3-sulfopropyl)-disulfide with Cu Surfaces," *Journal of The Electrochemical Society*, vol. 153, pp. C97-C107, February 1, 2006 2006.

[48] K. G. Schmitt, R. Schmidt, H. F. von-Horsten, G. Vazhenin, and A. A. Gewirth, "3-Mercapto-1-Propanesulfonate for Cu Electrodeposition Studied by in Situ Shell-Isolated Nanoparticle-Enhanced Raman Spectroscopy, Density Functional Theory Calculations, and Cyclic Voltammetry," *The Journal of Physical Chemistry C*, vol. 119, pp. 23453-23462, 2015/10/15 2015.

[49] J. Y. Lee, S. K. Lee, and J. H. Park, "Fabrication of void-free copper filled through-glass-via for wafer-level RF MEMS packaging," *Electronics Letters*, vol. 48, pp. 1076-1077, 2012.

[50] S. Bamberg, R. Brüning, J. Etzkorn, and F. Brüning, "NOVEL WET CHEMICAL COPPER METALLIZATION FOR GLASS INTERPOSERS," 2011.

[51] C. Jouwersma, "On the theory of peeling," *Journal of Polymer Science*, vol. 45, pp. 253-255, 1960.

[52] X. Ramis, J. M. Salla, C. Mas, A. Mantecón, and A. Serra, "Kinetic study by FTIR, TMA, and DSC of the curing of a mixture of DGEBA resin and γ-butyrolactone catalyzed by ytterbium triflate," *J. Appl. Poly. Sci.*, vol. 92, pp. 381-393, 2004.

[53] D. M. Pozar, *Microwave Engineering*, 4th ed. Hoboken, NJ: Wiley, 2011.

[54] S.-J. Cho, K.-W. Paik, and Y.-G. Kim, "The effect of the oxidation of Cu-base leadframe on the interface adhesion between Cu metal and epoxy molding compound," *IEEE Trans. Compon. Packag. Manuf. Technol.*, vol. 20, pp. 167-175, 1997.

[55] K. Demir, K. Ramachandran, Y. Sato, Q. Chen, V. Sukumaran, R. Pucha, *et al.*, "Thermomechanical and electrochemical reliability of fine-pitch through-package-copper vias (TPV) in thin glass interposers and packages," in *Proc. 2013 IEEE 63rd ECTC*, 2013, pp. 353-359.

[56] M. Broas, K. Demir, Y. Sato, V. Sundaram, and R. Tummala, "A comparative reliability study of copper-plated glass vias, drilled with CO2 and ArF excimer lasers," in *Proc. 2014 ESTC*, 2014, pp. 1-5.

[57] T. Huang, V. Sundaram, P. M. Raj, H. Sharma, and R. Tummala, "Adhesion and reliability of direct Cu metallization of through-package vias in glass interposers," in *Proc. 2014 IEEE 64th ECTC*, 2014, pp. 2266-2270.

[58] N. Kim, D. Wu, J. Carrel, J. H. Kim, and P. Wu, "Channel design methodology for 28Gb/s SerDes FPGA applications with stacked silicon interconnect technology," in *Proc. 2012 IEEE 62nd ECTC*, 2012, pp. 1786-1793.

[59] S. Sitaraman, J. Min, M. R. Pulugurtha, M. S. Kim, V. Sundaram, and R. Tummala, "Modeling, design and demonstration of integrated electromagnetic shielding for miniaturized RF SOP glass packages," in *Proc. 2015 IEEE 65th ECTC*, 2015, pp. 1956-1960.

[60] T. P. Moffat, D. Wheeler, M. D. Edelstein, and D. Josell, "Superconformal film growth: Mechanism and quantification," *IBM Journal of Research and Development*, vol. 49, pp. 19-36, 2005.

[61] B. M. D. Sawyer, Y. Suzuki, R. Furuya, C. Nair, T. C. Huang, V. Smet, *et al.*, "Design and Demonstration of a 2.5-D Glass Interposer BGA Package for High Bandwidth and Low Cost," *IEEE Transactions on Components, Packaging and Manufacturing Technology*, vol. 7, pp. 552-562, 2017.